Electrical Properties of ZrO_2-Gd_2O_3 Ceramics

By

Sreya Dutta

Roll No: 9911209

TH
MSP/2001/M
D95Hc

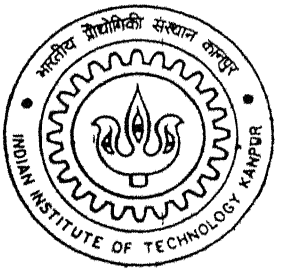

MATERIALS SCIENCE PROGRAMME

Indian Institute of Technology Kanpur

Kanpur-208016

India

Electrical Properties of ZrO_2-Gd_2O_3 Ceramics

by
Sreya Dutta

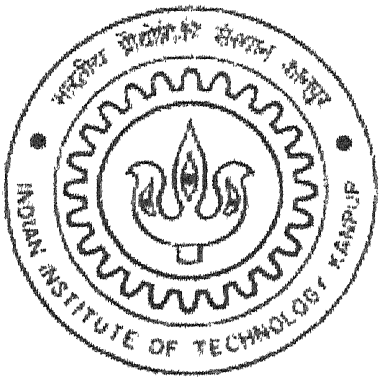

Materials Science Programme
Indian Insitute of Technology Kanpur
Kanpur-208016
India

29 APR 2002

IIM.S.P
पुरुषोत्तम काशीनाथ केलकर पुस्तकालय
भारतीय प्रौद्योगिकी संस्थान कानपुर
वर्गांक सं० A... 139593

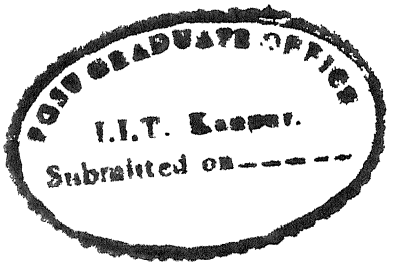

CERTIFICATE

This is to certify that the work contained in the thesis entitled " **Electrical Properties of ZrO_2-Gd_2O_3 Ceramics**" by Ms. Sreya Dutta has been carried out under my supervision and has not been submitted elsewhere for a degree.

(D.C. Agrawal)

Professor

Materials ScienceProgramme

Indian Institute of Technology

Kanpur 208 016

India

August, 2001

Acknowledgement

I would like to thank my supervisor Dr. D. C. Agrawal for introducing me to field of zirconia ceramics and impedance spectroscopy. I thank him for his patience, constant encouragement and excellent guidance. During my stay in this institute I have learned many things from him. I am grateful to him for his generosity. I wish that he will keep in touch with me in future and will continue to give his valuable advice.

I am very grateful to Dr. Shahi for his help and advices during my thesis work. I want to thank all the staff of the ACMS, MSP, Glass Blowing Lab and Physics Lab for their help and support during the entire course of work. I would also like to thank all the staff of ACMS and MSP for their cooperation. Especially I would like to thank Mr. Umashankar Singh, Mr. G. S. Thapa, Sardarji, and Mr. B.Sharma for their constant help.

Thanks are in store for my lab mates Aditi, Arpana, Animesh, Niraj, Sandesh and Sahooji for their help and cooperation. It was a nice and memorable association with all of them.During this long stay at I.I.T. Kanpur many people helped in different ways and it is not possible to acknowledge each of them in this small space. I thank them all for their help and their cooperation. The list would be incomplete if I don't thank Anshuman Dalvi, Sudha, Ashutosh and Feroz who rendered help whenever asked for

I wish to give a heartfelt thanks to Prof. Malay Chaudhuri, his wife and daughter Mahua for their constant help and support. Kakima's, Mrs Malay Chaudhuri, delicious Bengali dishes always made me feel at home away from home.

The silent support from my family members was always a constant source of inspiration for me during my stay.

Sreya Dutta

ABSTRACT

Impedance measurements are carried out on 1 75, 2 5, 4,5, 8, 9, and 11 mole% $Gd_2O_3 - ZrO_2$ samples prepared via coprecipitation route The Cole- Cole plot comprises of two semi circles, one due to grain (high frequency) and the other due to grain boundary (low frequency) conduction and an arc due to electrode effect The DC conductivity for grain is seen to be maximum at all temperatures for 4 mole% Gd_2O_3 and does not change much for rest of the composition. At around 585K, the value of DC conductivity for grain boundary is around 0.6×10^{-6} $(\Omega\ cm)^{-1}$ for all the compositions from 2.5 mole% to 9 mole%; however is significantly higher at 1.5×10^{-6} $(\Omega\ cm)^{-1}$ for 11 mole% Gd_2O_3.The activation enthalpy for conduction in grain varies between 0.58 to 1.01 eV, as the composition varies from 1.75 to 8 mole%. Similar trend is seen for activation enthalpy for grain boundary conduction. The activation enthalpy for grain conduction is quite low at 9 mole% and 11 mole% Gd_2O_3 indicating that there is no significant association of vacancy clusters. The values of migration enthalpies are nearly equal to activation enthalpies for grain conduction. This result also supports that association of vacancies is not significant. The activation enthalpy calculated from the modulus is nearly in agreement with that obtained from the Cole-Cole plot. A single peak is seen for all the compositions except for 1.75 and 9 mole% Gd_2O_3 compositions in the modulus plot of M" vs log (frequency) indicating a single relaxation mechanism. The carrier concentration is calculated at 603K. It is of the order of 10^{21}/ cm^{-3}. The Jonscher's constant is calculated by AC curve fitting & depression angle method and is found to vary between 0.8-1. The difference in the values indicates that the Cole-Cole plot is not exactly a semicircle. Both the ac conductivity vs log (frequency) and permittivity vs log

(frequency) show a dispersion step at the grain boundary relaxation frequency. From the dielectric loss vs log (frequency) plots, the dielectric loss peak is seen to decrease with increasing Gd_2O_3 content. Zirconia gadolinia thin films are prepared in the laboratory for studying the conductivity, but the film shows a shorting between top and bottom electrodes and could not be used fro impedance measurements

Contents

List of Tables

LIST OF FIGURES

1 INTRODUCTION

1.1 CONDUCTION IN IONIC SOLIDS

When an electric field is applied to an ionic solid an electric current is produced. The ionic solids have a large band gap and only a few electrons are excited even at high temperatures. So, the charge carriers in these materials are the anions or / and cations. The movement of these ions i.e. ionic transport occurs due to the presence of defects or disorder. These are mainly of two types

i) *Point Defect Type:* In this type, the transport is by Frenkel and Schottky defect pairs, which are thermally generated. The activation energy is generally high (~1eV or more).

Depending on the defect concentration density, this type of defects can be further subdivided as [1]

a) Dilute: Conventional ionic solids with number of mobile defects $10^{18}/cm^{-3}$ or less. Example: AgCl, β-AgI, NaCl, KCl etc.

Concentrated: The defect concentration is $10^{20}/cm^{-3}$ or less. Example: Stabilized

ZrO_2, HfO_2, CaF_2 etc.

(ii) *Molten Sublattice Type:* In this type of solids, the number of ions of particular type is less than the number of sites available for them in the sublattice So, as a result all these ions can hop and move like a free ion. Since all these ions are available for transport, the activation energy is low. Generally the number of mobile ionic charge carriers is $10^{22}/cm^{-3}$.

Depending on the magnitude of conductivity at moderate temperature, the ionic solids can be further subdivided into three groups.

i) *Poor/ Normal Ionic Conductors:* The conventional ionic solids having an ionic conductivity $< 10^{-6}(\Omega cm)^{-1}$ fall in this group. The charge transport is mainly through thermally generated Frenkel / Schottky defect. Example: AgCl, AgBr, β-AgI etc.

ii) *Moderate Ionic Conductors:* The range of conductivity for these ionic solids is from 10^{-6} to $< 10^{-3}$ $(\Omega cm)^{-1}$. Examples: CaF_2, PbF_2, CaO, ZrO_2.

iii) *Fast Ionic Conductors:* In this case all the ions in a sublattice are available for movement and conductivity is $> 10^{-3}$ $(\Omega cm)^{-1}$. Examples: α-AgI, $RbAg_4I_5$, Li_2SO_4.

Depending on the conducting ion, the ionic solids are classified in two groups:

(i) Cationic Conductors:

a. Li^+ and Na^+ ion conductors e.g. LiI, Li_2SO_4, Na-βAl_2O_3, Na_3PO_4.

b. Cu^+ and Ag^+ ion conductors e.g. α-AgI, $RbAg_4I_5$, α-CuI

c. Proton (H^+) Conductors e.g. H_3O, βAl_2O_3

(ii) Anionic Conductors: Oxide ion conductors e.g. doped ZrO_2, doped CeO_2

1.1.1 OXIDE ION CONDUCTORS [1]

Both cations and anions can move in the solid lattice. The common ions showing high mobility are Li^+, Na^+, K^+, Ag^+, Cu^+, F^- and O^{2-}. Of these F^- and O^{2-} show high conductivity only at high temperature. The first solid oxide electrolyte was probably 15 Y_2O_3-ZrO_2 ceramic, used by Nernst (1899) as an incandescent lighting material. Later Baur and Preis (1937) used this material for a fuel cell. Wagner (1943) proposed a definite conductivity mechanism in terms of oxygen vacancies, which was later, verified by Hund (1952). After Kiukola and Wagner (1957a, 1957b) proposed their use in high temperature thermodynamic measurements and fuel cells, there was a sudden surge of interest in these material.

Most of the oxygen ion conductors generally conduct at higher temperature (~1000°C) and their conductivity is of mixed nature (ionic + electronic + electron-hole). Other than temperature, their conductivity also depends on doping by aliovalent dopants (Ca^{2+}, Y^{3+}, Sr^{2+} etc in ZrO_2, HfO_2, CeO_2 etc). These dopants control the number of point defects and their mobility. Another unique property of these oxygen ion conductors is the dependence of conductivity on the ambient pressure. If the ambient oxygen pressure is low, the oxygen ions (O_o) would leave the solid electrolyte according to the following mechanism

$$2O_o \Leftrightarrow O_2\,(g) + 2V^{\cdot\cdot}_o + 4e$$

At high ambient oxygen pressure the defect equilibrium can be expressed as

$$\tfrac{1}{2}\,O_2\,(g) \Leftrightarrow O_i'' + 2h^{\cdot}$$

So, at low oxygen pressure and also at high temperature conduction is of electronic nature (n-type) and at high oxygen pressure the conductivity is predominantly hole conductivity

(p-type). In the intermediate pressure range, the conductivity is mostly ionic in nature and practically independent of the oxygen pressure Fig.(1.1).[1]

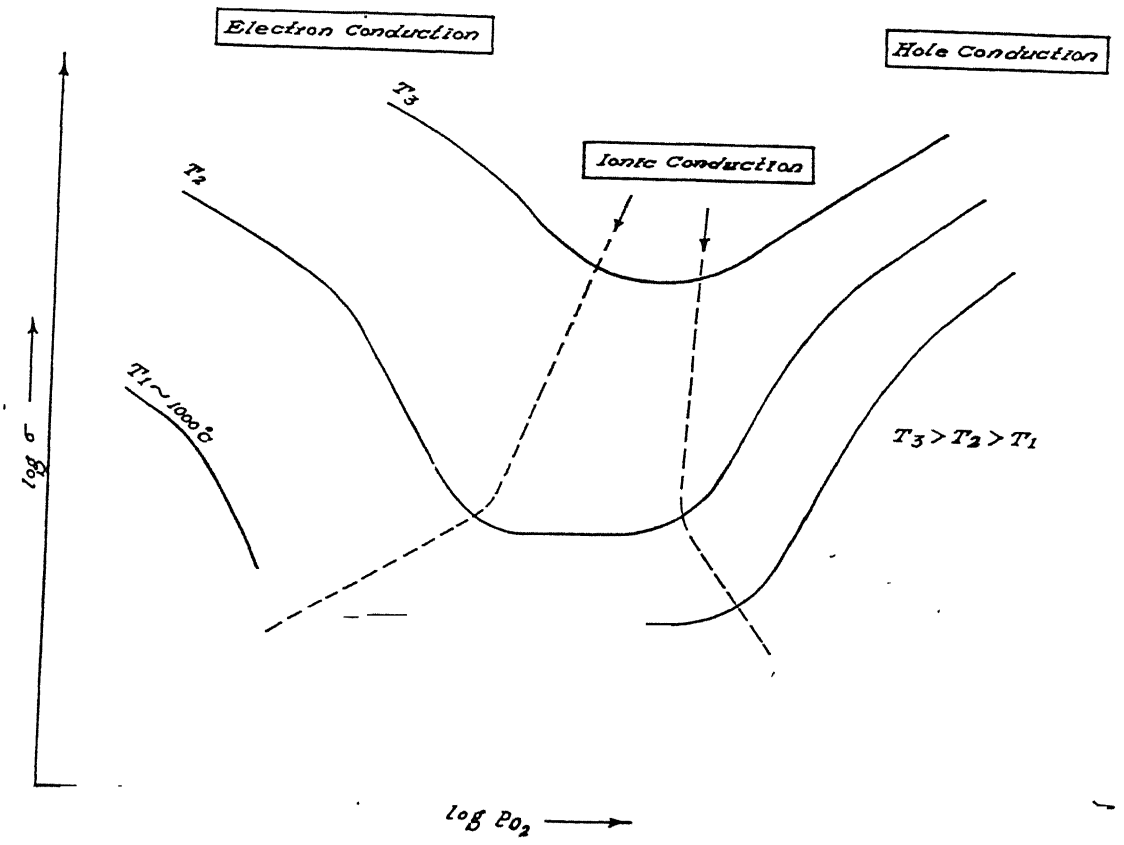

Fig.1.1 Schematic representation of the dependence of conductivity of any oxide ion electrolyte on oxygen partial pressure at three temperatures [1]

Most of the oxide electrolytes developed so far are based on ThO_2, CeO_2, ZrO_2 and HfO_2. The common feature, which sustains oxygen ion conduction, is the fluorite structure. In this structure the metal ions are dispersed in the body corners and face centers i.e. total four cations are there. All the eight tetrahedral voids are filled up by oxygen ions Fig.(1.2). The structure is quite open and the dopant concentration range over which the fluorite structure is retained is tabulated for ZrO_2 (Table1.1).

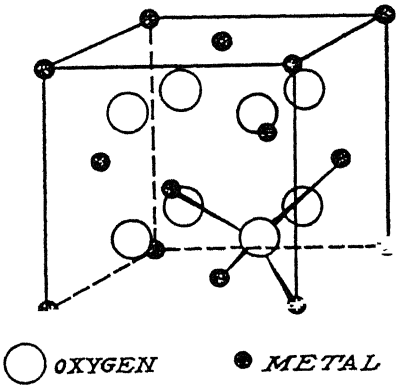

Fig.1.2 The fluorite crystal structure [1]

Table 1.1 Fluorite phase boundaries in doped ZrO_2 solid solutions [1]

Oxide solid solution	Boundaries (dopant mol%)	Temperature (°C)
ZrO_2. CaO	14 and 20	1500
: Nd_2O_3	15 and 40	1300
: Sm_2O_3	10 and 50	1000
: Eu_2O_3	10 and 55	1300
: Gd_2O_3	9 and 50	1000
: Dy_2O_3	5 and 41	1600
: Ho_2O_3	4 and 56	1300
: Yb_2O_3	7 and 46	1000
: Y_2O_3	10 and 36	1000
: CeO_2	50 and 100	1500

It is seen that as the concentration of dopant changes, the lattice parameter also changes.

Lattice parameters for ZrO_2 for different dopants are tabulated below (Table 1.2)

Table1.2: Lattice parameters of ZrO_2 with different dopants [1]

Material	Lattice Parameter (A°)
ZrO_2 : 10 % CaO	5.118
: 10% Nd_2O_3	5.183
: 10% Sm_2O_3	5.172
: 10 % Gd_2O_3	5.162
: 10 % Sc_2O_3	5.089

Stabilized Zirconia received wide attention as solid electrolytes, electrodes in fuel cells, oxygen sensors etc. It behaves as a mixed conductor depending on the crystal structure. Electronic conduction dominates in the monoclinic phase, while tetragonal form shows mixed ionic and electronic conduction. The cubic zirconia exhibits predominant ionic conduction.

1.2 ZIRCONIA CERAMICS

Zirconia ceramics is an important class of ionic conductors. Pure zirconia exists in three different crystal structures i.e. cubic, tetragonal and monoclinic. The transformation to various phases occurs as follows:

$$\text{Monoclinic (m)} \xleftrightarrow{1170^\circ C} \text{Tetragonal (t)} \xleftrightarrow{2370^\circ C} \text{Cubic (c)} \xleftrightarrow{2680^\circ C} \text{Liquid (l)}$$

At higher temperatures an orthogonal form also exists. The t→m conversion is accompanied by 4 to 6 % volume increase and 1 to 2 % shear strain. Due to this disruptive effect it is difficult to fabricate pure zirconia bodies. Hence aliovalent oxides such as CaO, MgO, Y_2O_3 and Gd_2O_3 etc. are added to ZrO_2 to stabilize the fluorite type cubic phase at room temperature. In fully stabilized zirconia (FSZ) with a lower content of the stabilizer a two phase material containing cubic and tetragonal (or monoclinic) phases termed as partially stabilized zirconia (PSZ) is obtained.[2]

When ZrO_2 is doped with oxides of elements of lower valence, the lower valence elements occupy the Zr^{4+} sites and for charge compensation vacancies are introduced at oxygen lattice sites. A typical trivalent ion substitution reaction with ZrO_2 is

$$(1\text{-}x)\ ZrO_2 + x/2 A_2O_3 \longrightarrow A_xZr_{1-x}O_{2-x/2} + x/2\ V''_o$$

where x is the mol% of A_2O_3, A being the dopant ion [3]. Depending on the substituent, ZrO_2 ceramics exhibit significant oxygen ion conductivity at elevated temperature. This factor along with good thermo mechanical properties of ZrO_2 alloys has resulted in their wide use as electrolyte material in high temperature solid oxide fuel cells (SOFC), oxygen sensors and in electrical heating elements in oxidizing atmosphere. Most frequently used materials for these applications are CaO, Y_2O_3 stabilized ZrO_2 [4,5].

The elastic energy associated with dopant cation mismatch is an important parameter in determining the ionic conductivity. The maximum conductivity is related to the minimum difference in the ionic radii between the Zr^{4+} and the dopant ion. The variation of conductivity with dopant follows roughly the sequence:

$Yb_2O_3 > Gd_2O_3 > Y_2O_3 > CaO > MgO$ [5]. The sizes of the various ions are:

Dopant Ion	Radius of Ion (nm)
Yb^{3+}	0.086
Gd^{3+}	0.097
Ca^{2+}	0.099
Mg^{2+}	0.066
Zr^{4+}	0.079
Y^{3+}	0.092

Y_2O_3 is the most commonly employed dopant in ZrO_2 used for ionic conductivity related applications. The use of Yb_2O_3 and Gd_2O_3 has not been practiced so far due to the difficulty in preparation of the doped ceramics. Bhattacharya and Agrawal have recently reported the preparation of ZrO_2-Gd_2O_3 ceramics [6]. Gd_2O_3 appears to be an attractive dopant due to higher conductivity expected in ZrO_2- Gd_2O_3 ceramics. Addition of Gd_2O_3 in amounts more than 10 % forms a large cubic phase region with ZrO_2. At a higher mole% of Gd_2O_3, a pyrochlore phase is reported [7].

Generally, it is seen that with increase in the dopant level, conductivity of the ZrO_2 ceramics increases due to the formation of oxygen vacancy defects. It becomes maximum at a dopant concentration where fully stabilized highly defective fluorite structure is obtained. Beyond that there is a decrease in conductivity due to defect association and micro domain ordering [5].

For a wide range of ZrO_2 ceramics there is a strong correlation between electrical properties, phase content, and microstructure. Of the three phases, the t and c phases have significantly greater conductivity than m phase. In the polycrystalline material, oxygen ion conduction across grain boundaries is influenced by the presence of the second phase

especially if it is glass. Solute segregation and presence of the thin siliceous film at the grain boundaries lead to the blocking nature of grain boundaries in ZrO_2.

1.3 IMPEDANCE SPECTROSCOPY TECHNIQUE

In a typical polycrystalline stabilized ZrO_2, both the grain and the grain boundary resistance add up to give the total resistance. Baurle [8] was the first to apply impedance spectroscopy technique to ZrO_2 to separate the grain and grain boundary contributions. The information extracted, by using this technique can be related to the grain interior microstructure and presence of resistive grain boundary films (if any), which can affect high temperature applications.

1.3.1 IMPEDANCE SPECTROSCOPY: THE TECHNIQUE

Impedance Spectroscopy (IS) is a well-known method to study the electrical properties of materials and their interfaces with electronically conducting electrodes. The parameters derived from an IS spectrum fall generally into two categories [9]:

a. Those pertinent only to the material itself such as conductivity, dielectric constant, mobility of charges, equilibrium concentration of charged species etc.

b. Those pertinent only to an electrode material interface such as adsorption reaction rates, constants and capacitance of the electrode itself.

The standard method is to measure the impedance directly in a frequency domain by applying a small voltage to the interface and measuring the phase shift θ and amplitude $|Z|$ of the impedance. The data obtained is analyzed in a complex impedance plane known as Cole-Cole plot ($Z\sin\theta$ vs $Z\cos\theta$). By this method contribution from different processes can be separated out.

1.3.2 COMPLEX IMPEDANCE PLANE ANALYSIS

The five frequency dependent properties that can be represented in a complex plane are [9]:

Complex Impedance (Z^*) Complex Admittance (Y^*)

Complex Permittivity (ε^*) Complex Modulus (M^*)

Dielectric Constant (χ)

They are related as

$$\varepsilon^* = \varepsilon' - j\varepsilon'' \quad (1.1)$$

$$\chi^* = \varepsilon^*/\varepsilon_0 = \chi' - \chi'' \quad (1.2)$$

$$Z^* = Z' - Z'' = 1/j\omega C_0\varepsilon^* \quad (1.3)$$

$$Y^* = 1/Z^* = Y' + jY'' = j\omega C_0\varepsilon^* \quad (1.4)$$

$$M^* = 1/\varepsilon^* = M' + jM'' = j\omega C_0 Z^* \quad (1.5)$$

where ω = angular frequency and C_0 = capacitance of the cell in vacuum

An AC sinusoidal signal $v(t) = V_M\sin(\omega t)$, involving a single frequency $f = \omega/2\pi$, is applied to a cell. The steady state current [$I(t) = I_M\sin(wt + \theta)$] is measured.Here θ is the phase difference between the voltage and the current. Then one can write

Complex Impedance $Z^*(\omega) = v(t) / i(t)$

Magnitude, $Z(\omega) = V_M / I_M(\omega)$ and phase angle = $\theta(\omega)$

Resistivity for ionic conduction in solids can be represented in terms of equivalent RC circuit, such that complex impedance (Z^*) at an applied frequency (ω) can be written as

$$Z^* = Z_R + jZ_I \quad (1.6)$$

where Z_R = real part of the complex impedance

Z_I = imaginary part of the complex impedance

Z_R (Z') and Z_I (Z'') can be represented

$$Z_R = |Z|\cos\theta,\ Z_I = |Z|\sin\theta \qquad (1.7)$$

$$\therefore\ |Z| = (Z_R^2 + Z_I^2)^{1/2} \text{ and } \tan\theta = Z_R/Z_I \qquad (1.8)$$

Some of the simple RC circuits are represented in terms of complex impedance and admittance plots.

I. Pure Resistor R

For only a resistor impedance can be written as

$$Z^* = R \qquad (1.9)$$

$$\therefore\ Z' = R \text{ and } Z'' = 0 \qquad (1.10)$$

Here the impedance is frequency independent as shown in Fig.1.3 (a and b).

II. Pure Capacitor C

For a pure Capacitor

$$Z^* = 1/j\omega C \qquad (1.11)$$

$$= -j/\omega C \qquad (1.12)$$

$$\therefore\ Z' = 0 \text{ and } Z'' = -1/\omega C \qquad (1.13)$$

The plot is a straight line along Z'' axis as shown in Fig. 1.4 (a and b)

III. Series combination of R and C

When R and C are in series, then from equation 1.10 and 1.13 we get

$$Z^* = R + 1/j\omega C \qquad (1.14)$$

$$= R + j(-1/\omega C)$$

$$\therefore Z' = R, \text{ and } Z'' = -1/\omega C \quad (1.15)$$

This combination leads to a straight line parallel to Z' axis as shown in Fig1.5.

IV. Parallel Combination of R and C

When R and C are in series then from equation 1.10 and 1.13 we get

$$Z^* = (R/j\omega C)/(R+1/j\omega C) \quad (1.16)$$

$$= R(-j/\omega C)/(R-j/\omega C) \quad (1.17)$$

$$= R(R+j/\omega C)(-j/\omega C) \quad (1.18)$$

$$\text{or } Z^* = [R/(1+\omega^2C^2R^2)] + j[-\omega CR^2/(1 + \omega^2C^2R^2)] \quad (1.19)$$

Thus the real and imaginary parts can be given as

$$Z' = R/(1+\omega^2C^2R^2) \quad (1.20)$$

$$Z'' = -\omega CR^2/(1 + \omega^2C^2R^2) \quad (1.21)$$

Eliminating ω from both the equations, we get

$$Z'^2 + Z''^2 = RZ' \quad (1.22)$$

$$(Z' - R/2)^2 + Z''^2 = (R/2)^2 \quad (1.23)$$

which is the equation of a circle with center at (R/2,0) and radius R/2 (Fig. 1.6).

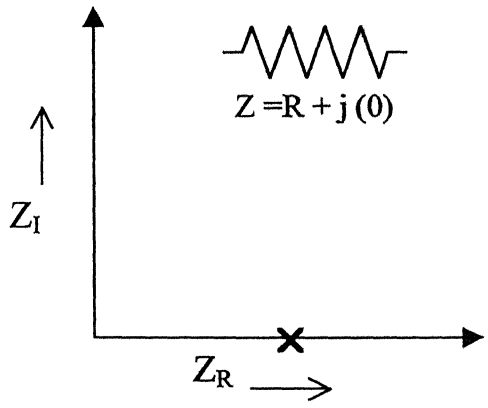

Fig. 1.3 (a) Impedance plot for pure resistive circuit

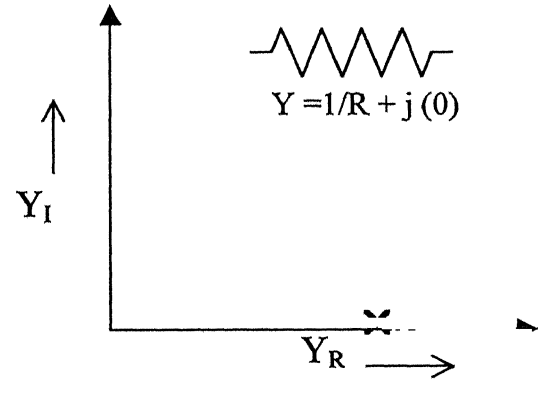

Fig. 1.3 (b) Admittance plot for pure resistive circuit

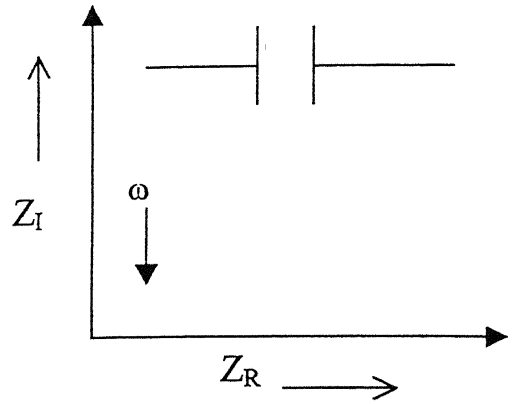

Fig. 1.4 (a) Impedance plot for pure capacitive circuit

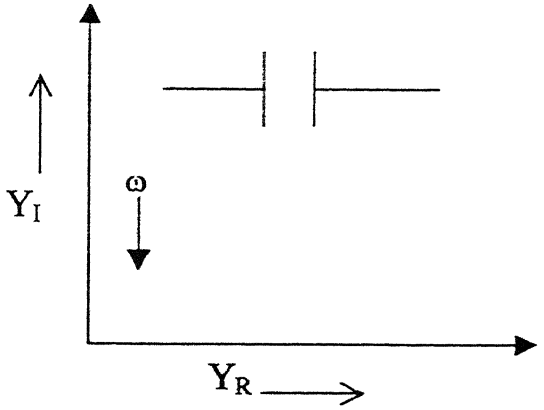

Fig. 1.4 (b) Admittance plot for pure capacitive circuit

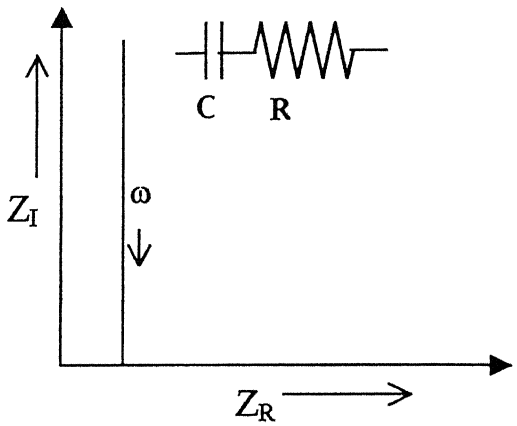

Fig. 1.5 Impedance plot for a resistor and capacitor in series

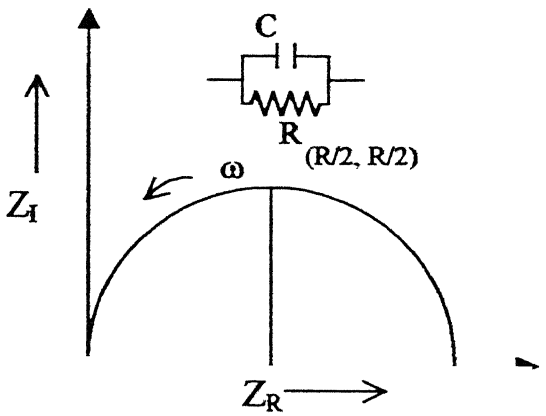

Fig. 1.6 Impedance plot for a resistor and capacitor in parallel

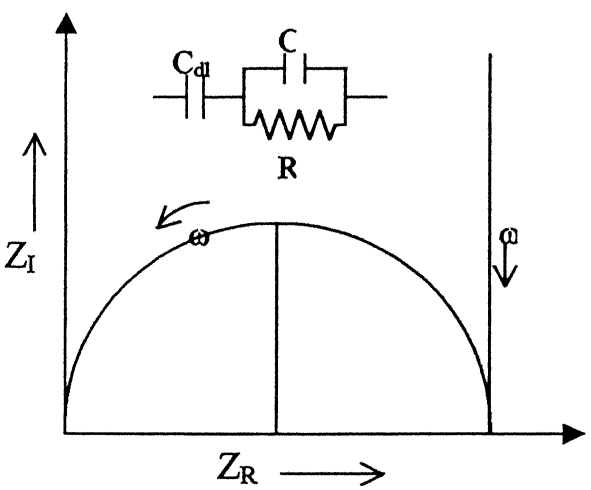

Fig. 1.7 Impedance plot for a sample with blocking electrodes (ideal case) [10]

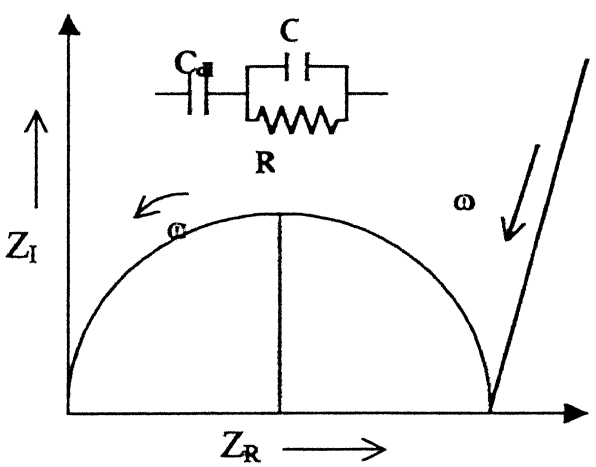

Fig. 1.8 Impedance plot for a sample with blocking electrodes (real case) [10]

Plot (1.7) and (1.8) are for ionic conductivity of the sample and due to the blocking electrode [10]. Blocking electrodes are the polarizable electrodes, which form a blocking interface between electrode and solid electrolyte and inhibit charge transfer across the interface within certain limits of voltage. This generally happens when the electrode metal (e.g. Pt/C) is in contact with the electrolyte (e.g. $RbAg_4I_5$). Then silver electrode will be non-blocking. For blocking electrodes a double layer is formed which resists charge transfer. Curve in Fig. (1.7) is seen in ideal case when we get a line 90° to x-axis i.e. when the electrode surface is very smooth (at low frequencies). At higher frequencies, there is contribution due to electrolyte. In case of surface roughness and other factors, the line due to electrode polarization gets inclined to x- axis in Fig (1.8) at low frequencies.

In case of non-blocking electrode, there is charge transfer due to anodic polarization. Ag electrode in contact with $RbAg_4I_5$ is such a case. Charge transfer occurs but there is also an additional charge transfer resistance. So, in the equivalent circuit charge transfer resistance R_{ct} is in parallel with the double layer capacitance C_{dl}. The plot will yield two semicircles, one at high frequency due to the electrolyte and the other at low frequency due to electrode effect (Fig.1.9).

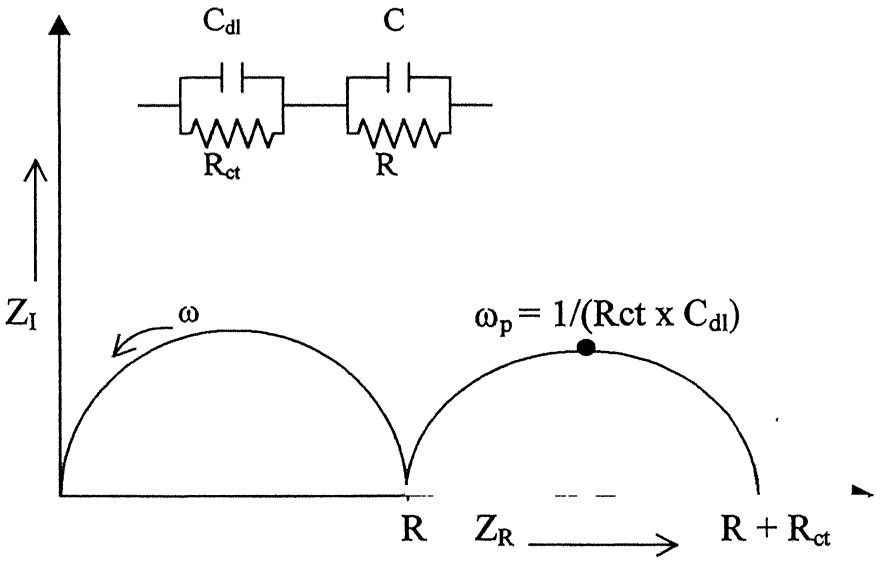

Fig. 1.9 Impedance plot for a sample with non-blocking electrodes (ideal case) [10]

From these curves, the intercept of the full semicircle with the x-axis gives the resistance values. From the peak frequencies ω_p, we get the capacitance value as $\omega_p = 1/RC$.

In real cases for polycrystalline sample, we generally get depressed semi-circles. By finding out their diameter we get an idea about their DC resistivity. In these solids there is ionic conduction due to both grain and grain boundary effects. So, there are two semicircles with plus an arc due to electrode effect. The typical plot is shown in Fig.1.10.

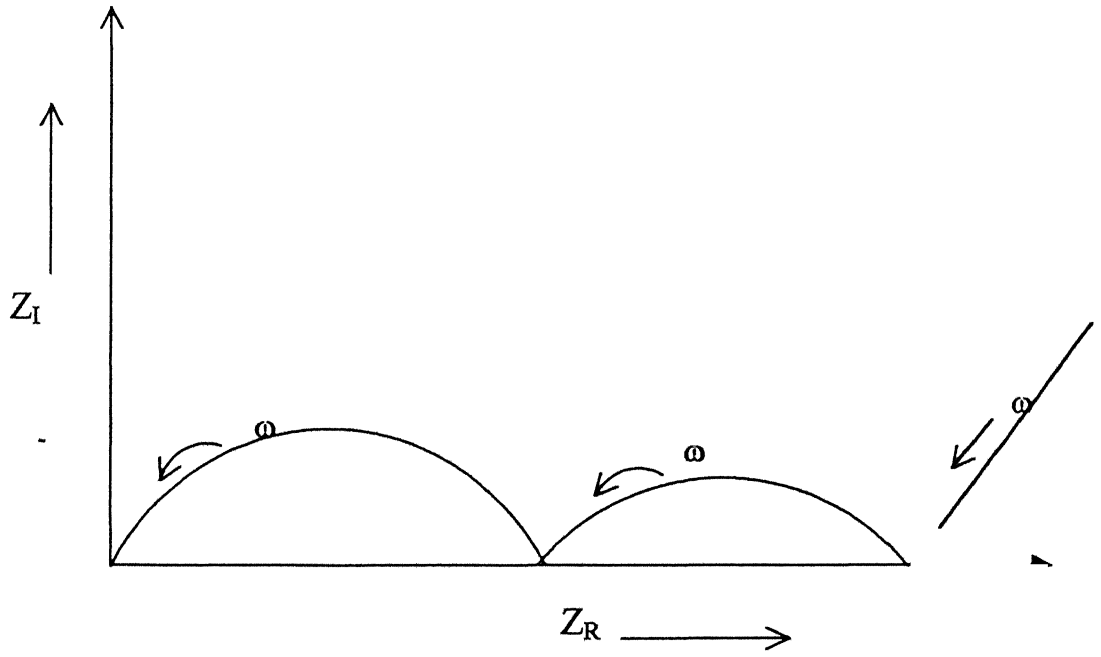

Fig. 1.10 Impedance plot for real polycrystalline samples

1.4 ANALYSIS OF THE IS DATA WITH REFERENCE TO ZIRCONIA CERAMICS

A typical measurement is made by applying a small sinusoidal voltage to the electroded sample. Phase shift (θ) and amplitude of the impedance (Z_o) are measured directly from the analyzer. If the applied voltage is $U = U_o e^{i\omega t}$, the current passing in the cell would be $I = I_o e^{i(\omega t+\theta)}$, the impedance is given by the formula

$Z = U/I = U_o e^{-i\theta}/I_o = Z_o e^{-i\theta} = Z_o(\cos\theta + \sin\theta)$

Where θ = phase shift and ω = angular frequency = $2\pi f$, f being the frequency at which measurement is done.

$Z_o\sin\theta$ is plotted against $Z_o\cos\theta$ in the Cole-Cole plot or in the complex impedance plane. Generally the complex impedance plots of the polycrystalline solid electrolytes show 3 characteristic semicircles (Fig. 1.11)[10]. The high frequency semicircle is mainly due to the intra-grain conductivity while the intermediate frequency semicircle is due to the grain boundary conductivity. The low frequency arc is due to the electrode-sample interface. The diameter of the semicircle corresponds to the corresponding resistance. The resistance measured by the first real intercept and the conductivity calculated from it is usually called intra-grain resistance and conductivity respectively. The resistance measured using the second intercept and the conductivity from it is usually called the grain boundary resistance and conductivity respectively, which include the blocking effect.

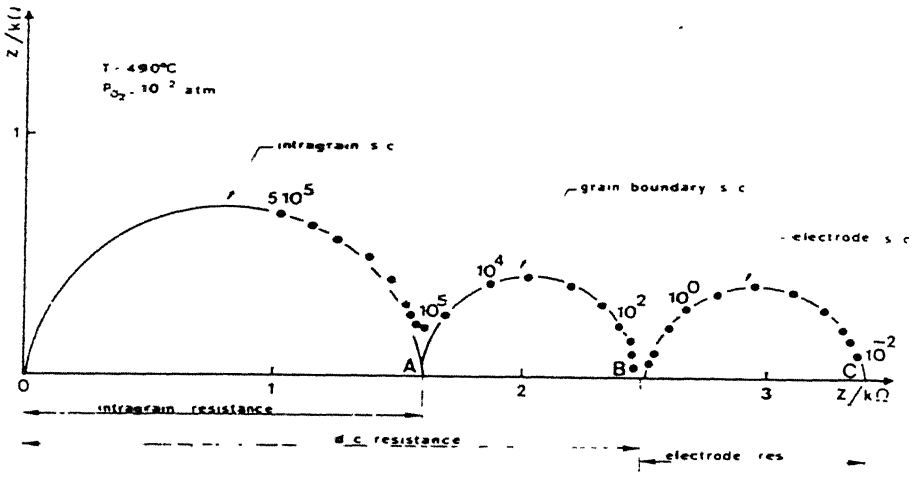

Fig. 1.11 Impedance plot for a sintered zirconia sample at low temperature [10]

A careful observation of the recent results has indicated the presence of two semicircles due to the electrode contribution. The complex impedance plot for a polycrystalline material in this situation can be schematically represented as shown in Fig1.12.

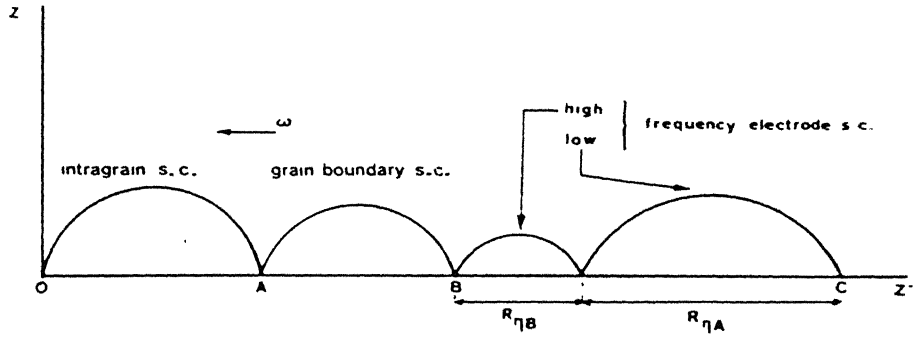

Fig.1.12. Impedance diagram of a sintered zirconia pellet where $r\eta_a$, low frequency semicircle resistance; $r\eta_b$, high frequency semicircle resistance [10]

1.4.1 CONDUCTIVITY AND ACTIVATION ENTHALPY

The analysis of the impedance data is carried out by assuming that an equivalent parallel R-C circuit can represent the ionic conductor. As discussed earlier, for an ideal R-C circuit, the real and imaginary parts of the impedance generate a semicircle. The diameter of the semicircle is equal to R: and C is obtained from $\omega_p = 1/RC$, where ω_p is the peak frequency i.e. the frequency for which $Z\sin\theta$ is maximum. The DC conductivity of the ionic materials is derived by considering the diffusion of charge carriers in an electric field as [12]

$$\sigma_{DC} = (\gamma J_d^2 q^2 N_c f_h)/kT \qquad (1.24)$$

where γ = geometrical factor which is dependent on the crystal structure

J_d = jump distance related to lattice parameter

q = charge on the charge carrier

N_c = free charge carrier concentration

and f_h = vacancy hopping rate

The charge carrier concentration is given by [10]

$$N_c = N_o \exp(\Delta G_a/kT) \qquad (1.25)$$

$$= N_o \exp(\Delta S_a/k)\exp(-\Delta H_a/kT) \qquad (1.26)$$

= total vacancy concentration

ΔG_a, ΔS_a, ΔH_a are the free energy, entropy and enthalpy for the formation of vacancy clusters respectively.

In diffusion , hopping is a thermally activated process. The hopping rate can be written as:

$$f_h = f_{ho}\exp(-\Delta G_m/kT) = f_{ho}\exp(\Delta S_m/k)\exp(-\Delta H_m/kT) \qquad (1.27)$$

where f_{ho} = attempt frequency and ΔG_m, ΔS_m, ΔH_m are the free energy, entropy and enthalpy for migration of oxygen ions respectively.

Substituting the expression (1.27) in (1.24) we get

$$\sigma_{DC} = (\gamma J_d^2 q^2 N_c f_h)/kT \qquad (1.28)$$

$$= ((\gamma J_d^2 q^2)/kT)N_o\exp(\Delta S_a/k)\exp(-\Delta H_a/kT)f_{ho}\exp(\Delta S_m/k)\exp(-\Delta H_m/kT) \qquad (1.29)$$

$$=(A/T)\exp[-(\Delta H_a + \Delta H_m)]/kT \qquad (1.30)$$

$$\text{or } \sigma_{DC}T = A\exp(-\Delta H_\sigma/kT) \qquad (1.31)$$

$$\text{where } A = ((\gamma J_d^2 q^2)/kT)N_o\exp(\Delta S_a/k)\, f_{ho}\exp(\Delta S_m/k)$$

$$\text{and } \Delta H_\sigma = \Delta H_m + \Delta H_a$$

The slope of the plot of log ($\sigma_{DC}T$) versus 1/T gives the value of $\Delta H\sigma$ and the intercept

gives the value of A. As mentioned earlier the AC conductivity in real materials is frequency dependent. Almond and West have given the following expression for AC conductivity [12,13]

$$\sigma(\omega) = K\,\omega_p[1+(\omega/\omega_p)^n] \qquad (1.32)$$

Here ωp is a characteristic frequency which in dipolar dielectrics is associated with the frequency of the dielectric loss peak. Almond and West call it a *hopping frequency*. They also noted that

$$\sigma_{DC} = K\,\omega_p \qquad (1.33)$$

So that

$$\sigma(\omega) = \sigma_{DC}[1+(\omega/\omega_p)^n] \qquad (1.34)$$

For $\omega = \omega_p$, $\sigma(\omega) = 2\sigma_{DC}$. Hence ω_p is the frequency at which the AC conductivity is twice the DC conductivity. The frequency ω_p can also be evaluated by curve fitting the conductivity data to the equation (1.34). The AC conductivity is obtained from the (Z,θ) data using the relation

$$\sigma_{AC} = (\cos\theta/Z)(L/A) \qquad (1.35)$$

Here L is the thickness of the sample and A is the cross-section area.

Luo et al [13] have fitted the high frequency data corresponding to the intra-grain conductivity to equation (1.32). At this frequency the contribution of grain boundaries and the electrode to the conductivity can be neglected. The high frequency range suitable such a plot can be found from an impedance plot for each temperature. It was observed

that the best fit is obtained when the frequency is around ω_p. Value of n can also be obtained by such curve fitting. It was found that the value of n would not remain constant if the frequency range used for the curve fitting is far away from ω_p.

The hopping frequency is temperature dependent. A plot of $\ln\omega_p$ versus 1/T gives the activation enthalpy for migration (ΔH_m). Knowing the activation enthalpy for conduction (ΔH_σ) as discussed above, the activation enthalpy for association of vacancies (ΔH_a) can be obtained since $\Delta H_\sigma = \Delta H_m + \Delta H_a$.

Results of the AC impedance measurements were carried on ZrO_2-Y_2O_3 systems are summarized below from literature.

R. Ramamoorthy [14] prepared Y_2O_3 stabilized ZrO_2 (YSZ) samples of compositions 2, 3, 4.5, 6 and 9 mole% Y_2O_3 using chemical precipitation technique. The grain sizes vary between 1μm to 5μm. The measurements were done between 1Hz to 1MHz. The results are tabulated below in Table1.3 .for temperatures 573K and 773K as obtained from the Fig.1.13 (σ vs Y_2O_3 concentration).

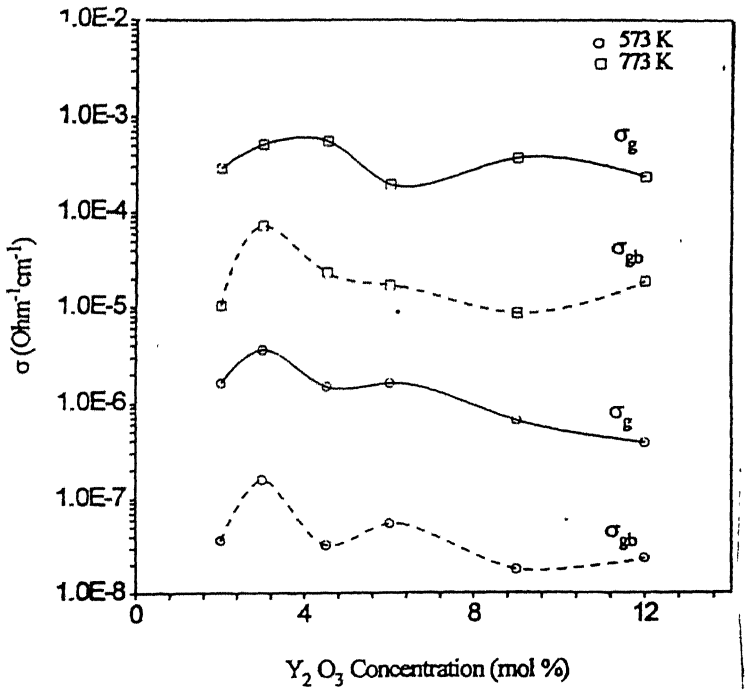

Fig.1.13 Variation of conductivity in grain and grain boundaries with yttria concentration at temperatures 573K and 773K [14]

Table 1.3 Data for activation enthalpy and conductivity at 573K and 773K for different compositions [14]

Mole % of Y_2O_3	Phases	$\Delta H_{\sigma g}$ (eV)	$\Delta H_{\sigma gb}$ (eV)	σ_g $(\Omega cm)^{-1}$ at 573K	σ_{gb} $(\Omega cm)^{-1}$ at 573K	σ_g $(\Omega cm)^{-1}$ at 773K	σ_{gb} $(\Omega cm)^{-1}$ at 773K
2	Mainly t + small amount of c	0.98	1.2	$1.7x10^{-6}$	$3.8x10^{-8}$	$2.8x10^{-4}$	$1.0x10^{-5}$
3	Purely t	0.97	1.21	$3.5x10^{-6}$	$1.7x10^{-7}$	$5x10^{-4}$	$7x10^{-5}$
4.5	Mainly c with little amount of t	1.12	1.27	$1.7x10^{-6}$	$3x10^{-8}$	$5.1x10^{-4}$	$2.1x10^{-5}$
6	c	1.02	1.27	$1.6x10^{-6}$	$5x10^{-8}$	$1.8x10^{-4}$	$1.5x10^{-5}$
9	c	1.17	1.31	$6x10^{-7}$	$2x10^{-8}$	$3x10^{-4}$	$7x10^{-6}$
12	c	1.22	1.35	$3.5x10^{-7}$	$2.6x10^{-8}$	$2x10^{-4}$	$1.5x10^{-5}$

The conductivity of 2 mole% YSZ is lesser than 3 mole% due to the presence of the monoclinic phase. 3 mole% showed the maximum conductivity at 573K and then decreases with increasing mole% of Y_2O_3 above 3 mole%. The 3 mole% composition also showed the maximum grain boundary conductivity for both the temperatures. At 773K, σ_g is higher for 4.5 mole% and then decreases after that. The activation enthalpies for grain and grain boundary increase generally from 3 mole% onwards for both the temperatures.

J. Luo et al [12] carried out impedance measurements on YSZ samples containing

3, 4.8, 5 7, 6.6, 7.5, 8.4, 10.2 and 12 mole% using Solartron 1264 impedance measurements. Fig.1.14 shows the impedance plot for 7.5 mole% Y_2O_3 at 290°C.

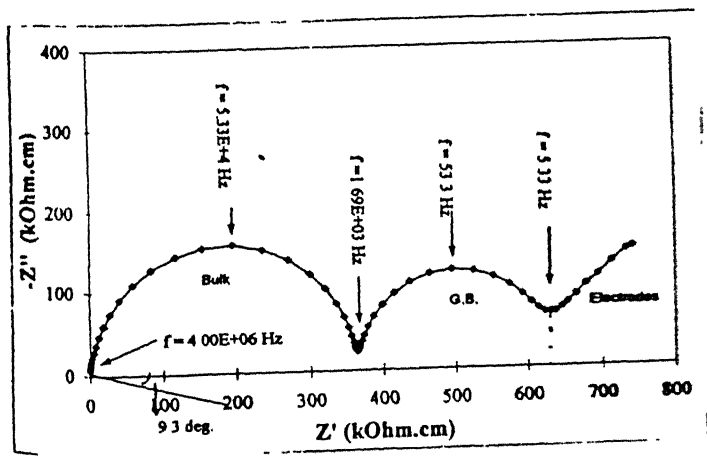

Fig.1.14 Complex impedance plot of 7.5 mole% Y_2O_3-ZrO_2 ceramics at 290°C [12]

J. Luo et al [12] has tabulated the data for phases, activation enthalpy at different temperatures for different mole% (Table 1.4).

Table 1.4 Enthalpies and phases for different mole% of Y_2O_3-ZrO_2 [12]

Y_2O_3 conc (mole %)	Cubic (%)	Tetragonal (%)	Monoclinic (%)	ΔH_σ (eV)	ΔH_m (eV)	ΔH_a (eV)
3	-	72	28	0.95	0.92	0.03
4.8	49	51	-	1.01	0.91	0.1
5.7	66	34	-	1.06	0.91	0.15
6.6	100	-	-	1.09	0.96	0.13
7.5	100	-	-	1.10	0.92	0.18
8.4	100	-	-	1.18	1.05	0.13
10.2	100	-	-	1.24	1.05	0.19
12	100	-	-	1.25	1.06	0.19

The activation enthalpies are seen to increase with increasing mole% of Y_2O_3 as reported by J. Luo et al [12].

The conductivity data for different compositions at different temperatures are read from log(σT) vs 1/T plot (Fig.1.15).

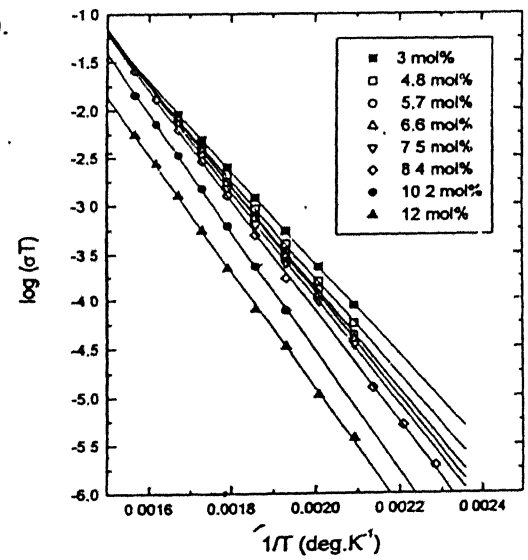

Fig 1.15 Arrhenius plots of DC conductivity temperature product of eight ZrO_2-Y_2O_3 specimens studied by J.Luo et al. [12]

Table1.5. Values of grain conductivities at different temperature for different mole% of Y_2O_3

	Mole % of Y_2O_3							
Temperature (°C)	3	4.8	5.7	6.6	7.5	8.4	10.2	12
476	2.10×10^{-7}	1.18×10^{-7}	8.86×10^{-8}	8.36×10^{-8}	$7\ 45\times10^{-8}$	6.64×10^{-8}		
503	4.08×10^{-7}	3.53×10^{-7}	2.65×10^{-7}	2.29×10^{-7}	2.29×10^{-7}	1.99×10^{-7}		
513	1.09×10^{-6}	9.99×10^{-7}	9.76×10^{-7}	7.76×10^{-7}	6.16×10^{-7}	3.47×10^{-7}	1.46×10^{-7}	7.08×10^{-8}
533	1.88×10^{-6}	1.49×10^{-6}	1.30×10^{-7}	1.23×10^{-6}	1.23×10^{-6}	1.23×10^{-6}	3.85×10^{-7}	2.06×10^{-8}
553	3.71×10^{-6}	3.21×10^{-6}	2.86×10^{-6}	2.80×10^{-6}	2.27×10^{-6}	2.27×10^{-6}	1.04×10^{-6}	5.72×10^{-8}
573	7.35×10^{-6}	6.95×10^{-6}	5.65×10^{-6}	5.52×10^{-5}	5.39×10^{-6}	5.09×10^{-6}	2.69×10^{-6}	1.36×10^{-7}
593	1.46×10^{-5}	1.34×10^{-5}	1.09×10^{-5}	1.06×10^{-5}	1.06×10^{-5}	1.06×10^{-5}	5.33×10^{-6}	1.98×10^{-6}
613							$1\ 06\times10^{-5}$	4.46×10^{-6}
633							2.10×10^{-5}	7.69×10^{-6}

Table 1.5 gives the values of conductivities at different temperature for different mole% of Y_2O_3.

It is seen that at particular temperature, the conductivity decreases with increasing Y_2O_3 content and at any particular composition; the conductivity increases with increasing temperature. However it has been pointed out by these authors that on extrapolating the curves, the 7.5 and 8.4 mole% Y_2O_3 compositions show higher conductivities at higher temperature (> 633K).

The data from the two papers are compared at 573K and tabulated in Table1.6.

Table 1.6: Conductivity and activation enthalpy data at 573K as reported by J. Luo et al and R. Ramamoorthy et al [12,14]

Data given by J. Luo et al			Data given by R. Ramamoorthy et al	
ΔH_σ (eV)	σ_g $(\Omega cm)^{-1}$	Mole% of Y_2O_3	σ_g $(\Omega cm)^{-1}$	ΔH_σ (eV)
0.953	7.35×10^{-6}	3	3.5×10^{-6}	0.97
		4.5	1.7×10^{-6}	1.12
1.011	6.95×10^{-6}	4.8		
1.059	5.647×10^{-6}	5.7		
		6	1.6×10^{-6}	1.02
1.091	5.519×10^{-6}	6.6		
1.104	5.39×10^{-6}	7.5		
1.179	5.09×10^{-6}	8.4		
		9	6×10^{-7}	1.17
1.238	2.69×10^{-6}	10.2		
1.255	1.356×10^{-12}	12	3.5×10^{-7}	1.22

It is seen that the activation energy and conductivity broadly agree in the investigations. In both the cases the conductivity decreases with increasing Y_2O_3 content. It should be noted that at high temperature (> 633K) the conductivity is highest for 8 mole% Y_2O_3. If the plot of Luo et al is extrapolated to this temperature then their 7.5 and 8.4 mole% samples are found to have higher conductivities than the other samples, which is in agreement with earlier results. The data shows the conductivity of Y_2O_3-ZrO_2 is around $5x\ 10^{-6}\ (\Omega cm)^{-1}$ and $\Delta H_\sigma$is of the order of 1 eV. The values of ΔH_σ are seen to increase from 3 mole% in both the cases. But Ramamoorthy et al has pointed out higher activation energy at 4.5 mole% than 6 mole%. This could be due to the presence of a two phase mixture (t+c) in 4.5 mole% samples. Except this deviation the values of activation enthalpy determined by the two investigations are comparable of around 1 eV.. Furthermore they increse slightly as the mole% of Y_2O_3 increases. The values of activation enthalpy given by A. Pimenov et al [15] for 4, 8, 10 and 12 mole% Y_2O_3 is seen to increase from 4 to 12 mole% slightly and the values are ~1 eV.

Several authors have measured electrical properties of ZrO_2-Gd_2O_3 ceramics and single crystals [3,7,16,17,18]. However, except one all the studies have been carried out at very high Gd_2O_3 content (> 20 mole%). Table1.7 summarizes the conductivity and activation enthalpy results on ZrO_2-Gd_2O_3 containing 10 and 12.5 mole% Gd_2O_3 [16].

Table 1.7: Conductivity and activation enthalpy of ZrO_2-Gd_2O_3 single crystal containing 10 and 12.5 mole% Gd_2O_3 [16]

Temperature (K)	σ_g $(\Omega cm)^{-1}$ for 10 mole%	σ_g $(\Omega cm)^{-1}$ for 12 mole%	$\Delta H_{\sigma g}$ (eV) for 10 mole%	$\Delta H_{\sigma g}$(eV) for 12 mole%
833	0.0478	0.019		
769	0.013	4.613×10^{-3}		
714	3.76×10^{-3}	2.49×10^{-4}		
667	4.74×10^{-3}	1.49×10^{-4}	1.1856	1.248
625	8.997×10^{-3}	1.6×10^{-5}		
588	3.02×10^{-3}	9.56×10^{-6}		
546	3.25×10^{-3}	1.03×10^{-3}		

Conductivity of the 10 mole% sample is higher than the 12.5 mole% sample at all the temperatures. Fig.1.16 compares the results on the single crystals with that on polycrystals. The electrical conductivity of the single crystals is higher than that of polycrystals. At 909K, the grain conductivities of 12 mole% Gd_2O_3 doped ZrO_2 are $0.011(\Omega cm)^{-1}$ for single crystals and 0.0027 $(\Omega cm)^{-1}$ for polycrystalline sample and at 1000K these values are 0.044 $(\Omega cm)^{-1}$ and 0.01 $(\Omega cm)^{-1}$ respectively.

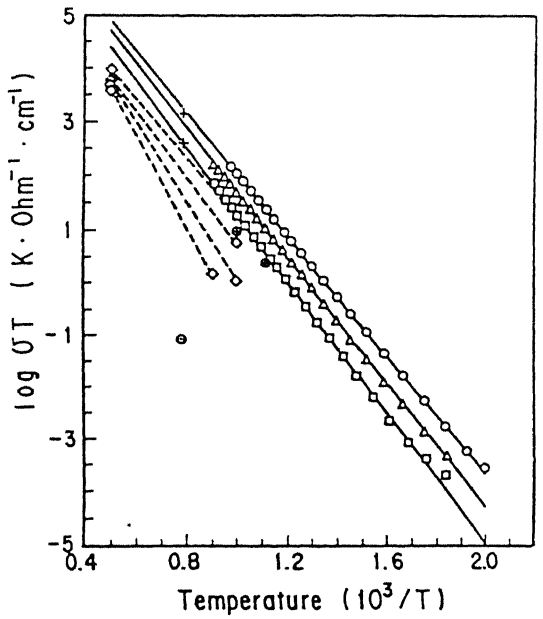

Fig.1.16 Temperature dependence of conductivity of ZrO_2-Gd_2O_3 solid solutions [16] (Solid lines are (○) 10, (Δ) 12.5 and (□) 15 mole% Gd_2O_3.)(Dashed lines are for 12 mole% Gd_2O_3 polycrystals :(+)[17], (⊗)[7], (◇)[18] and (⊙)[17])

The conductivity of the polycrystals is an order of magnitude lower due to the presence of grain boundaries [3,7,17]. The activation energy is found to be ~1.2 eV for 10-12 mole%.

T. Van Dijk [3] studied conductivity of cubic solid solutions of $Gd_xZr_{1-x}O_{2-x/2}$ with x in the compositional range of $0.2 < x < 0.6$. A bell shaped pyrochlore (P) phase region is seen to exist within the defect fluorite (F) structure in the compositional range of 46 to 53 mole%. Electrical measurements are carried on the samples prepared through wet chemical method using Solartron FA 1172 apparatus between temperature 500°C and 750°C. The complex admittance diagram is shown in Fig. 1.17 for $Gd_{0.51}Zr_{0.49}O_{1.745}$ at

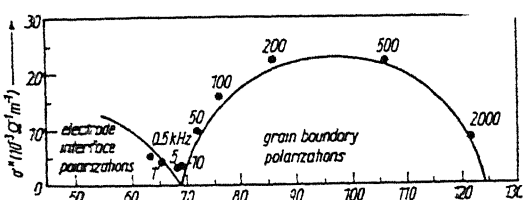

Fig.1.17 Complex admittance diagram for $Gd_{0.51}Zr_{0.49}O_{1.745}$ at 600°C [3]

From Fig.1.18 conductivity variation shows a particular trend with composition at different temperatures. The conductivity is found to decrease sharply with composition between 19 and 30%. It remains constant between 30 to 38 mole% and then increases continuously until it reaches the peak at 50 mole% (composition $Gd_2Zr_2O_7$). Beyond this, conductivity decreases strongly. The conductivity is higher in pyrochlore phase than fluorite phase.

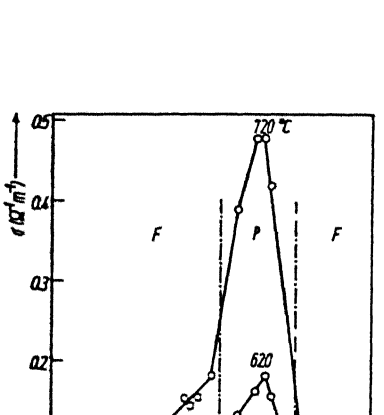

Fig.1.18 Grain conductivity at 520°C, 620°C and 720°C as a function of composition in the ZrO_2-Gd_2O_3 system [3]

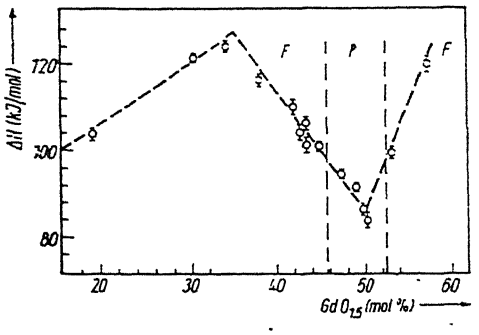

Fig.1.19 Variation of activation enthalpy with composition [3]

In another paper T. Van. Dijk[7] did complex admittance measurements on $Gd_xZr_{1-x}O_{2-x/2}$ prepared by three different routes which are skull melting procedure producing single crystals, alkoxide synthesis producing dense ultrafine grain ceramics and citrate route producing dense fine grain ceramics. The values of bulk and grain boundary conductivity at different compositions are tabulated in Table1.8.

Table 1.8: Values of bulk and grain boundary conductivities at different compositions of $Gd_xZr_{1-x}O_{2-x/2}$ prepared through different methods at three different temperatures [7]

Method	$GdO_{1.5}$	Phase	500°C		600°C		700°C	
			σ_g $x10^{-3}$ $(\Omega m)^{-1}$	σ_{gb} $x10^{-3}$ $(\Omega m)^{-1}$	σ_g $x10^{-3}$ $(\Omega m)^{-1}$	σ_{gb} $x10^{-3}$ $(\Omega m)^{-1}$	σ_g $x10^{-3}$ $(\Omega m)^{-1}$	σ_g $x10^{-3}$ $(\Omega m)^{-1}$
Citrate	44.8	F	4.1	16	28	140	102	1000
Alkoxide	49.5	P	24	4	110	30	267	160
Citrate	49.8	P	31	13	140	70	345	300
Single Crystal	52	P	9.5		52		173	
Citrate	53.2	P	4.1	70	25	60	25	

Both the grain and the grain boundary conductivities increase with increasing temperatures. σ_{gb} of citrate materials exceed that of alkoxide by one order of magnitude. While the σ_g is nearly of the same order independent of the preparation technique. The activation enthalpies are tabulated in Table1.9.

Table 1.9: Activation Enthalpies for different compositions of $Gd_xZr_{1-x}O_{2-x/2}$ [7]

Method	$GdO_{1.5}$	$\Delta H_{\sigma g}$ (eV)	$\Delta H_{\sigma gb}$ (eV)
Citrate	44.8	1.11	1.21
Alkoxide	49.5	0.83	1.22
Citrate	49.8	0.83	1.24
Single Crystal	52	1.01	
Citrate	53.2	1.03	1.21

The $\Delta H_{\sigma gb}$ is always higher than $\Delta H_{\sigma g}$ for both the routes. The $\Delta H_{\sigma g}$ is around 1eV and $\Delta H_{\sigma gb}$ is around 1.2eV.

1.4.2 THE PARAMETER n IN THE CONDUCTIVITY EQUATION

The values of the n in the conductivity equation can be obtained by different methods [13]. The values differ from one and another and provide insight into the validity of the analysis procedure.

(1) As described above, the value of n can be obtained by curve fitting the AC conductivity data to the grain interior AC conductivity in the valid frequency range (around ω_p)

(2) The parameter n is also related to the angle φ by which the semicircle is depressed by the relation

$$n = 1-2\varphi/\pi \qquad (1.36)$$

(3) The third procedure is to obtain n using the following expression for the dielectric loss:

$$\chi'' = (\sigma_{AC} - \sigma_{DC})/\omega\varepsilon_o \qquad (1.37)$$

This expression is very sensitive to the value of σ_{DC}. Luo et a [13] estimated σ_{DC} by two different methods and used their average to fit the equation. One estimation is from diameter of the semicircle in the Cole-Cole plot. The other estimation is by curve fitting equation (1.34), to AC conductivity data.

When χ'' is plotted against frequency Fig (1.20)[11] is obtained. Combining equation (1.34) and (1.37) one gets

$$\chi'' = \sigma_{DC}(\omega^{n-1}/\omega_p^{n}) \qquad (1.38)$$

Hence a plot of $\log\chi''$ versus $\log\omega$ should have a slope of n -1.

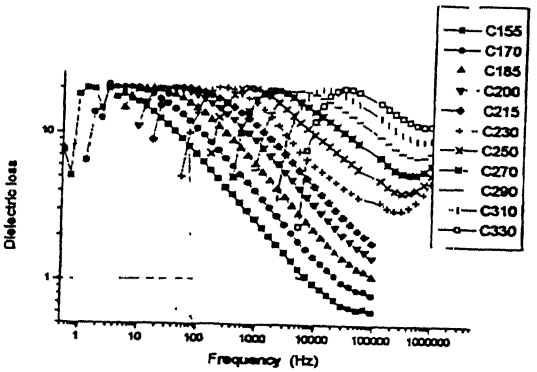

Fig.1.20 The effect of frequency on the dielectric loss at various temperatures for 12 mole% Y_2O_3-ZrO_2 [13]

As seen in Fig.1.20 the relation is obeyed after the peak frequency. This slope is –0.44 so that n = 0.56. The value of n obtained by the three methods by Luo et al [13] are 0.7 to 0.8, 0.88 and 0.56 respectively. This difference in the values of n leads to the conclusion that n = 0.56 is the most correct value as a linear fit is satisfied only in the corresponding frequency range. The semicircle fit is done in the whole frequency range. Thus, the universal expression for conductivity is not satisfied in the system used by Luo et al [13] and the semicircle in the Cole-Cole plot is not really a semicircle.

A value for n can also be obtained by plotting log (σ_{AC}-σ_{DC}) vs logfrequency (Fig. 1.21). The slope should be n. This value was also found to be close to 0.6.

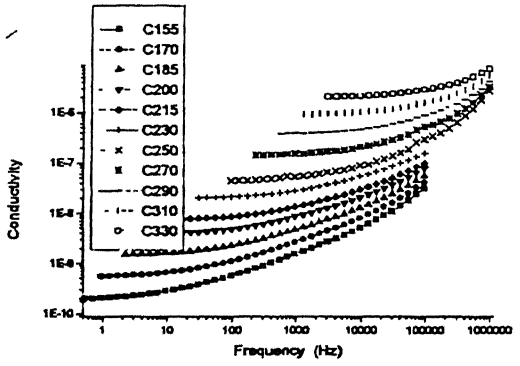

Fig.1.21. The effect of frequency on the difference between ac and dc conductivity for 12 mole% Y_2O_3-ZrO_2 [13]

1.4.3 THE VARIOUS CHARACTERISTIC FREQUENCIES AND ACTIVATION ENERGIES ASSOCIATED WITH THEM

From the description above, three characteristic frequencies can be obtained

a. Frequency f_R corresponding to the peak in the Cole-Cole plot which is also the frequency for which $\sigma_{AC} = \sigma_{DC}$.

b Frequency f_p obtained by curve fitting the AC conductivity data to equation (1.34)

c The dielectric loss peak frequency obtained for the plot of dielectric loss vs frequency plot

All the frequencies are thermally activated and can be fitted to Arrhenius equation. Luo et al[13] obtained the following equations for the three frequencies:

$f_R = 4.3 \times 10^{14} \exp(-1.10/kT)$ (1.35)

$f_p = 5.4 \times 10^{15} \exp(-1.12/kT)$ (1.36)

$f_d = 5.0 \times 10^{14} \exp(-1.13/kT)$ (1.37)

All the three frequencies can be related to the hopping rate of the change of carriers. The corresponding activation enthalpy (1.1 to 1.3 eV) is found to be about 0.1eV smaller than the activation enthalpy for conduction [13] The difference can be taken to be the defect association enthalpy

Luo et al in another paper [12] had found the hopping frequency determined from methods (a) and (b) above to be identical They also found the migration enthalpy as determined from the Arrhenius plot to be smaller than the conductivity activation enthalpy and attributed the difference to the enthalpy of association Table 1.4[12] reproduces the results for ZrO_2-Y_2O_3 alloys of different compositions

The association enthalpy is found to increase with cubic content upto 5 mol%, above which it is not sensitive to composition even though, both the activation enthalpies for conduction and migration, are found to increase with the Y_2O_3 content (Fig. 1.22)[12]

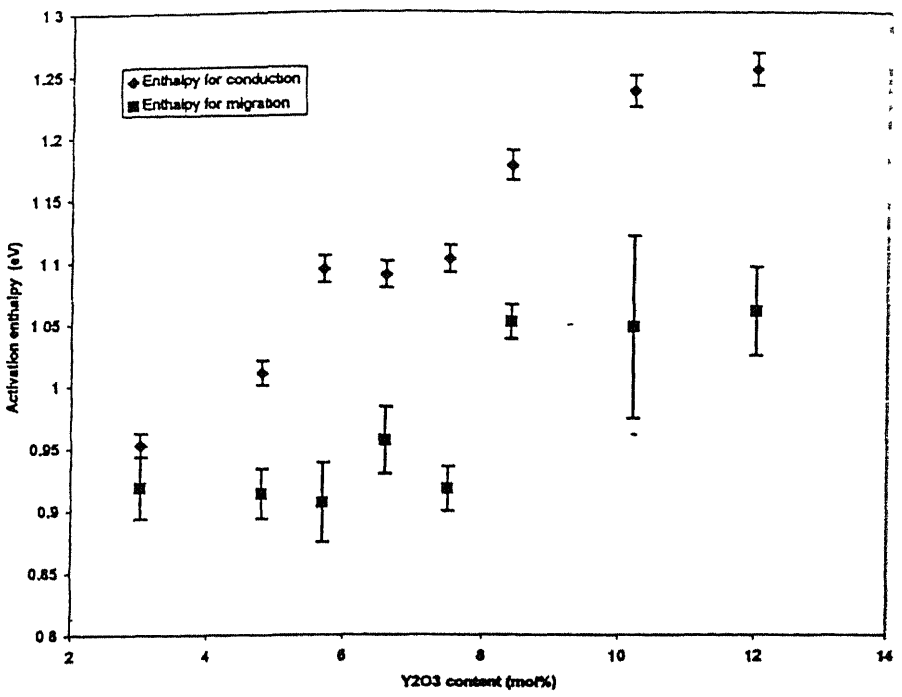

Fig. 1.22 Effect of yttria on activation enthalpies for conduction and migration [12]

The association enthalpy is in the range of 0 15-0 2 eV for fully stabilized zirconia. Henn et al used dielectric measurement to get a value of 0.29 eV for the association enthalpy in ZrO_2-Y_2O_3 In the CeO_2 fluorite materials, the binding energy for dopant cations with ionic radii similar to Ce^{4+} has been found to be 0 12 to 0 26eV [10].

As suggested by A. Pimenov [15], the frequency dependence of the intrinsic part of the conductivity is given by Universal Dielectric Response expression. But due to the influence of grain boundary relaxation, the frequency range of the applicability of the expression is very small Hence as an alternative way to represent the data $M^*(f) = 1/\varepsilon^*(f)$ is used to analyze the dielectric behavior of the ionic conductors [15] M vs logv plot (Fig 1 23) is sigmoidal for 4 mol% Y_20_3 doped ZrO_2 ceramics M" vs logv shows peak (Fig. 1 23) at ν_{max}, which represents the characteristics frequency

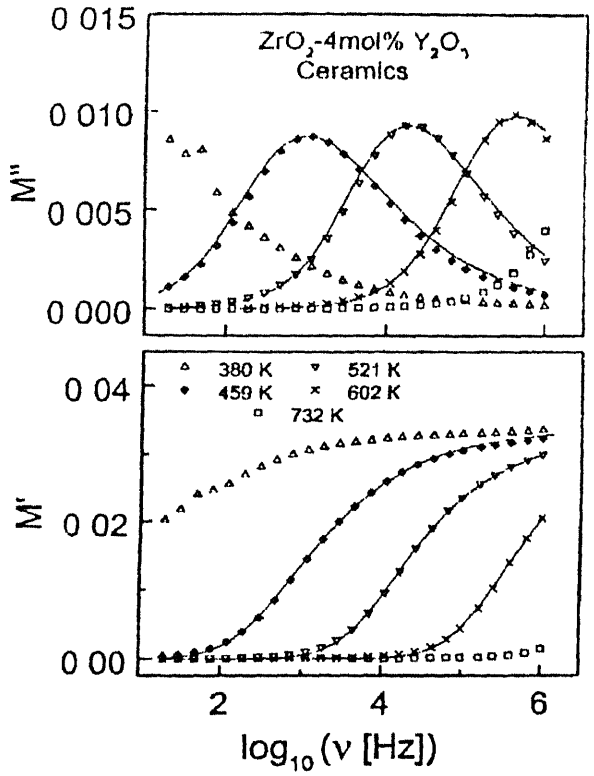

Fig.1.17. Frequency dependence of M' and M'' at different temperatures for 4 mole% Y_2O_3-ZrO_2 [15]

It is suggested that if necessary correction factor is incorporated, the modulus peak generally lies in the transition region from DC to AC conductivity Advantage of using modulus spectroscopy is that the grain boundary and the blocking electrode influence are effectively suppressed.

The concentration of the mobile ions can be estimated using the expression

$$\sigma_{DC} = (Nq^2d^2\gamma/6)\,(\omega_H/kT) \qquad (1\ 38)$$

Here N = carrier concentration, q = charge on the carrier, d = characteristic hopping distance, γ = geometrical factor The value of $d^2\gamma$ can be taken to be $0\ 35a^2$ when a = lattice parameter of the cubic zirconia is taken to be 0 516nm Typical values obtained for yttria doped zirconia by A.Pimenov et al [15] are tabulated in Table1 20

Table 1.10 Conductivity parameters for Y_2O_3-ZrO_2 [15]

Mole% of Y_2O_3	$\sigma_{DC}(\Omega cm)^{-1}$ (400°C)	ΔH_σ (eV)	N (cm^{-3})
4	$3.2x10^{-5}$	1.01	$9.4x10^{20}$
8	$7.3x10^{-5}$	1.05	$9x10^{20}$
10	$9.7x10^{-6}$	1.22	$1.3x10^{20}$
12	$1.6x10^{-5}$	1.22	$9x10^{20}$

1.5 ZIRCONIA THIN FILM

Zirconia films are used as insulating layers in multilayer electronic devices These films have high dielectric constant ~ 18[19] and greater impermeability to impurity diffusion ZrO_2 film has a potential use for storage capacitor in the dynamic random access memory Charge storage in anodic ZrO_2 films and oxygen sensor elements having thin layer of stabilized ZrO_2 sintered on a substrate are also in use[20,21] The zirconia films are synthesized by a variety of method Chemical vapor deposition using hydrolysis of β-diketone chelates such as $Zr(C_{11}H_{19}O_2)_4$, electron beam evaporation, plasma arc spraying and sol-gel process have been reported for the preparation of zirconia thin films In the present work we have attempted sol-gel process for the preparation of the zirconia –gadolinia film

1.5.1 SOL-GEL PROCESS

Sol-gel technology has been developed to prepare metal oxide fibers, monoliths, microspheres, thin films and fine powders etc. The sol-gel prepared films have large number of applications such as antireflection coatings, protective coatings, catalysts,

piezoelectric devices, wave-guides, and coating of optical lenses

The sol-gel processes offer the following advantage over the conventional methods

1) High purity of the products is obtained
2) Mixing takes place at the molecular level so that one can get molecular level homogeneity in the multicomponent materials
3) Lower processing temperature leads to low energy requirements
4) Thickness of the films can be controlled by modifying the sol concentration and varying the number of the coatings
5) Dopants can be easily introduced for desired electrical and physical properties

However it has some disadvantages

1) Long processing time
2) Residual fine pore after drying and annealing
3) Large shrinkage in films during heating and annealing, which cause crack formation in the film

Two type of sol-gel processing are generally used

a *Colloidal Processing*

Particles of size 1-1000 nm are used They form a gel network and subsequently sinter to yield a continuous film

b *Polymeric Processing*

Different metal alkoxides $M(OR)_x$ are used as precursors In the sol-gel synthesis, $M(OR)_x$ is mixed with water and appropriate solvent (usually an alcohol) A small amount of acid or base is added to catalyze the reaction To avoid or minimize self-

condensation, some metal salt like chloride, nitrate and acetate are used Alcohol, chloride, nitrate and acetate play an important role is determining the thickness and volume shrinkage During polymeric gel formation, hydrolysis and condensation reactions takes place simultaneously The reactions which lead to the formation of a gel from the sol are of two types a) *hydrolysis* and b) *condensation*

(1) **Hydrolysis Reaction:** By this, the alkoxy group is replaced by an –OH group

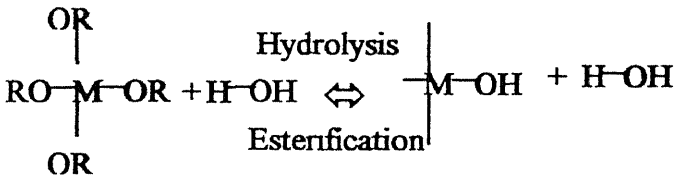

(2) **Condensation Mechanism:** The –OH group is eliminated and M-O-M linkages form.

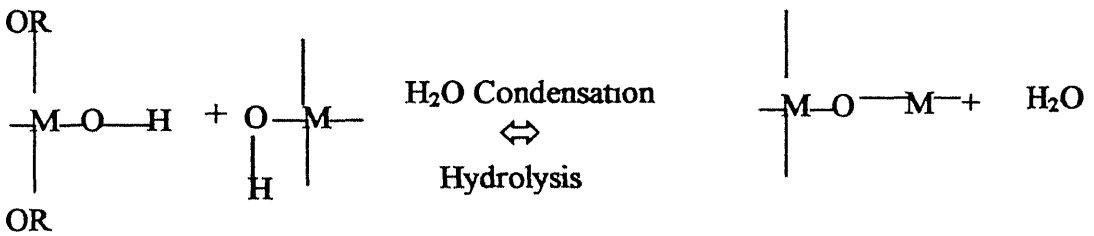

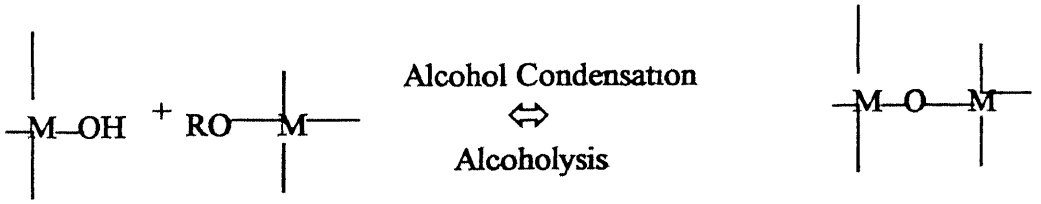

The sol is eventually transformed into a 3-d network by the elimination of water or some other group like alcohol This process is known as gelation The relative rate of both hydrolysis and condensation reactions depends on the experimental conditions Like solvent, water, alkoxide ratio etc water is a by-product of the condensation reaction Increasing the amount of water inhibits the condensation reaction.

1.5.2 SOL-GEL CHEMISTRY

For Zr-n-propoxide the main reactions are as shown below

$$Zr(OR)_4 + 4H_2O \rightarrow Zr(OH)_4 + 4ROH$$

$$Zr(OH)_4 \xrightarrow{\Delta} ZrO_2 + H_2O$$

Zirconium alkoxide form hydrous zirconium oxide like ZrO_2nH_2O or $ZrO(OH)_2nH_2O$ and/ or hydrated polymeric species having a number of Zr-O-Zr bridges. Hydrolytic polycondensation reactions of zirconium alkoxides result in the formation of Zr-O-Zr bridges based on a octrahedrally six coordinated zirconium [22]

1.5.3 SOL CHARACTERISTICS FOR THIN FILM FORMATION

The sol prepared should possess the following features for an good coating on the substrate

1 Adequate solubility of the initial compounds like materials, which dissolve in colloidal or polymeric state They should have a tendency towards crystallization on evaporation of the solvent.

2 Sufficiently small contact angles between the solution and the substrate to be coated to give good coating. Surface structure and cleanliness also affect the wettability

3 Adequate durability of the solution and constancy of the process

conditions

4 Transformability of deposited gel film into the solid homogenous oxide layer By drying and heating the film, high bonding strength to the substrate should develop On solidification the film should not crack or haze

1.5.4 COATING TECHNIQUES

Coating on the substrates can be obtained by using any one of the following processes·

1) *Dipping Process*

Substrates to be coated are immersed and withdrawn very carefully and slowly from the sol when it gets covered with a thin layer of the sol

2) *Lowering Process:*

The object is fixed and the liquid level is slowly lowered. Controlling rate of lowering controls the thickness of the film

3) *Spraying Process*

Suitable for non-optical coatings since it is very difficult to obtain homogenous films of sufficiently uniform thickness with this method. The solution to be coated is sprayed from stationary spray guns on to a preheated glass plate, which is moved across the jet s at a predetermined speed

4) *Spinning Process*

It is done by spreading the liquid film by spinning the wetted surfaces There are no marginal disturbances The sol is poured on a rotating, horizontal substrate, when it spreads on the surface completely and evenly Controlling the rotational speed can control the thickness.

2 EXPERIMENTAL PROCEDURE

2.1 SAMPLE PREPARATION

2.1.1 BULK SAMPLES

Samples of ZrO_2 containing 1.75,2 5,4,5,8 and 11 mol % Gd_2O_3 in the form of disks were available in the laboratory [23] Those were prepared by Santanu Bhattacharya by a coprecipitation method followed by calcinations and sintering.

2.1.2 THIN FILMS

Table2.1 Chemicals and Substrates:

Precursors	Source	Molecular wt.	Assay
Zirconium-IV-propoxide	Fluka Chemika	327.58	70% in propanol
Acetic acid	Thomas Baker	60 05	99.8%
Ethyl alcohol	Merck	46 07	99.8%
Gadolinia (Gd_2O_3)	Kemphasol	362 5	99.0%
Triple distilled water	Prepared in lab	18	
Nitric acid	S-D Fine Chemicals	63.01	69-71%

Substrates: Microscopic glass slides, Sapphire $\{\alpha - Al_2O_3(1\bar{1}20 orientation)\}$, Silicon and Platinum(1 cm× 1 cm)

2.1.2.2 SOL PREPARATION

Zirconia sols containing 1 75, 5 0, 8 0, 11 0 mole% gadolinia (Gd_2O_3) are prepared Concentrations and ratios of different chemicals are optimized to get a clear and transparent sol and a coating of sub-micron range

High mol% of ZrnP created a rough and thicker coating whereas a higher acetic acid content causes rapid gelling of the sol. Acetic acid is used to reduce the cracking tendency of the sol-gel film when it is drying

2 1 2 2 1 CALCULATIONS

The table2.2 gives the concentrations and optimized ratios of the constituents of the unstabilized sol

Table 2.2 Data for Concentrations of Various Constituents

Constituents	Concentration
Zirconium-n-Propoxide (ZrnP)	0 2 M/L
Acetic Acid ($\frac{Aceticacid}{ZrnP} = 3$)	0 6 M/L
Distilled Water ($\frac{H_2O}{ZrnP} = 1\ 8$)	0 36 M/L
Ethyl Alcohol	10L – volume of the rest of the constituents

Ethyl Alcohol is used as a solvent

To prepare 10 ml of sol, following amounts of the constituents are required

1) *Zirconium-n- Propoxide*

Molecular weight = 327.57

Density = 1 05 gm/cc

Volume of 1 mole of ZrnP = $\frac{327\ 57}{1\ 05}$

= 311 95 cc

To prepare 1000ml of sol, ZrnP needed (concentration 0 2 M/l) = 62 39 ml

To prepare 10ml of sol, ZrnP needed = 0 6239ml

≈ 0 624 ml

2) *Acetic Acid·*

Molecular weight = 60 05

Density = 1 431 gm/cc

Volume of 0 6 M Acetic Acid = 25.178 cc

To prepare 1000ml of sol, 25 178 ml of acetic acid is required.

So, to prepare 10ml of sol, 0 2518ml of acetic acid is required.

3) *Distilled Water:*

Molecular Weight = 18

Density = 1gm/cc

Volume of (1 8×0 2) mole or 0.36moles of water = $\frac{0\ 36\times18}{1}$ = 6 48 ml

To prepare1000 ml of sol 6 48 ml of water is required

To prepare 10ml of sol 0 0648 ≈ 0.065ml of water is required

4) *Ethyl Alcohol·*

Volume of the solvent used in 10ml sol is {volume of sol – volume of (ZrnP + acetic acid + water)} = {10 – (0 624 + 0 252 + 0 065)} ml

= 9 059 ml

Gadolinia (Gd_2O_3) in the form of gadolinium nitrate is added to the Zirconia sol to stabilize the high temperature tetragonal and cubic phases of Zirconia Gadolinium nitrate is soluble in ethyl alcohol, which is also used as a common medium for alkoxide and water

Gadolinia and Nitric acid·

Molecular Weight of Gd_2O_3 = 362 5

Molecular weight of Nitric Acid = 63

Density of HNO_3 = 1 4gm/c c

From the chemical equation,

$$Gd_2O_3 + 6\ HNO_3 = 2\ Gd(NO_3)_3 + 3\ H_2O$$

1 mole of Gd_2O_3 requires 6 moles of HNO_3 acid and 3 moles of H_2O are also produced.

Concentration of zirconia in Zirconium –n-propoxide is 0 2M/L We have to prepare $Gd_2O_3 - ZrO_2$ containing x mole % of Gadolinia So the rest i e (100-x) mole % is zirconia Thus, the weight of the gadolinia powder required for preparing 1L of zirconia sol is given by

$$W = \frac{x}{(100-x)} \times 0\ 2 \times M \qquad (2\ 1)$$

Where M = Mol Wt Of Gadolinia

Now W/M moles of Gd_2O_3 require (6 W/M) moles of nitric acid and (3 W/M) moles of water for preparing 1L of the zirconia sol

So, the volume of HNO_3 required is

$$V_{acid} = \frac{6W/M}{Density of HNO3}\ L \qquad (2\ 2)$$

And the volume of water required is

$$V_{water} = \frac{3W \quad M}{Density of H_2O} L \qquad (2.3)$$

For preparing 1.75 mol% Gd_2O_3 doped Zirconia sol of 0.2 M/l concentration, moles of Gd_2O_3 required $= \frac{1.75}{98.25} \times 0.2 = 3.56 \times 10^{-3} M$

(Since 100 mole % of ZrO_2 alloy contains 1.75 mole% of the additive Gd_2O_3 and rest i.e 98.25 mole% of ZrO_2)

Weight of Gd_2O_3 required = $(3.56 \times 10^{-3} \times 362.5)$ gm = 1.291 gm

To prepare 100ml of Zirconia sol 1.291 gm of Gd_2O_3 is required

To prepare 10 ml of sol, 0.129 gm ofGd_2O_3 is required

Performing similar calculations for 5, 8 and 11 mol% Gd_2O_3 , amount of Gd_2O_3 powder required for 10 ml of sol is calculated. Volumes of Nitric Acid and water are also calculated. The values are tabulated below in table 2.4

Table 2.3: Volume of Nitric Acid and Water Required

Mol% of Gd_2O_3	Wt in 10ml sol (gm) (W/100)	Vol of HNO_3 (ml) (V_{acid}/100)	Vol of H_2O (ml) (V_{water}/100)
1.75	0.129	0.016	0.0064
5.0	0.382	0.047	0.019
8.0	0.611	0.078	0.03
11.0	0.839	0.11	0.04

2.1.2.2.2 APPARATUS CLEANING

Glassware used like pipettes, beakers, measuring cylinder, teflon coated magnetic beads are thoroughly cleaned with dilute nitric acid, then with a glassware cleaning

solution (Thomaklin), finally with distilled water For faster drying a quick rinsing of the glassware and bead with propanol is done before keeping in oven at $50^{\pi}C$.

2 1 2 2 3 PREPARATION

All the glassware, bead, aluminium foil are transferred inside the glove box The relative humidity level inside was maintained at ≤ 35% by keeping silica gel (heated to 100°C) in the glove-box to prevent the reaction of the alkoxide with the moisture of the air. Initially the measuring cylinder is rinsed with little ethyl alcohol and the washing is discarded in a wash beaker Approximately 9 059ml of ethyl alcohol is kept aside in the measuring cylinder Then with the help of a pipette about 0.25 ml of acetic acid is transferred to a dry 25 ml beaker (containing the bead) Immediately half of the alcohol is added to the beaker The pipette is rinsed with some more ethanol and the washings are added to the contents of the beaker.

Then 0 62 ml of Zr-n-P is pipetted out and poured into the beaker Rinsing of the pipette is done in the same way with some ethanol The remaining ethanol is kept in the measuring cylinder

The beaker is covered with an aluminum foil to avoid moisture absorption from the atmosphere The solution is stirred for 2 hrs on the magnetic stirrer A clear transparent sol is obtained

In the mean time, gadolinia powder is weighed and dissolved in specified volume of HNO_3 and triple distilled water outside the glove-box After 2hrs of stirring the sol, the prepared gadolinium nitrate solution is taken inside the glove box and mixed with the remaining ethyl alcohol The solution is added to the sol and then kept stirred for 15min Finally a clear transparent gadolinia stabilized zirconia sol is obtained Such zirconia sols

are prepared for 1 75, 5, 8 and 11 mol% gadolinia composition within the glove box. All the beakers containing the sols are labeled and refrigerated to reduce gelling tendency

2.1.2.3 PREPARING THE SUBSTRATES

Platinum, Sapphire and Silicon substrates are used

2 1 2 3 1 POLISHING

The Pt and sapphire substrates are polished before cleaning them The Pt substrates were successively polished with 2/0, 4/0 emery paper followed by 0 25μm diamond paste on a cloth to give a mirror like finish

The sapphire substrates are polished with 0 3 μ m alumina paste on a glass plate for about 15 min, followed by polishing on glass plate with 0 05 μ m alumina powder

2 1 2 3 2 CLEANING

The polished substrates are subjected to cleaning

Platinum and Sapphire substrates are cleaned using the following steps.

i) Boiled in soap solution for 5 mins

ii) Ultrasonicated 3 times in distilled water for 5 mins each time

iii) Ultrasonicated in acetone for 5 mins

iv) Ultrasonicated in trichloroethylene for 5 mins

v) Ultrasonicated in ethyl alcohol for 5 mins

vi) Ultrasonicated in ethyl alcohol for 5 mins

vii) Dried in oven around 50 ° C

Cleaning silicon substrate created red and green colors on it with variable thickness This discoloring made the substrates unsuitable for thin film preparation and electrical characterization

After cleaning and polishing the substrates are stored in clean sample boxes They are handled with forceps to prevent the formation of fingerprints on them

2.1 2.4 THIN FILM DEPOSITION

The substrates are coated by spin coating technique Thickness of the coatings are increased by applying multiple coatings with intermediate drying in the oven at 80 ° C for about 5 mins Viscosity of the sol, sol concentration and the speed of the spinner are the important factors controlling the thickness of the film. The speed of the centrifuge is optimized at 3000rpm. Higher speed of about 5000rpm gives very thin coating whereas lower speed of about 2000rpm and also higher sol concentration of about 0 5M/L gives a thicker and rough coating.

For electrical characterization of the thin film, there should be a bottom electrode and a top electrode and in between the insulating thin film. Pt is itself conducting whereas for silicon and sapphire, which are non-conducting, Au-Pd bottom electrode is deposited on their surface using sputtering technique A thin layer of Au-Pd is deposited on the clean surface of sapphire and on silicon substrate by using HUMMER (6-A) Sputtering System (Anatech Ltd) The settings used are discussed in section 2 3 1. For better adherence, the substrate with the Au-Pd film is heat treated at 400 ° C for 5 mins. The film retained its conductivity after the heat treatment

Spin coating with the stabilized ZrO_2 sol is attempted on the Pt and sapphire and silicon substrates coated with Au-Pd layer Before coating the substrate, a little area of it is covered with a teflon tape carefully with the help of a forcep Thus a step is formed between the coated and uncoated portion so that film thickness can be measured using the surface profilometer

The substrate is fixed on the top of the spinner of the centrifuge and rotational speed is kept constant at 3000rpm Lower speed of 2200rpm gives a rougher and thicker coating as seen from its thickness profile This kind of film is more prone to cracking during the heat treatment At a higher speed of 4000rpm the film thins out and is barely discernible

Single drop of sol is added to the substrate while it is spinning at 3000rpm and spun for about a minute The coat is dried for 5 minutes at about 80°C. About 6 to 8 coatings are applied and after each coating the substrate is seen under optical microscope (100 magnification) to check the microstructure and the presence of cracks.

Initially the glass slides are used for optimizing the sol concentration, number of coatings, speed of rotation and heat treatment by studying the thickness of the deposited film on it Surface profilometer is used for measuring the thickness

At first the sol concentration was kept at 0 5M/L A 0.5 mole% stabilized sol and 2 coatings are used at a speed of 2200 rpm on the glass slide with heat treatment at 350°C for 1hr The average thickness of the film is 5 μm and it is very rough as seen in Fig 2 1(a) So the sol concentration is reduced to 0 2M/L.

With 0 2M/L concentration, few glass slides are coated with the sol by varying different conditions Then the thickness is measured using the Surface profilometer. The results are tabulated in Table 2 5

Table 2.5: Data for Spin Coating on Glass Substrates

Serial No	No. of Coatings	Rotational Speed	Heat Treatment	Thickness (μm)	Nature of the Film
1	2	2200	350°C for 1hr	0 25 to 0.5	Rough
2	2	3000	450°C for 1hr	0 1 to 0 2	Less rough
3	2	2200	450°C for 1hr	0 2 to 0 4	Rougher than 2
4	1	3000	450°C for 1hr	0 05	Thin and rougher than 1
5	1	2200	450°C for 1hr	0 1	Rougher than 4

The conditions given in the serial no 2 of the table is seen to produce a better thin film than the rest On the clean and polished sapphire substrates, 2 coats of the sol (5 mole% stabilizer, 0 2M/L concentration) are applied with a spinning speed of 3000rpm and the film is heat treated at 450°C for 1hr From the Fig 2 1(b) it is seen that the film thickness is 0 1 μm but on checking the film with multimeter, it is seen the film shows a very low resistance The conducting film cannot be used for electrical characterization, as the film has to be capacitive in nature sandwiched between the electrodes

In a view of getting a non-conducting film the number of coatings are increased 6 coatings of 1 75 mole% Gd_2O_3 (0 2M/L concentration) are applied to a sapphire with a rotational speed of 3000 rpm, and then heat treated at 700°C for 15 min. The film is seen to be very rough and thick Now the number of coatings is reduced to 4 and heat treatment temperature of 500°C for 1hr is used Films of 8 and 11 mole% Gd_2O_3 additives are prepared in this way and their average thickness are 0.5μm and 1μm (with some 4μm features) respectively as seen from the Figs 2.1(c), 2 1(d). Even with 6 and 4 coatings the

पुरुषोत्तम काणीनाथ केलकर पुस्तकालय

film is conducting The reduction of heat treatment temperature to 500°C did not show any better results XRD of the 8 mole% Gd_2O_3 containing thin film showed that cubic peaks are just developing (Fig 2 1f) There is little chance of getting crystalline film lower than this temperature

As an alternative the silicon wafers are used But after the heat treatment of the sol on it some patterned red and green areas are seen on it When studied under the profilometer, a change in thickness across red to green area is noticed Fig 2.1 (e), this makes it unsuitable for conductivity measurement

Finally Pt substrates are used keeping the conditions similar to the sapphire substrates 4 coats of the sol (0 2M/L) are applied at a rotational speed of 3000 rpm The film is then non-conducting After the heat treatment at 500°C the film showed very less resistance Thickness of the film is not measured, as it cannot be used for electrical characterization.

The Pt substrate showed very high resistance after initial heat treatments during the spin coatings But when subjected to heat treatment for the crystallization of the film to a temperature as low as 400°C for 15 mins, the film became conducting

Microwave treatment of the film after spin coating and application of dip coating also did not help The probable reason could be proper wetting of the substrate was not taking place So at some places the film was continuous and in others it is discontinuous The electrical characterization of the film therefore could not be done

2.2 CHARACTERISTICS OF THE BULK SAMPLES

2.2.1 DENSITY

The density of the samples was determined by Archimedes method using xylene as the immersion medium The relative density of the samples as a function of Gd_2O_3 is shown in fig (2.2) The relative density increases with increasing Gd_2O_3 content reaches a maximum at 4 mole% and then falls off again The density of samples upto 5mole% Gd_2O_3 are all $\geq$ 90% of the theoretical

2.2.2 PHASES

XRD date is used for determining the relative amounts of the phases present The relative amounts of different phases in the sintered samples vs Gd_2O_3 content is shown in fig (2 3) Even with 1 75 mole % Gd_2O_3 only ~ 12 vol % monoclinic phase is present The 2 5 and 4 mole % compositions are single-phase tetragonal material Higher compositions i e 5 and 8 mole % Gd_2O_3 samples show the presence of t and c phases But the amount of c phase in 5 mole % sample is only about 9 vol % but it increases to about 80 vol% for 8 mole % Gd_2O_3 samples 9 mole% samples were prepared to check the presence of different phases, it is seen it contains little t phase and rest is cubic.

2.2.3 MICROSTRUCTURE

Figs (2.4) show the microstructure of the polished and sputtered surface of sintered ZrO_2-Gd_2O_3 samples Except for 8 mole% Gd_2O_3 all the grains are rounded and have extremely fine grain size (0 1-0 15μm) The average grain size does not match above 4 mol% Gd_2O_3 as seen in table 2 2

Table 2.3: Variation of Grain Size and Relative Density with Composition

Mole percent of Gd_2O_3	Average Grain Size (μm)	Relative Density
1 75	0.14	0 9
2 5	0.13	0 93
4	0 13	0 96
5	0 17 0.35	0 92
8	0 67 0 2	0 88

For compositions 1.75 and 2 5 mole% there is a bimodal grain size distribution Almost uniform grain size is observed for 4 mole% samples At a higher mole% of 8, majority of the grains are large (0 6μm) although for this composition, smaller grains are found at the junction of 3-4 grains These large grains unlike the small grains are faceted i e they have sharp corners they also may contain intergranular porosity Electrical measurements were done on Zirconia samples containing 1 75, 2 5, 4, 5, 8, 9 and 11 mol % gadolinia

2.3 ELECTRICAL CHARACTERIZATION

This can be divided into the following heads

1) Polishing and electrode deposition
2) Sample holder
3) Electrical measurements
4) Data analysis

2.3.1 POLISHING AND ELECTRODE DEPOSITION

For good results smooth and polished samples are necessary The samples are ground on 400 grit SiC slurry on a glass plate for 10 minutes followed by 600 grit and 1000 grit SiC slurry for 10 minutes each After that the samples are polished using 1μm alumina paste for 10 minutes followed by 0 3 μm alumina paste to a mirror finish Finally the samples are polished with 0 25 μm diamond paste on a diamond microcloth. XRD diffractogram of the samples are taken at this point if required.

The polished samples are then coated in HUMMER VIA Sputter Coater (Anatech Ltd) with Gold –Palladium target Three to four samples at a time are mounted on the sample holders and are kept inside the chamber The chamber is flushed for two three times with Argon gas from cylinder Following parameters are optimized for a good conducting layer

Vacuum in the sputtering chamber = 80 millitorr

Plasma discharge current = 10 mA

Voltage control setting = 3 4

Time of sputtering = 10 -15 mins

Violet colored gas plasma is formed as the gas atoms are ionized by the electric field. The ionized atoms hit the Au-Pd target and the metal atoms are dislodged and adhere to the specimen surface to form a thin conducting layer Both the surfaces of the samples are coated in this manner. The specimens are now ready for impedance analysis.

2.3.2 SAMPLE HOLDER

A sample holder is fabricated for high temperature electrical measurements as shown in Fig (2 5) It contains four identical lava discs of diameter 27 mm and thickness

10 mm and a nylon block of diameter 22 mm and thickness 51 mm Each of these discs and nylon block has a hole of diameter 2 mm at the center and four other holes situated symmetrically at the periphery The lava discs are used to support the different parts of the sample holder at least upto 500°C One quartz tube of outer diameter 12 mm, inner diameter 10 mm and length 220 mm is placed between the two inner lava discs as shown in the figure A spring of diameter 12 mm and length 30 mm is placed between the two lava discs near the nylon block. The lava discs are recessed to a depth of 1 mm in a circle of diameter 14 mm to accommodate the quartz tube and the spring After machining the lava discs, they are heated slowly to 700°C and soaked at the temperature for 5 hrs to harden the pyrophillite A pair of stainless steel rods of diameter 2.9 mm and length 400 mm is passed through the two diametrically opposite holes of the blocks to provide support to the sample holder For electrical contacts, two platinum discs of diameter 120 mm and thickness 1mm are brazed to silver wires to provide high temperature contacts One of the wires passes through the central hole within the quartz tube and the other passes through one of the peripheral holes The length of the wires is 400 mm each and their ends are connected to the Impedance Analyzer by means of crocodile clips The sample to be studied is placed between the two platinum discs supported by the two lava discs The spring and the quartz tube are used for providing enough pressure and to ensure proper contact between the sample and the electrodes Through one of the peripheral holes, a chromel–alumel thermocouple is passed for sensing the temperature of the sample The thermocouple is connected to HIL 2301 digital panelmeter The millivolt readings are converted to temperature readings according to the standard charts. The sensitivity of the panelmeter is ± 0 05 mV

2.3.3 ELECTRICAL MEASUREMENTS

A block diagram of the experimental set-up is shown in fig (2.6) Various parts of the set-up are described below

2.3.3.1 FURNACE AND TEMPERATURE CONTROLLER:

A horizontal furnace with a mullite tube muffle of internal diameter 50 mm and length 59 mm is used It is an electrical resistance furnace with a Kanthal wire wound over the mullite tube The space between the tube and the outermost aluminum body is filed up by insulating glass wool. The resistance of the heating element is nearly 32Ω.

The length of the sample holder was so adjusted that when the sample is in the center of the furnace the spring and the nylon block is just in the outer edge of the furnace

A S-type (Platinum / Platinum-10% Rhodium) thermocouple is placed in the center of the furnace from the other end. It is then connected to the Microprocessor based Programmable Temperature Controller (Indotherm –161, MPC-500) It consists of a temperature programmer and a power controller The temperature control method is of P I D type The accuracy of the controller is ± 0 5°C

2.3.3.2 IMPEDANCE ANALYZER

A HP 4192A LF fully automatic, high performance analyzer is used with a HP 1607A test fixture for a wide range of complex impedance measurement The inbuilt frequency synthesizer is used to generate frequency in the range 5Hz-13MHz with 1 mHz resolution The two display modes 'A' and 'B' can be selected to measure quantities of interest Table2 3

Table2.5: The Displays 'A' and 'B' of the Impedance Analyzer:

Display A Function	Display B Function
|Z| Absolute value of Impedance	θ(deg/rad) Phase angle
|Y| Absolute value of Admittance	
R Resistance	X Reactance
G Conductance	B Susceptance
L Inductance	Q Quality Factor
	D Dissipation Factor
C Capacitance	R Resistance
	G Conductance

The equivalent circuit modes are auto, series and parallel

2.3.4 IMPEDANCE MEASUREMENTS

The coated sample is placed between the platinum electrodes of the sample holder and the silver wire ends are connected to the bridge of the Impedance Analyzer The temperature of the furnace is increased with the help of programmable power controller. The temperature is raised from room temperature to 150°C at the rate of 5°C/min, when the first measurement is generally taken The impedance value Z and phase angle θ are noted by varying the frequency f between 5Hz to 13MHz. the temperature is fixed at this temperature for about 15 mins The temperature takes sometime to stabilize at this soaking period and the readings are noted down as the panelmeter reading becomes more or less stable After this the controller is reprogrammed to ramp at 5°C/min to the next temperature and stay there The measurements are repeated This is continued upto a temperature of 450 °C An ammeter of rating 0 to 6 amps is connected to the circuit. For dielectric measurements the displays can be set to 'C' and 'D' which gives the values of the capacitance and dielectric loss, but they can be calculated using only Z and θ values.

2.3.5 DATA ANALYSIS

2.3.5.1 CONDUCTIVITY AND ACTIVATION ENTHALPY CALCULATION

At a particular temperature the values of f, Z and θ are noted from the impedance analyzer Cole-cole plot (Zsinθ vs Zcosθ) is plotted using the Origin Software Using the non-linear square fitting program, 2 semicircles are fitted, one for the grain and the other for the grain boundary effect, in the impedance plane The semicircles are depressed in nature The values of the center and the radius are obtained from the program The diameter of the semicircles gives the grain and the grain boundary resistances R_g and R_{gb} respectively The DC conductivity in each case is obtained from the relation

$$\sigma_{DC} = (L/A)(1/R_{DC}) \qquad (2\ 4)$$

where L = thickness of the sample and A = area of the electroded surface

Log ($\sigma_{DC}T$) vs 1/T is plotted in each case The slope of the linear fit gave the value of the activation enthalpy (ΔH_σ) for conductivity

To find out the migration enthalpy the following technique is used As suggested by Almond and West,

$$\sigma_{AC} = \sigma_{DC}[1+(\omega/\omega_p)^n] \qquad (2\ 5)$$

where σ_{AC} = AC conductivity,ω_p = characteristic frequency at which the dielectric loss is maximum (hopping frequency), n = Jonscher's universal exponent (varying between 0 5 to 1)

Now σ_{AC} is calculated using the following expression

$$\sigma^* = (L/A)\ (\cos\theta/Z^*)$$

$$= (L/A)[1/(Z'-jZ'')]$$

$$= (L/A)\ [(Z' -jZ'')/Z^2]$$

$$= (L/A)\ (\cos\theta/Z_o - i\sin\theta/Z_o) \qquad (2\ 6)$$

The real part of the complex conductivity gives the value of AC conductivity as

$$\sigma_{AC} = (L/A)(\cos\theta/Z) \qquad (2\ 7)$$

putting the value of σ_{AC} and σ_{DC} to equation A, we get

$(L/A)(\cos\theta/Z) = (L/A)(L/R_{DC}[1+(2\pi f/2\pi fp)^n])$

Taking log on both the sides, we get

$$\log[R_{DC}(\cos\theta/Z)-1] = n\log f - n\log f_p \qquad (2\ 8)$$

Knowing the value of R_{DC}, $\cos\theta$, Z and f at each temperature, n and f_p can be obtained by plotting log $[R_{DC}(\cos\theta/Z-1]$ vs logf. The slope of the fit corresponds to the n value and the intercept of the when divided by n gives the $\log f_p$ value. Generally n varies between 0 5 and 1 Then $\log f_p$ is plotted against the inverse of the corresponding temperature. From the slope of the linear fit, migration activation enthalpy (ΔH_m) is calculated. The association enthalpy (ΔH_a) is obtained from the difference between ΔH_σ and ΔH_m.

2.3.5.2 MODULUS SPECTROSCOPY

The dielectric constant ε^* is given by the equation

$$\varepsilon^* = Y(1/j\omega C_o) \qquad (2.9)$$

where ω= frequency of the applied signal, C_o = vacuum / air capacitance, Y^*= complex admittance

$$\text{Now} \quad \varepsilon^* = \varepsilon' - j\varepsilon''$$

$$= 1/(Z\ j\omega C_o)$$

$$= 1/(Z' - jZ'')j\omega C_o$$

$$= 1/(Z'' + jZ')\omega C_o$$

$$= (Z'' - jZ')/(Z''^2 + Z'^2)\omega C_o$$

$$= (Z'' - jZ')/Z_o^2\omega C_o \qquad (2\ 10)$$

Equating the real and the imaginary parts

$$\varepsilon' = Z_0 \sin\theta / Z_0^2 \omega C_o$$

$$= \sin\theta / Z_0 \omega C_o \qquad (2\ 11)$$

$$\varepsilon'' = Z_0 \cos\theta / Z_0^2 \omega C_o$$

$$= \cos\theta / Z_0 \omega C_o \qquad (2\ 12)$$

M* is the reciprocal of ε^*, so

$$M^* = 1/\varepsilon^*$$

$$= Z^* j\omega C_o$$

$$. M' + jM'' = (Z' - jZ'')j\omega C_o \qquad (2\ 13)$$

Equating the real and the imaginary parts

$$M' = Z''\omega C_o$$

$$= Z \sin\theta 2\pi f C_o$$

$$M'' = Z'\omega C_o$$

$$= Z \cos\theta 2\pi f C_o \qquad (2\ 14)$$

Under an AC field, dispersion or dielectric relaxation is observed due to different polarization mechanisms like electronic, ionic, dipolar and space charge polarization. Each relaxation mechanism is characterized by a relaxation time given by

$$\tau_r = 2\pi/\omega_r$$

where ω_r = relaxation frequency

The plot of M' and M'' vs log ($\omega/2\pi$) are known as Modulus Spectra. Sigmoidal fit is applied to M' vs log ($\omega/2\pi$) and Lorentzian fit is applied to M'' vs log ($\omega/2\pi$). Frequency

dependence of the real part of conductivity (σ_{AC}) and the real part of permittivity (ε') is also studied for all the compositions

2.3.5.3 ESTIMATION OF CARRIER CONCENTRATION

For all compositions the carrier concentration N can be calculated at a particular temperature using the formula

$$\sigma_{DC} = (Nq^2d^2\gamma/6)(\omega_R/kT) \qquad (2\ 15)$$

where q = charge

d and ω_R = characteristic hopping distance and frequency

γ = geometrical factor

$d^2\gamma = 0\ 35a^2$ (a = 0 516 nm for ZrO_2-Gd_2O_3 system)

Knowing the values of σ_{DC} and ω_R at a particular composition N can be calculated as $N = (6\sigma_{DC}/q^2d^2\gamma)\ (kT/\omega_R)$

2.4 X-RAY DIFFRACTION ANALYSIS

X-ray diffraction of all the bulk samples is carried out to determine the phases in different samples X-ray Diffractometer (Rich Seifert Iso-Debyeflex 2002, Germany) is used with the CuK_α radiation (λ = 1 5405 A°) The following operating parameters have been used

Characteristic	Values
Accelerating Voltage	30KV
Accelerating Current	20mA
Scanning Speed	3°/min in 2θ
Chart Speed	30 mm/min
Time Count	10 sec
Count Per Min (CPM)	5K

The value of interplanar spacing (d) is used to calculate the index of an X-ray line using the Bragg's relation

$$n\lambda = 2d \sin\theta \qquad (2\ 16)$$

where θ = Bragg's angle

n = order of diffraction

λ = wavelength of X-ray (in this case 1 54A°)

All the XRD patterns are recorded at room temperature

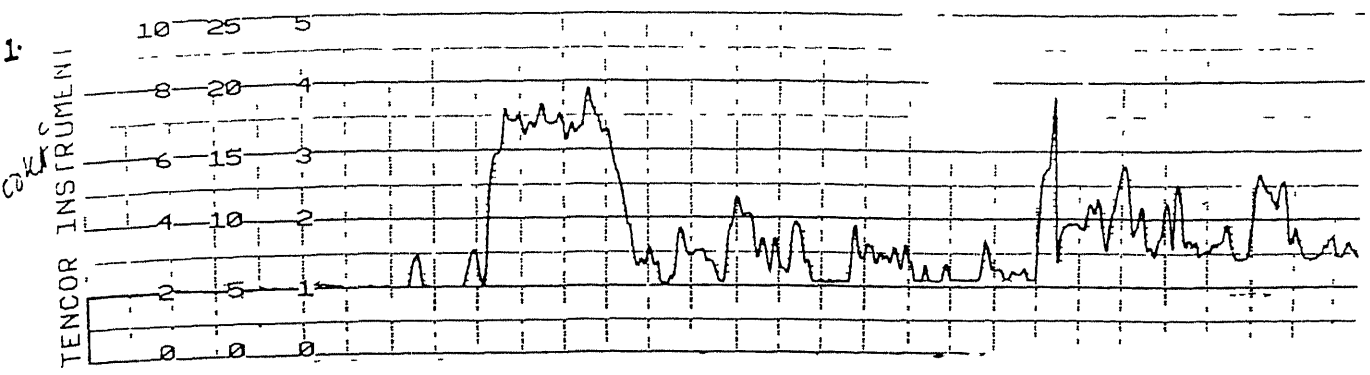

Fig. 2.1a. Thickness profile of ZrO_2-5Gd_2O_3 (2 coatings, 350°C for 1 hr.) thin film deposited on a glass substrate. Sol of molar conc. 0.5M/l and rotational speed of 2200rpm is used.

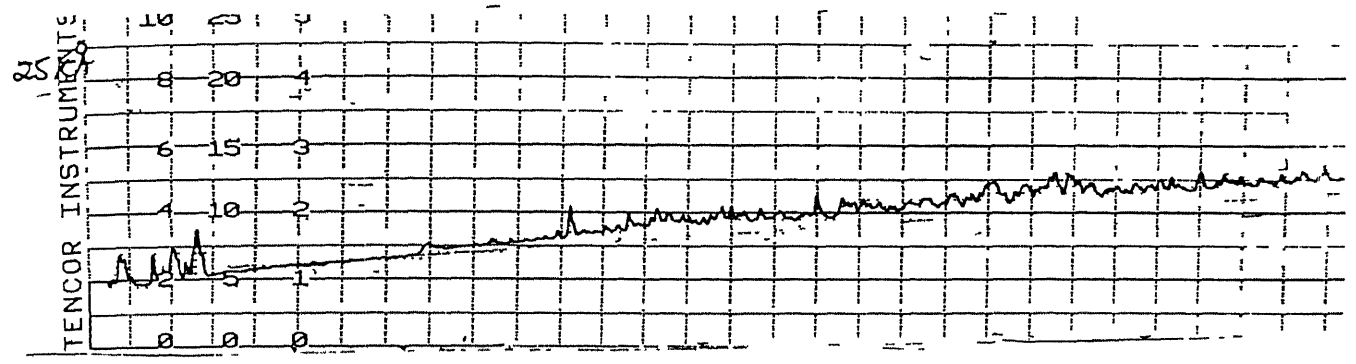

Fig. 2.1b. Thickness profile of ZrO_2-5Gd_2O_3 (2 coatings, 450°C for 1 hr.) thin film deposited on a sapphire. Sol of molar conc. 0.2M/l and rotational speed of 3000rpm is used.

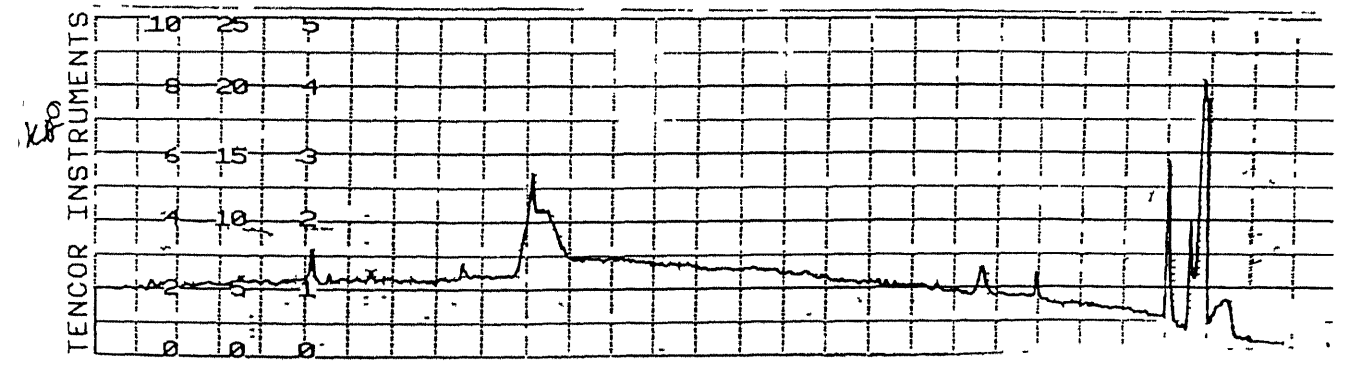

Fig. 2.1c. Thickness profile of ZrO_2-8Gd_2O_3 (4 coatings, 500°C for 1 hr.) thin film deposited on a sapphire. Sol of molar conc. 0.2M/l and rotational speed of 3000rpm

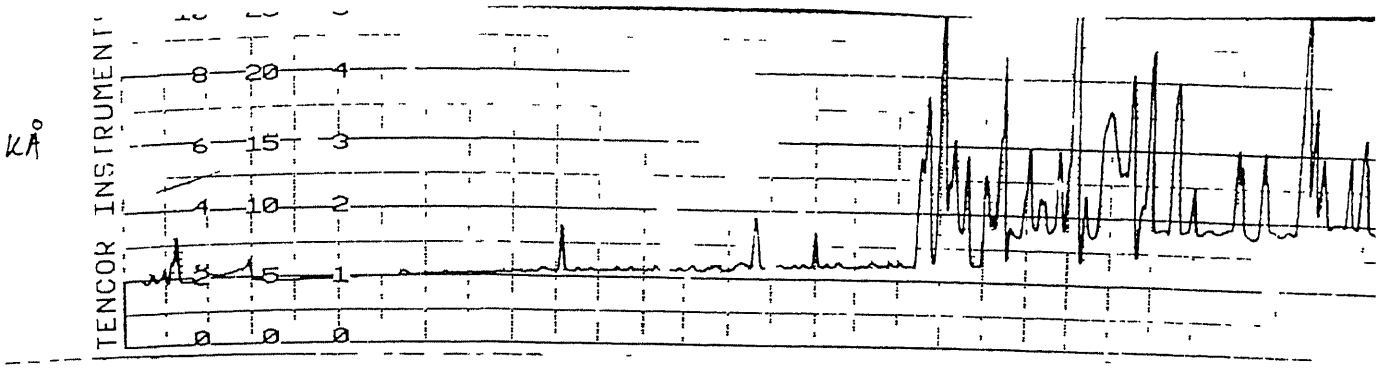

Fig. 2.1d. Thickness profile of ZrO_2-11Gd_2O_3 (4 coatings, 500°C for 1 hr.) thin film deposited on a sapphire. Sol of molar conc. 0.2M/l and rotational speed of 3000rpm is used

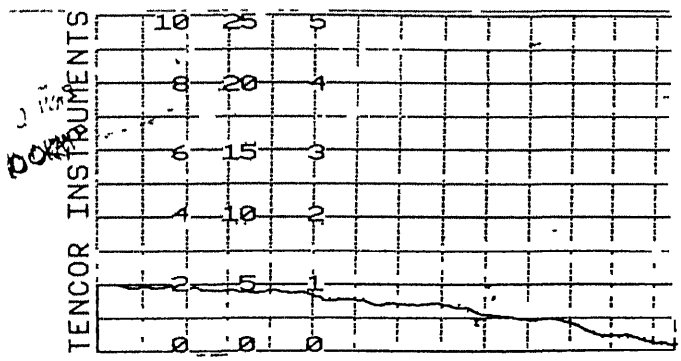

Fig. 2.1e. Thickness profile of ZrO_2-1.75Gd_2O_3 (4 coatings, 500°C for 1 hr.) thin film deposited on a silicon. Sol of molar conc. 0.2M/l and rotational speed of 3000rpm is used.

Fig. 2.1(f) XRD plot of 8 mole% zirconia- gadolinia thin film on sapphire substrate

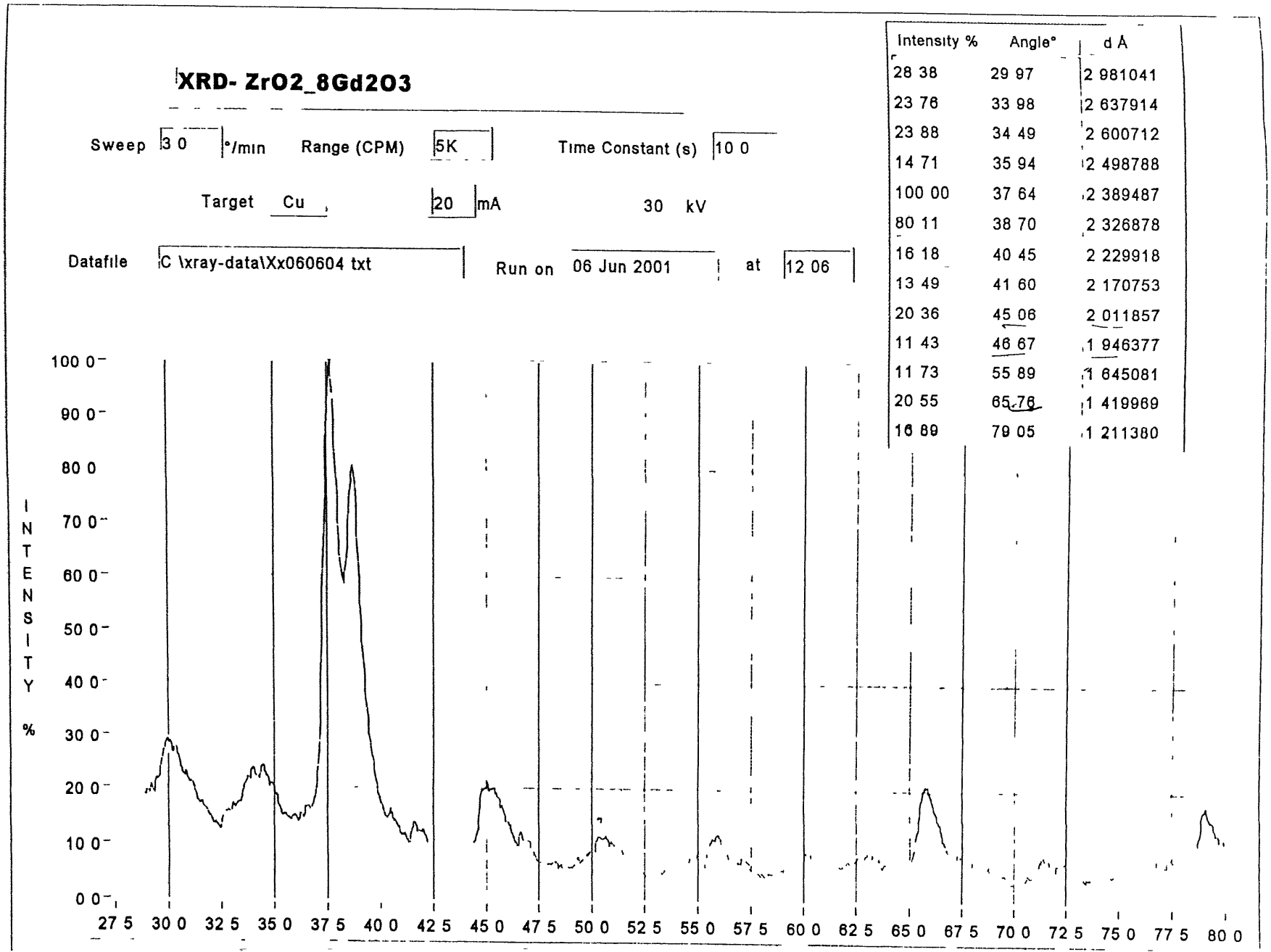

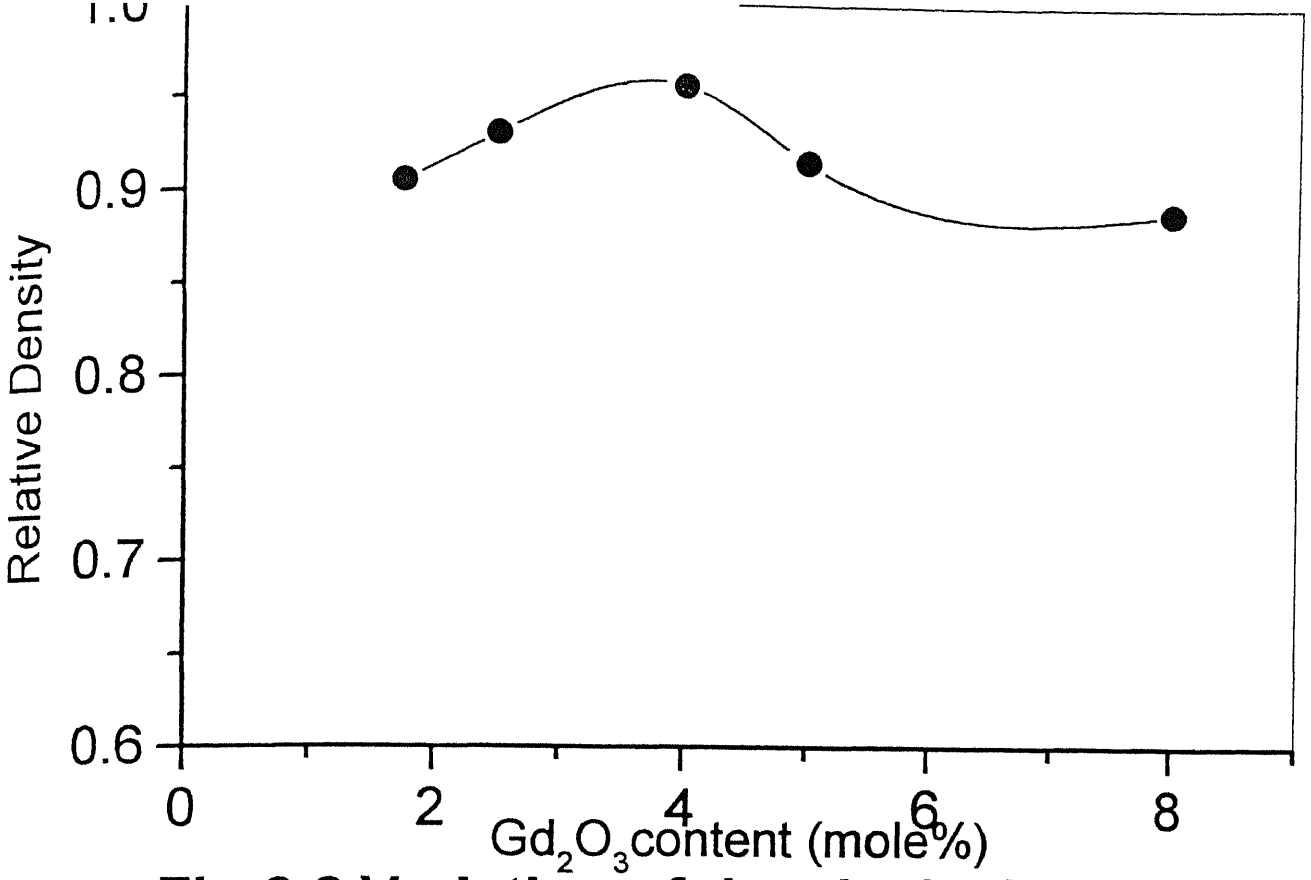

Fig.2.2 Variation of density in Gd_2O_3-ZrO_2 samples at different mole% of Gd_2O_3

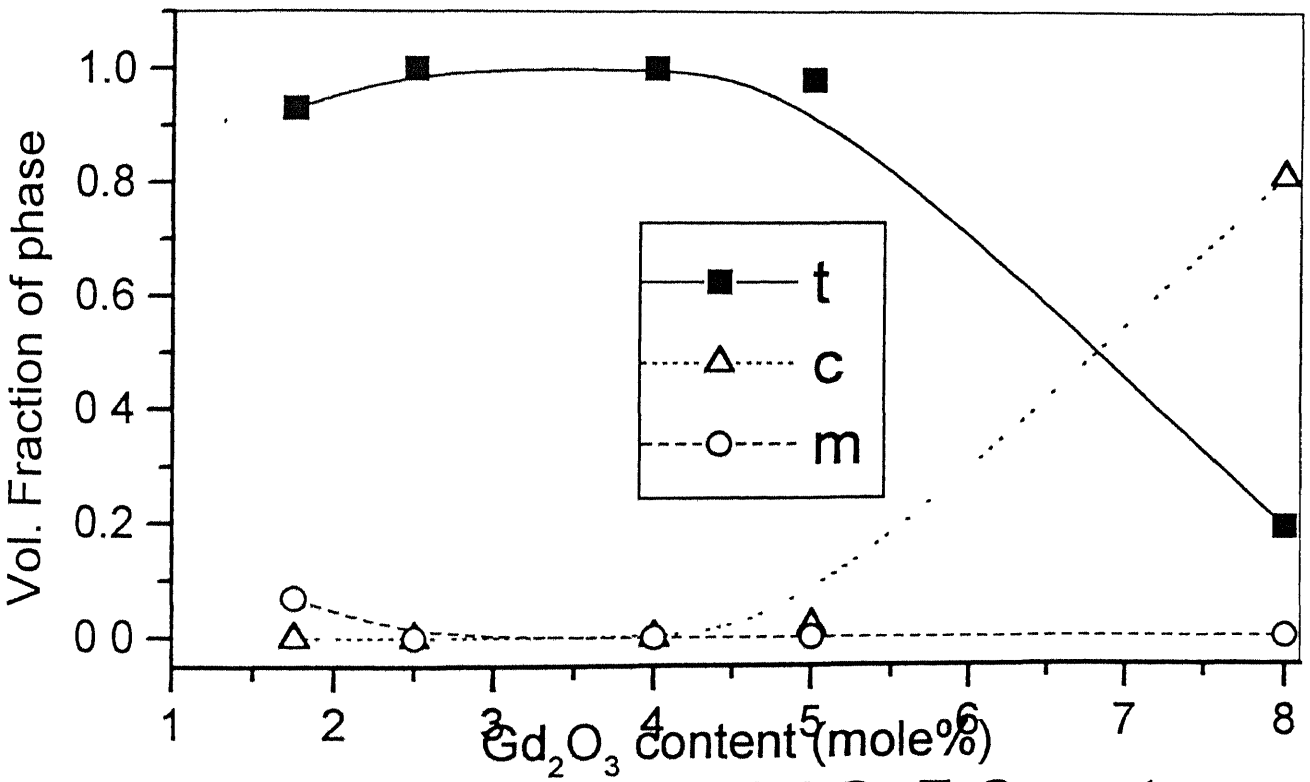

Fig.2.3 Phase content of Gd_2O_3-ZrO_2 system for different mole% of Gd_2O_3

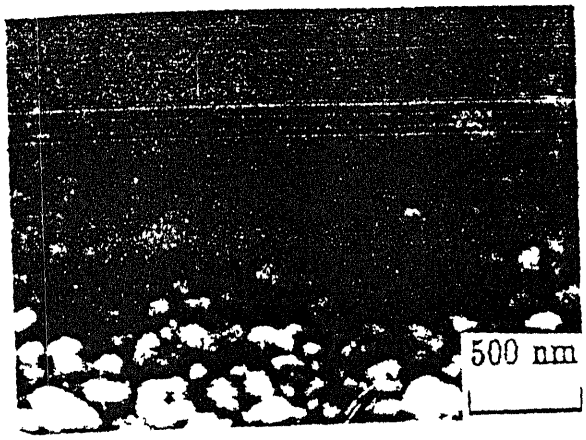

a

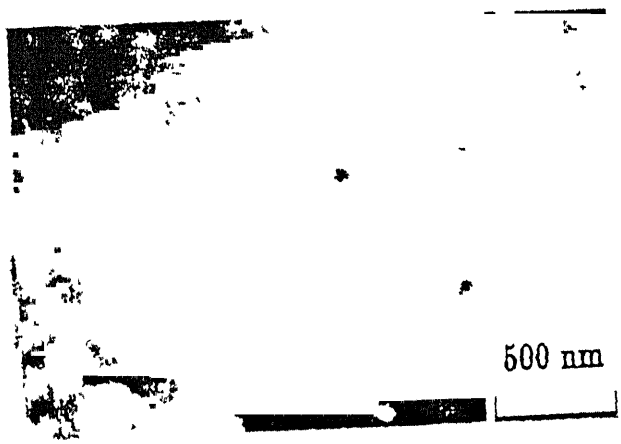

b

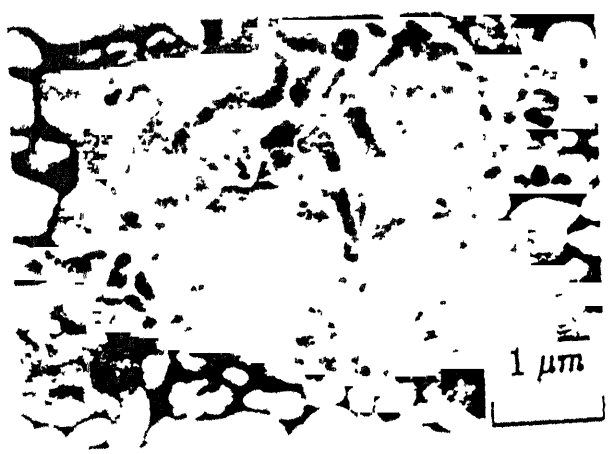

c

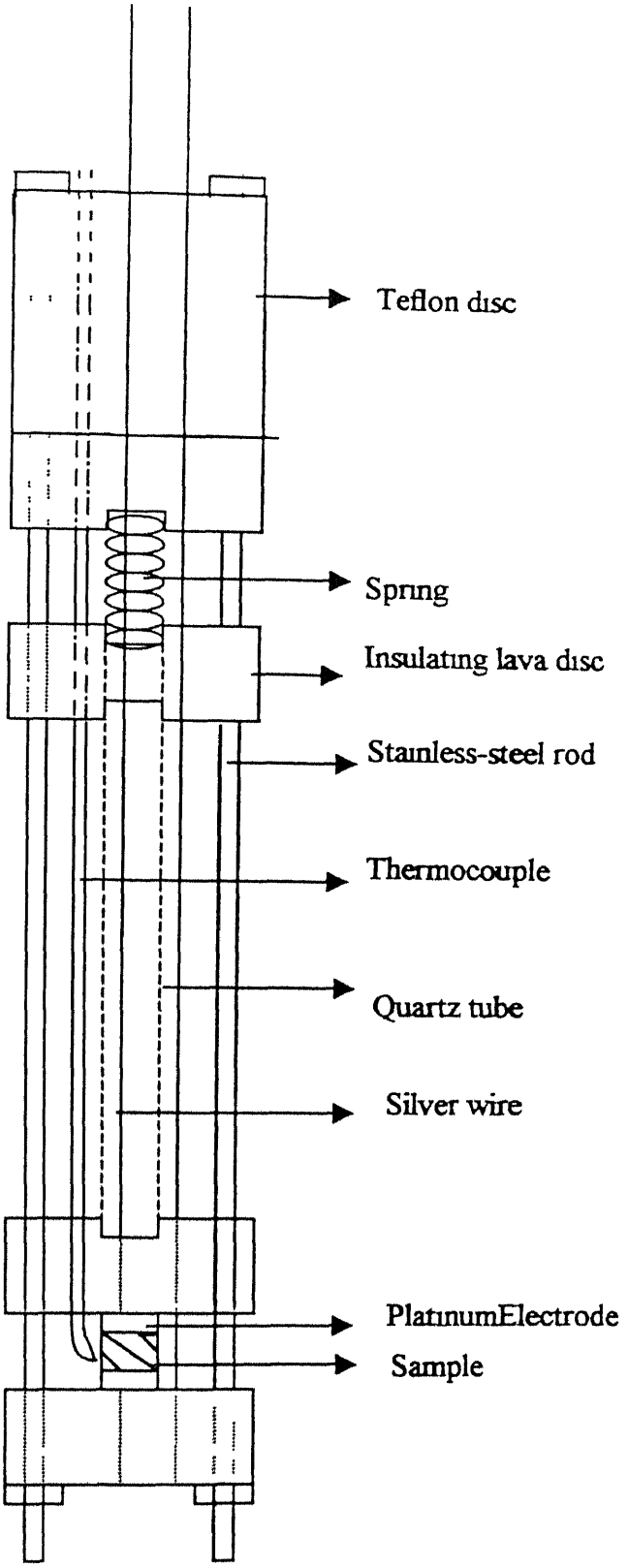

Fig. 2.5 Sample-holder for complex impedance analysis

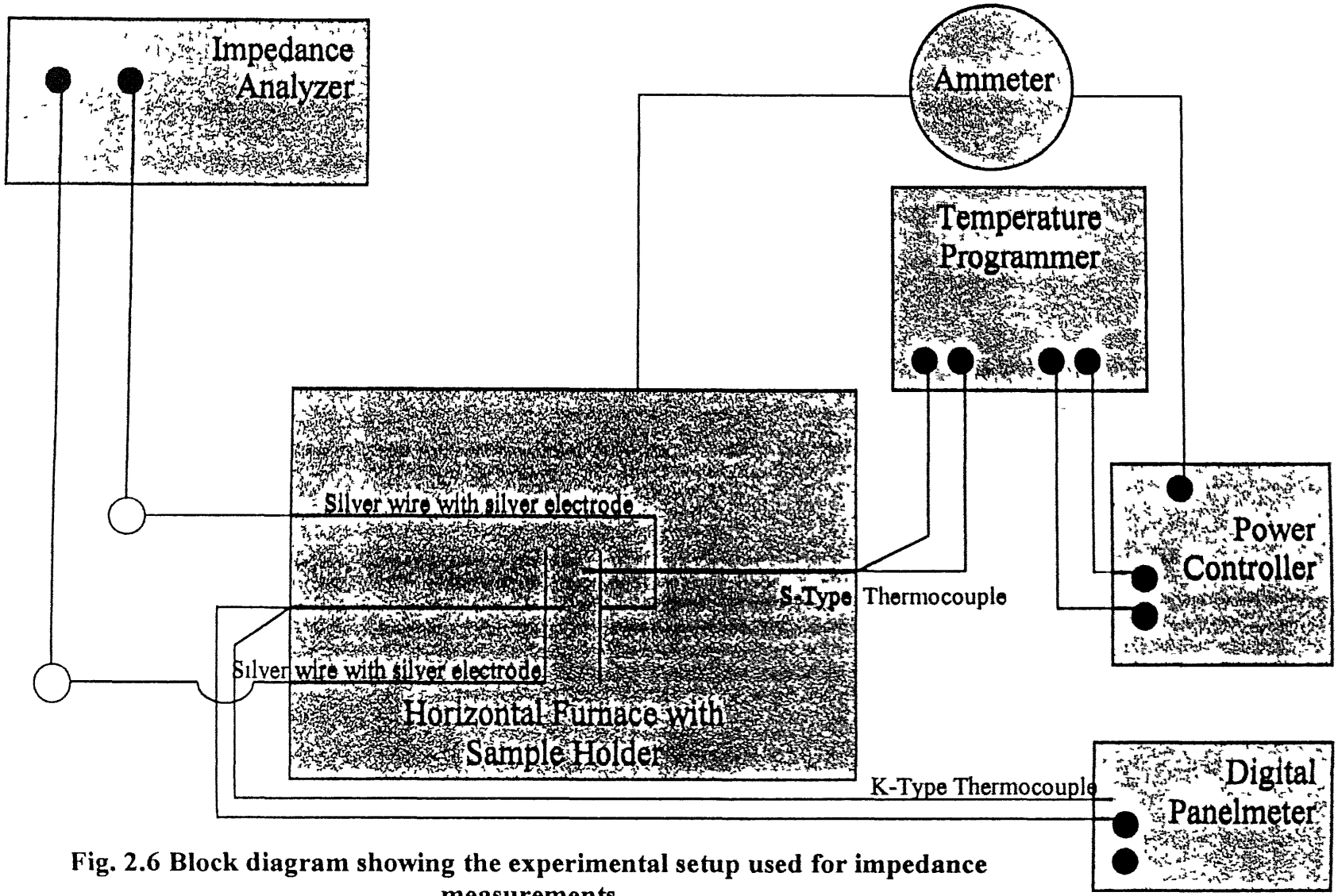

Fig. 2.6 Block diagram showing the experimental setup used for impedance measurements

RESULTS AND DISCUSSIONS

3.1 XRD ANALYSIS

The XRD patterns are recorded for 1 75, 2 5, 4, 5, 8, 9 and 11mol% samples using the computerized Richeifert powder Diffractometer. All the XRD plots are shown in Fig 3.1-3.7

The plots of 1.75 and 2.5 mole% samples showed prominent peaks corresponding to (t + m) phases. The 1.75 mole% sample contains more high intensity peaks of monoclinic than 2.5 mole%. Both of them contain t phase but the peak at 50 07 is more prominent in 2.5 mole%.

The 4 mole% sample contains tetragonal and little cubic phase The 5 mole% sample contains more prominent peaks of cubic phase with a sharp peak at 30.07° and also tetragonal phase.

The 8 mole% contains higher proportion of cubic phase with a little amount of t phase as seen from the less prominent peaks. The 9 mole% and the 11 mole% contains purely cubic phase.

3.2 IMPEDANCE MEASUREMENTS

3.2.1 COLE-COLE PLOT

Using the impedance analyzer the Z and θ values are measured for the doped zirconia samples containing 1 75, 2 5, 4, 5, 8, 9 and 11 mole% gadolinia at various temperatures Zsinθ vs Zcosθ is plotted to obtain the Cole-Cole plot The Cole-Cole plots are shown for different samples at various temperatures in Fig 3 8-3 14 The grain and the grain boundary resistances are calculated by using the non-linear square fitting to the semicircular arcs In all this plots a and b are the co-ordinates of the center of the semicircle and c is the radius of the semicircle The diameter of the semicircles represents the resistance Generally two depressed semicircles and a small arc are obtained in the impedance plane at elevated temperature within the frequency range of 5 Hz –13 MHz At lower frequencies arc due to electrode polarization is seen In the mid-frequency range the grain boundary semicircle and at higher frequencies grain/ bulk semicircular arc is seen All these semicircles are depressed having centers below the positive y-axis as seen in the case of real polycrystalline samples For the higher mole% of Gd_2O_3, above 5 mole % the grain and the grain boundary semicircles are distinct (Fig 3 11-3 14) At lower mole percent both the semicircles (Fig 3 8-3 10) tend to overlap and at 1 75 mole% it is very difficult to separate them (Fig 3.8)

Similar overlapping is seen in the case of zirconia samples studied by J Luo et al [12] The grain arc is seen at higher frequencies within the entire experimental temperature range where as the grain boundary is seen at higher temperatures and lower frequencies In all the cases above 1 75 mole % Gd_2O_3, the grain arc is smaller than the grain boundary arc At higher temperature the

contribution to the total resistivity is mainly due to the grain boundary resistivity The grain size and relative density of different mole % of Gd_2O_3 is shown below in the Table 3 1

Table 3.1: Variation of Grain Size with Different Mole % of Gadolinia

Mole percent of Gd_2O_3	Average Grain Size (μm)	Relative Density
1 75	0 14	0 9
2 5	0 13	0 93
4	0 13	0 96
5	0 17 0 35	0 92
8	0 67 0 2	0 88

Due to smaller grain size, the grain boundary resistance is higher in all the cases As shown by R Ramamoorthy et al [14] with smaller grain size (1 to 0 5μm), grain boundary arc is smaller than grain arc and the activation energy for the grain boundary increases with mole percent of Gd_2O_3

3.2.1 DC CONDUCTIVITY

The DC conductivity is obtained from the Cole-Cole plot using the relation

$$\sigma_{DC} = (1/R)(L/A) \qquad (3\ 1)$$

where R is the diameter of the semicircle in the Cole-Cole plot, L is the length of the sample and A is the area of the electroded surface

Fig 3 15 shows the variation of conductivity with temperature for different compositions It is seen for all the compositions with increasing temperature both the grain and the grain boundary conductivity increases Table 3 2 gives the values of conductivity of ZrO_2-Gd_2O_3 ceramics for different compositions at temperatures around 585K

Table 3.2 Conductivity values of ZrO_2-Gd_2O_3 ceramics for different compositions at temperatures around 585K

Temperature (°C)	Mole % of Gd_2O_3	$\sigma_g x10^{-6}$ $(\Omega cm)^{-1}$	$\sigma_{gb} x10^{-6}$ $(\Omega cm)^{-1}$
588	1 75	0 6	-
581	2 5	1 2	0 6
581	4	2	0 65
581	5	1 5	0 2
595	8	1 6	0 4
584	9	1 4	0 6
584	11	1 8	1 5

The grain conductivity is seen to vary from 0 6 to 2 x 10^{-6} $(\Omega cm)^{-1}$ Although the value for the 4 mole% Gd_2O_3 is highest at 2 x 10^{-6} $(\Omega cm)^{-1}$ however in the range of the experimental error it appears the grain conductivity does not change much with composition from 1 75 mole% to 11 mole% Gd_2O_3 The σ_{gb} is around 0 6x10^{-6} $(\Omega cm)^{-1}$ for all compositions from 2 5 mole% Gd_2O_3 onwards However it is significantly higher at 1 5 x 10^{-6} $(\Omega cm)^{-1}$ for11 mole% Gd_2O_3 Comparing these values with the conductivity of zirconia-yttria ceramics, we find that the values of conductivity are

Comparable to data of R. Ramamoorthy et al[5,43] but somewhat lesser than those given by J. Luo[5,44] Also the conductivity of the grain

$$\frac{\sigma}{T} = \sigma_O \exp\left(\frac{-\Delta H_\sigma}{kT}\right) \qquad (3\ 2)$$

where σ is the conductivity, σ_O is the pre exponential factor, ΔH_σ is the activation enthalpy for conduction mechanism and T = temperature in Kelvin

Log (σT) versus 1/T is plotted and the data is fitted to a straight line using linear regression Fig 3 16 shows the linear fit of the data for all the compositions If the linear fits are extrapolated to higher temperatures (> 633K) then the conductivity will become highest at 8 mole% as reported by J Luo et al for ZrO_2-Y_2O_3 system.

3.2.2 ACTIVATION ENTHALPY FOR CONDUCTION

Using the relation given in the equation 3 2, separate plots of log (σT) versus 1/T for all the compositions in Fig 3 17 The slope of the linear fit to the data gives the value of ΔH_σ and the intercept gives σ_O The values of activation enthalpy for grain and grain boundary are tabulated in Table 3 3

Table 3.3: Variation of activation enthalpy (ΔH_σ) with different mole % of Gadolinia

Mole % of Gadolinia	$\Delta H_{\sigma b}$ (bulk) (eV)	$\Delta H_{\sigma gb}$ (grain boundary) (eV)
1.75	0 58	-
2.5	0.72	0 75
4	0 93	1 11
5	0.92	1 04
8	1.01	1 12
9	0 72	0 92
11	0 88	0 85

Fig 3 18 shows the variation of ΔH_σ with different mol% of gadolinia.

ZrO_2-Gd_2O_3 also showed increase in the activation energy similar to ZrO_2-CeO_2 and ZrO_2-Y_2O_3 [12] with increase in the mole% of Gd_2O_3 At 1 75 mole % Gd_2O_3 grain has minimum

activation enthalpy The activation enthalpies for grain and grain boundary increases from 0 72 to 1 01 eV as the Gd_2O_3 content increases from 2 5 mole% to 8 mole % The reason could be narrowing of the passage for the diffusing ions as relatively larger Gd^{3+} (0 097nm) replaces Zr^{4+} (0 079 nm) Similar trend could is seen with regards to the activation enthalpy for grain boundary (Table 3 3) Comparing this results with ZrO_2-Gd_2O_3 and ZrO_2-Y_2O_3 from literature as described earlier, it is seen that while the activation enthalpies are much lower for low Gd_2O_3 contents (1 75 and 2 5 mole%) than those reported for ZrO_2-Y_2O_3, the values are nearly 1 eV for both grain and the grain boundary conductions The activation enthalpy decreases after 8 mole% Gd_2O_3 and is seen to be lowest at 9 mole% Gd_2O_3 and then increases slightly for 11 mole% It should be noted that 9 mole% Gd_2O_3 corresponds to the lowest composition at which the cubic phase is obtained as has been reported in literature The activation enthalpies for ZrO_2-Y_2O_3 and the ZrO_2-CeO_2 systems are known to increase with stabilizer content in the cubic phase This has been attributed to the formation of vacancy clusters in this ceramics However in the ZrO_2-Gd_2O_3 samples prepared by us shows lower activation enthalpies for 9 and 11 mole%. This indicates that the vacancy cluster formation may not be significant in ZrO_2-Gd_2O_3 system

3.2.3 ANALYSIS OF DIELECTRIC MODULLI

The complex dielectric modulli M^* consists of real (M') and imaginary (M") parts where

$$M' = \omega C_o Z \sin\theta \qquad (3\ 3)$$

$$M'' = \omega C_o Z \cos\theta \qquad (3.4)$$

increase with stabilizer content in the cubic phase This has been attributed to the formation of vacancy clusters in this ceramics However , the ZrO_2-Gd_2O_3 samples prepared by us shows lower activation enthalpies for 9 and 11 mole% This indicates that the vacancy cluster formation may not be significant in ZrO_2-Gd_2O_3 system.

3.2.3 ANALYSIS OF DIELECTRIC MODULLI

The complex dielectric modulli M^* consists of real (M') and imaginary (M") parts where

$$M' = \omega C_o Z \sin\theta \qquad (3\ 3)$$

$$M'' = \omega C_o Z \cos\theta \qquad (3\ 4)$$

M' and M" are plotted against log (frequency) For all the samples from around 200°C and above sigmoidal curve fitting is applied for M' vs logf (frequency) (Fig 3 19) and Lorentzian curve fitting for M" vs logf curve (Fig 3 20) The nature is similar to what is reported by A Pimenov et al [15] for 4 mol% Y_2O_3 doped ZrO_2 At lower frequencies M' values tend to zero and level off at higher frequencies around 1MHz and droops down at still higher frequencies (not shown in figure) This may be due to grain boundary relaxation and interfacial effect For M" vs logf plot, presence of peaks in the Lorentz fit signify dielectric relaxation processes Except 1 75 (Fig 3 21) and 9 mol % (Fig 3 22) Gd_2O_3 all the other samples show one relaxation peak at a frequency which represents the characteristic frequency of the conductivity relaxation. The plots are more or less symmetric about the peak maxima indicating a single dominant dielectric relaxation mechanism e.g. for 2 5 mol%, 4 mol%, 5 mol%, 8 mol% and 11 mol% (Fig 3.20) The relation between relaxation frequency ω_r and temperature is represented in a plot of log ($\omega_r/2\pi$) and 1000/T (Fig 3 23) Linear fit of

the curve gives the activation energy for the conduction mechanism For all the samples except the 1 75 and 9 mole% samples, the data fall on a single line For the 1 75 mole% samples, two lines are obtained (discussed in further section 3 2 3 1) For the 9 mole% samples also, two lines are obtained but one has a positive slope This sample was very thin and cracked and this may be the reason of anomaly The values for the other samples are more or less comparable to the activation energy from log (σT) vs 1000/T (Fig 3 17) The values of activation energy for bulk are compared with those obtained from modulus spectra in the Table 3 4

Table 3.4 Comparison of values of ΔH_σ obtained from two different methods

Mol % of Gd_2O_3	ΔH_σ (bulk) (eV)	ΔH_σ (from modulus) (eV)	Phases present
2 5	0 72	0 678	m + t
4	0 93	0 89	t
5	0 93	0.99	t
8	1 01	1 04	c
11	0.88	0 97	c

It is seen that with increasing temperature at a fixed composition, the height of the relaxation peak increases Also with increasing Gd_2O_3 content at any particular temperature the peak height generally increases. The peak height values are tabulated for different mol% Gd_2O_3 in Table 3 5 at 533K

Table 3.5 Relaxation peaks for different mole% of Gadolinia

Mole % of Gadolinia	Height of Relaxation Peak
2 5	8 2267X10^{-5} units
4	9 671 X10^{-5} units
5	20 384 X10^{-4} units
8	62 272 X10^{-4} units
11	11 968X 10^{-4} units

The variation of relaxation time ($\tau_R = 2\pi/\omega_R$) with composition is tabulated in Table 3 6 at 533K.

Table 3.6 Variation of Relaxation time with different mole% of Gadolinia

Mole % of Gadolinia	Log ($\omega_R/2\pi$) (Hz)	τ_R (sec)
2 5	4 548	2 83 x10^{-5}
4	4 886	1 3 x10^{-5}
5	5 048	8 95 x10^{-6}
8	5 2037	6 256 x10^{-6}
11	5 529	2 95x10^{-6}

It is seen that with increasing mol% of Gd_2O_3, relaxation time decreases and is minimum for the highest conducting composition in the table

3.2 3 1MULTIPEAKS FOR MODULUS PLOTS OF 1 75 AND 9 MOL% Gd_2O_3 DOPED ZrO_2

The values of activation enthalpies obtain by curve fitting the two sets of relaxation frequency against inverse of temperature are tabulated in table 3 7

Table 3.7 Values of ΔH_σ for 1.75 and 9 mole% obtained from Modulus Spectra

Mol % of Gadolinia	ΔH_σ (bulk) (eV)	ΔH_σ (from modulus) (eV)	
1 75	0 60	0 36	0 68
9	0 72	-	0 84

For the 9 mol% sample up to 311°C, the two Lorentzian peaks can be fitted to the M'' vs logf curve (Fig 3 22) Beyond this temperature the curve is slightly asymmetric but only one peak can be fitted For 1 75 mol% up to 424°C, 2 peaks can be fitted (Fig 3 21)

Modulus plots for doped zirconia show a single relaxation peak as seen in the case reported by A Pimenov et al [15] This peak is due to the conductivity relaxation associated with ionic diffusion Another type of relaxation i e dielectric relaxation is seen due to the dipole reorientation This occurs at a lower frequency than ionic relaxation As discussed by V Provenzano et al [24] for Na_2O-SiO_2 glasses, asymmetric curves (for M'' vs logf) are seen which are broader on both the sides of the maxima than would be expected for a single conductivity mechanism Such modulus plots can be resolved into 2 curves both with log- Gaussian distribution of relaxation times. Two relaxation times corresponding to the peaks are obtained [24] Whether dipole reorientation and ionic relaxation both may have been occurring for 1 75 mol % and 9 mol% gadolinia is to be further investigated

3.2.4 CALCULATION OF CARRIER CONCENTRATION

For all the compositions the carrier concentration (N) is calculated at any particular temperature using the equation 2 15 in section 2 3 5 3 So, N can be expressed as

$$N = (6\sigma_{DC}/q^2d^2\gamma)\ (kT/\omega_R) \qquad (3\ 5)$$

The values of σ_{DC} and ω_R can be tabulated around 603K for different mol% of Gd_2O_3 in table 3 8

Table 3.8 Various parameters for different mole% of gadolinia around 603K

Temperature (K)	Mol% of Gd_2O_3	ω_R (KHz)	σ_{DC} $(\Omega cm)^{-1}$
606	2 5	169 107	1 93X10^{-6}
606	4	196 590	4 8 X10^{-6}
603	5	323 799	2 28 X10^{-6}
597	8	301 304	1 33 X10^{-6}
597	11	520 152	5 34 X10^{-5}

For each case, n is calculated putting the values of k, q, a

$N = [6x1\ 38x10^{-23}xTx\sigma_{DC}]/[\omega_Rx(0\ 35)x(0\ 516x10^{-7})^2x(2x1\ 6xx0^{-19})^2]$

here q = 2x1 6x10^{-19} Coulombs for the oxygen vacancies

The values of N are tabulated in table 3 9 against composition

Table 3.9 Variation of N with composition at 603K

Mol% of Gd_2O_3	N (cm^{-3})	T
2.5	6X10^{21}	606
4	12 8 X10^{21}	606
5	3 6 X10^{21}	603
8	2 29 X10^{21}	597
11	5 32 X10^{21}	597

The carrier concentration is seen to decrease from 2 5 mole% to 4 mole% and then decrease upto 8 mole% and again increase at 11 mole% No monotonic dependence is found to by other investigators (Table 1 20[15]) The numbers are however in agreement with the values found in literature The effective carrier concentration is in the range of 10^{21}

3.2.5 MIGRATION ENTHALPY

Using the equation 2 8 in section in 2 3 5 1

$$\log[(R_{DC}\cos\theta/Z)-1] = n\log f - n\log f_p \qquad (3\ 6)$$

values of n and f_p are calculated from the plot of $\log[(R_{DC}\cos\theta/Z)-1]$ vs logf Then $\log f_p$ is plotted against temperature (Fig 3 24) ΔH_m is calculated from the slope of the linear fit according to the equation

$$f_p = f_{po}\exp(-\Delta H_m/kT) \qquad (3\ 7)$$

where f_{po} pre-exponential constant

The values of ΔH_m obtained for composition are tabulated against composition in table 3 10

Table 3.10 Values of ΔH_m, ΔH_a and (ΔH_m-ΔH_a) for different mole% of Gd_2O_3

Mol% of Gd_2O_3	ΔH_m (eV)	ΔH_σ (eV)	(ΔH_σ-ΔH_m) (eV)
1 75	0 4	0 6001	+0 20
2 5	0 72	0 72	0
4	1 09	0 93	-0 16
5	1 08	0 92	-0 16
8	1 08	1 01	-0 07
9	0 71	0 72	+0 01
11	0 98	0 89	-0 09

For most of the cases, ΔH_m is higher than ΔH_σ So association of ions and vacancies are not expected here as we are getting negative values of ΔH_a ($\Delta H_a = \Delta H_\sigma - \Delta H_m$)

Only 1 75 and 9 mol% samples show association enthalpy values of 0 25eV and 0 01eV These values do not conform to the ΔH_a values as reported by J Luo et al for Y_2O_3 doped ZrO_2[12] A possible explanation could be close relaxation frequencies for grain and grain boundary arcs As reported by J Luo et al [13] a significant difference in relaxation time helped to estimate the migration enthalpy within the grains Also suggested by A Pimenov et al [15] that the frequency range of applicability of the dielectric response is very small due to the influence of grain boundary relaxation and does not allow a reliable determination of the parameters n and f_p also the values of ΔH_m and ΔH_σ are quite similar this indicates that no significant association of clusters has taken place

3.2.6 JONSCHER'S CONSTANT IN CONDUCTIVITY EQUATION

As discussed in section 1 4 1 the values of n are calculated by the three different methods

1) By curve fitting the AC conductivity data in the valid frequency range, n is calculated from the slope to the linear fit to the $\ln(\sigma_{AC}/\sigma_{DC}-1)$ vs ln(frequency) Fig 3 25 shows the values of n and f_p at the 585K At a particular composition generally the value of n increases and f_p decreases with decreasing temperature The values of n are seen to vary between 0 6 and 0 85 The values of n are tabulated for 1 75 mol% at different temperatures in table 3 11

Table 3.1.1 Variation of n and f_p with temperature for 1.75 mole%

Temperature (°C)	n	f_p (KHz)
279	0 74	1 50
300	0 71	1 74
316	0 67	1 89
332	0 69	3 06
347	0 66	3 48
363	0 64	4 01
378	0 64	5 32
393	0 63	5 69
408	0 63	7 06

At any particular temperature the value of n is seen to increase generally with dopant concentration (Table 3.12)

Table 3.12 Variation of n with composition around 333°C

Temperature (°C)	Mol% of Gd_2O_3	n
332	1 75	0 68833
333	2 5	0 69735
333	4	0 76347
327	11	0 88759

2) Another set of values for n is obtained from the depression angle φ

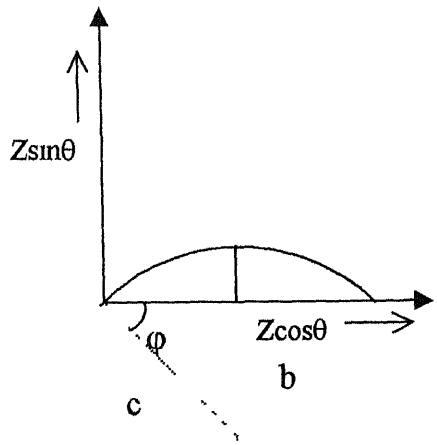

All the Cole-Cole plots show depressed semicircles The depression angle φ is given as $\varphi = \sin^{-1}(b/c)$ (3 8)

where b = ordinate of the center (negative) and c = radius of the semicircle

Now, $n = 1-2\varphi/\pi$, where φ is in radians

.. $n = 1-2\varphi/180$ when φ is in degrees

The values are mainly seen to vary between 0 8 and 1 The depression angle therefore varies between 10° and 15° occasionally as low as 4°

From both the methods it is seen that the values of n obtained from the calculations based on the depression angles is slightly higher than those from

$$\chi'' = (\sigma_{AC}-\sigma_{DC})/\omega\varepsilon_o$$

and $\chi'' = \sigma_{DC}(\omega^{n-1}/\omega_p^{n})$

$$\chi'' = \omega^{n-1}$$

$$\log\chi'' \propto (n-1) \qquad (3\ 9)$$

Figs (3 26) shows the curve plotted for logχ''vs log (frequency) at different compositions and at different temperatures From the peak heights dielectric losses are calculated The values are tabulated for different compositions in table 3.14

Table 3.14 Dielectric losses at different compositions

Mole% of Gadolinia	Dielectric Loss
1 75	Around 631
2 5	Peak heights are varying, few around 71
4	Mostly around 50
5	Not similar average peak height is 39 8
8	Around 25
9	Few peaks around 63, rest not developed
11	Very overlapping with average peak height of 8 9

The dielectric loss is seen to decrease with increasing mole% of Gd_2O_3 except at 9 mole%. It is seen from Fig . 3.26 that the plot is not amenable to analysis for obtaining n. For the analysis, plots such as that obtained by J Luo et al [13](Fig 1.20) should be available. Hence the analysis was not performed

3.2.7 RELATIONSHIP OF AC CONDUCTIVITY WITH FREQUENCY

AC conductivity σ_{AC} is plotted against frequency (1Hz to 10 MHz) in the log-log scale (3 27) The nature of the plots is largely the same as shown by A Pimenov et al [15] and J Luo et al [12]

Starting from the higher mol% Gd_2O_3 samples, for 11 mol% Gd_2O_3 dispersion step due to grain boundary relaxation is seen from 240°C The relaxation frequency is seen to increase with temperature The relaxation frequency varies in the range of 316 Hz to 10 KHz between 327°C to 430°C A power law increase in conductivity is seen at higher frequencies and frequency independent plateau of DC conductivity at lower frequencies is noticed At higher temperatures starting from 368°C the grain boundary effects modify the plateau and two frequency independent plateaus, one for the grain (higher frequency) and the other for the grain boundary (lower frequency) relaxation is seen At still higher frequency, the power law increase in conductivity is seen

Similar nature is seen for 8 mol% sample, the dispersion step is between 1KHz to 3 2 KHz, starting from 324°C The power law increase in conductivity and the plateau for DC conductivity is also seen 2 plateaus are seen prominently from around 362°C

For 9 mol% plots the nature is more or less similar to 11 and 8 mol% samples But the plateaus are not prominent and at temperatures around 262°, 311° and 322°C the behavior is somewhat different

The nature of the plot is somewhat similar for 5 mol% samples but here the dispersion step is quite prominent and the plateau at higher temperature is not so significant The relaxation frequencies lie in the range of 300 to above 1000Hz

For 4 mol% samples also the plateaus for DC conductivity and power law increase in AC conductivity is seen Here also the plateau at higher frequency is not very prominent

For 2 5 mol% also similar nature is seen i e plateau at higher frequency and higher temperature is nearly absent At lower frequencies beyond the plateau for DC conductivity power law increase in AC conductivity is seen The relaxation frequencies varied between 300 to 1000 Hz At higher temperature the plots are very overlapping

For the lowest mol% studied i e 1 75 mol% the plateaus at lower frequency are quite prominent and the plateaus at higher frequency are missing

The absence of plateaus at higher frequencies and decrease in prominence of the dispersion step may be overlapping nature of grain and grain boundary contributions From the Cole-Cole plot it can be seen that with decreasing gadolinia content it is more difficult to distinguish the two semicircles

3.2.8 VARIATION OF REAL PART OF PERMITTIVITY WITH FREQUENCY

ε' is plotted against frequency in the log-log scale (3 28) At all the compositions it is seen that the dispersion step due to grain boundary relaxation shifts to a higher frequency with increasing temperature

For 11 mol% the dispersion step is seen to increase with to shift to a higher frequency with increasing temperature Similar nature is seen for 9 mol% except at 353°C. For 8 mol% a strong dispersion step is seen starting from 291°C A small plateau for grain boundary relaxation is seen at ε' ~ 3162 starting from around 324°C

At a lower frequency, an increase in ε' is seen may be due to the blocking effect of the space charge near the electrodes on the AC conductivity Nature of 5 mol% is similar to 8 mol% but plateau for grain is seen only at 330°C The plots between 330°C to 416°C showed some sharp changes at lower frequencies and increasing at still lower frequencies For the 4 mol% sample, the dispersion step is seen for all temperature and the plateau for dielectric permittivity is seen at ε' ~ 3162 2 at higher temperature starting from around 318°C due to grain boundary relaxation. At a still lower frequency there is an increase inε' due to electrode polarization 2 5 mol% gadolinia showed a similar nature with 2 dispersions around the plateau of ε' ~ 2500 due to grain boundary relaxation The plot of 1 75 mol% is somewhat smoother with small and gradual dispersion due to the grain boundary relaxation. Decrease in steepness of dispersion step may be due to the overlapping semicircles for grain and grain boundary effects The plateau is also not so prominent The second dispersion step due to the blocking charge is also seen The dispersion step for grain boundary relaxation is more clearly studied for logε' vs logf plots than for $\log\sigma_{AC}$ vs logf plots

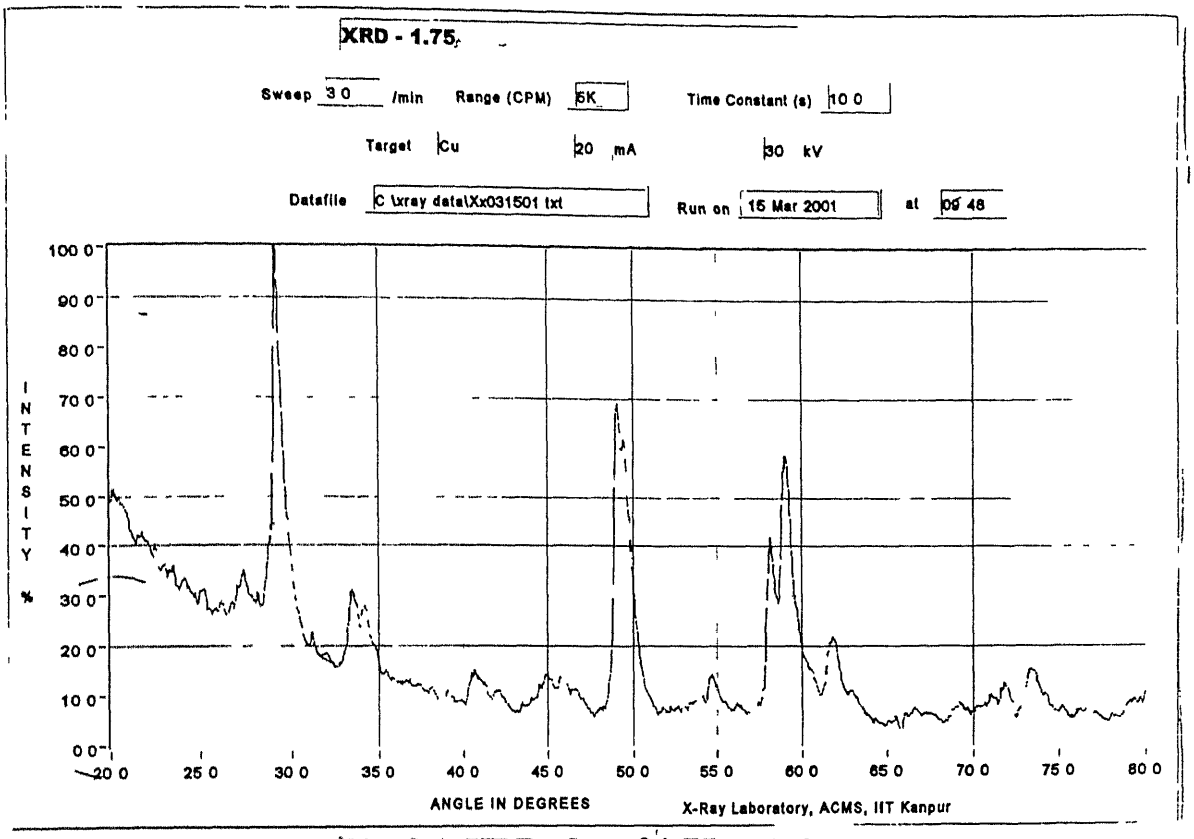

Fig. 3.1 XRD plot of 1.75 mole%

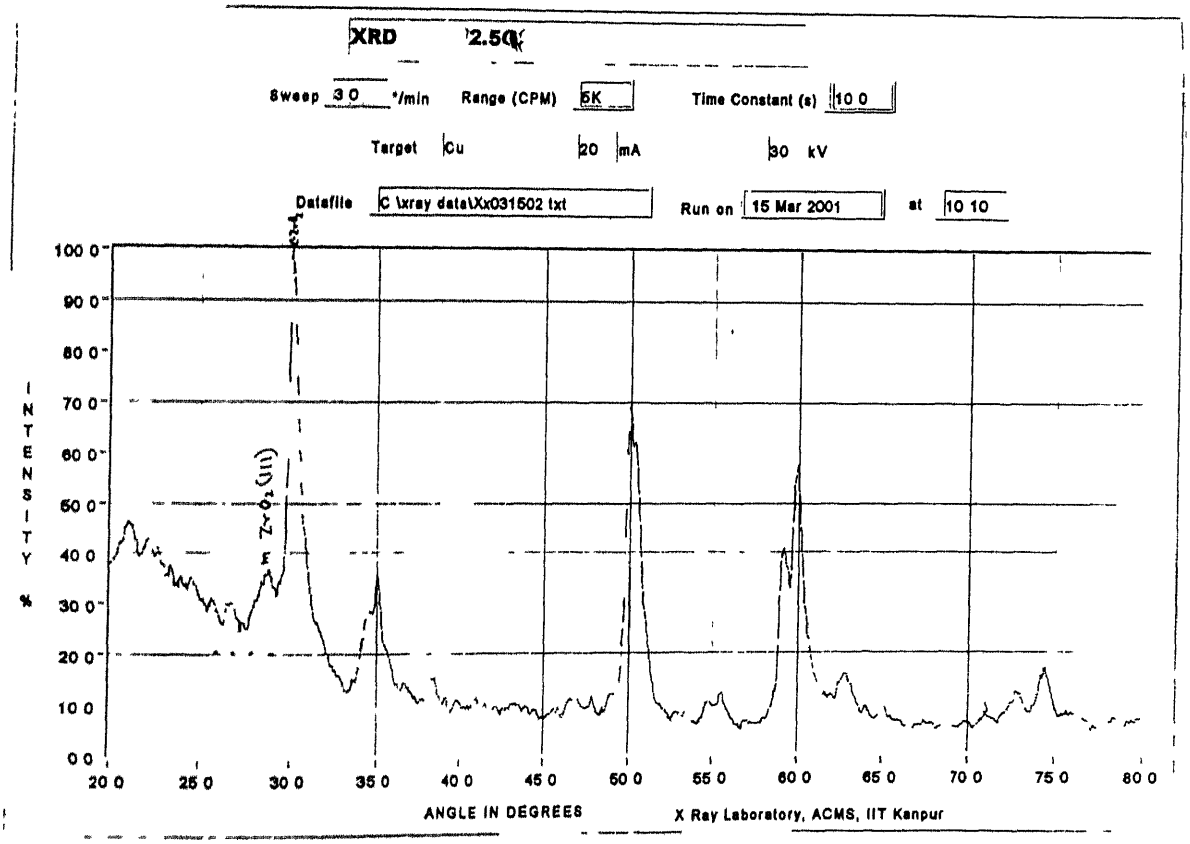

Fig. 3.2 XRD plot of 2.5 mole%

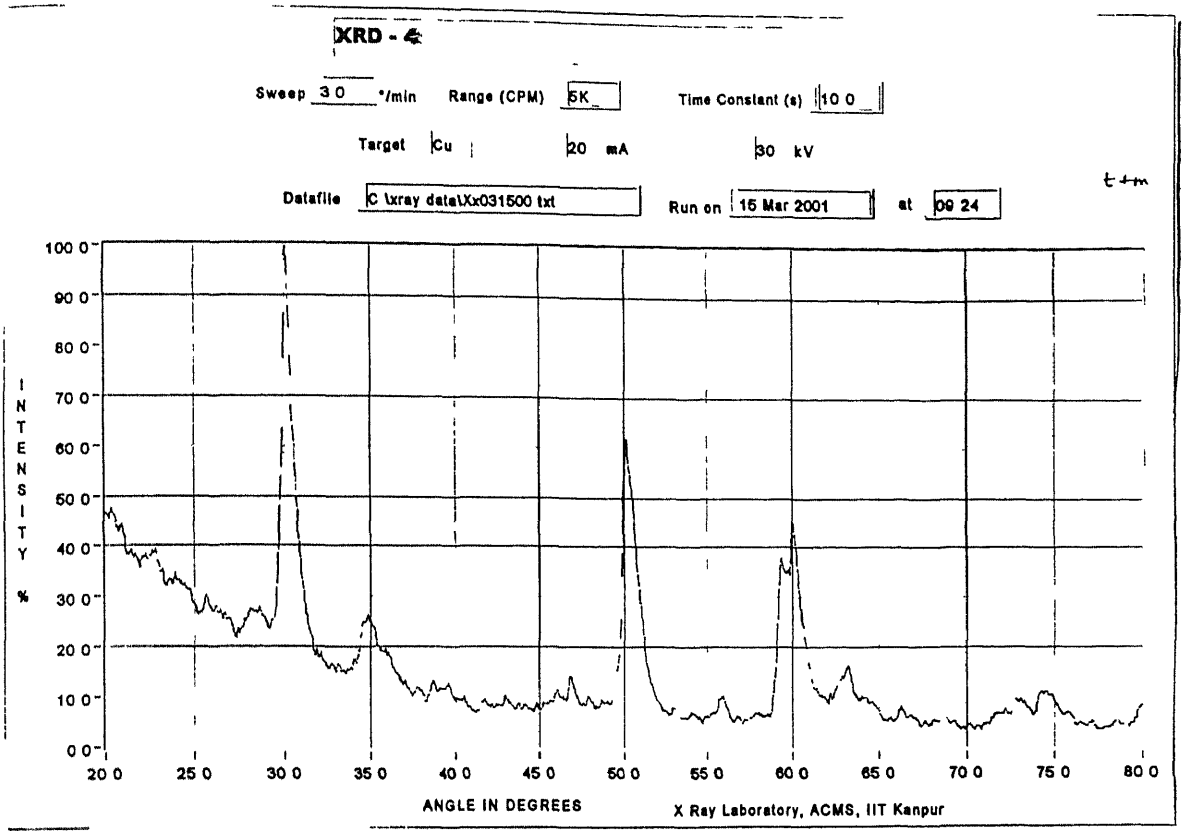

Fig. 3.3 XRD plot of 4 mole%

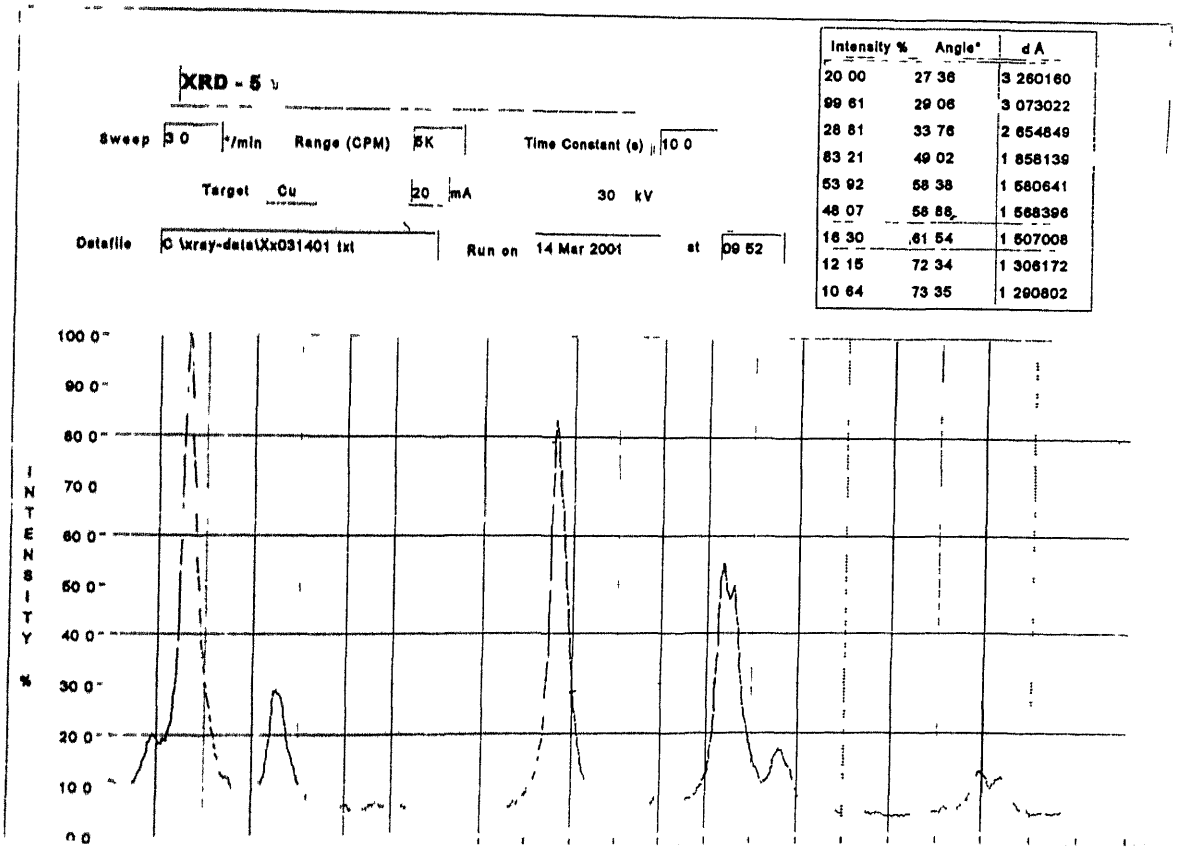

Intensity %	Angle°	d Å
20 00	27 36	3 260160
99 61	29 06	3 073022
28 61	33 76	2 654849
83 21	49 02	1 858139
53 92	58 38	1 580641
46 07	58 86	1 568396
16 30	61 54	1 507008
12 15	72 34	1 306172
10 64	73 35	1 290802

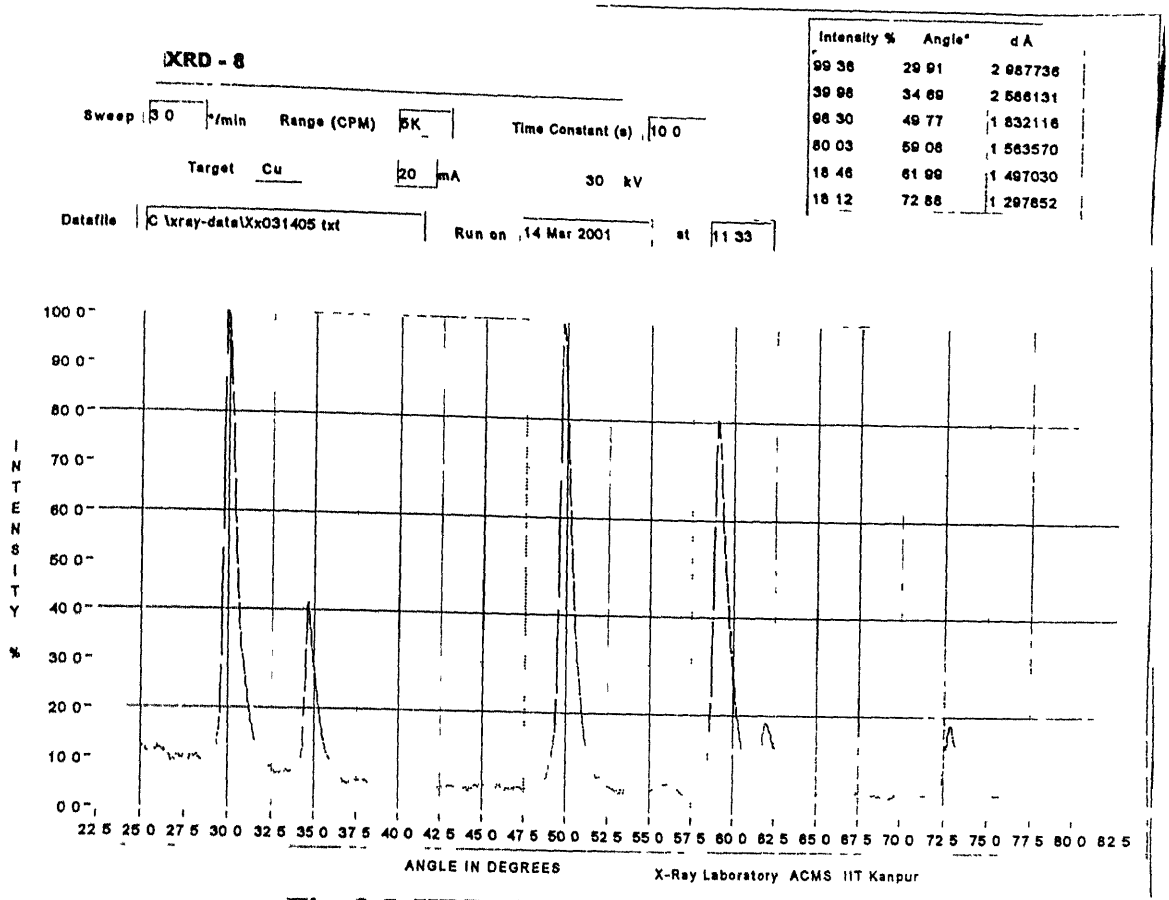

Fig. 3.5 XRD plot of 8 mole%

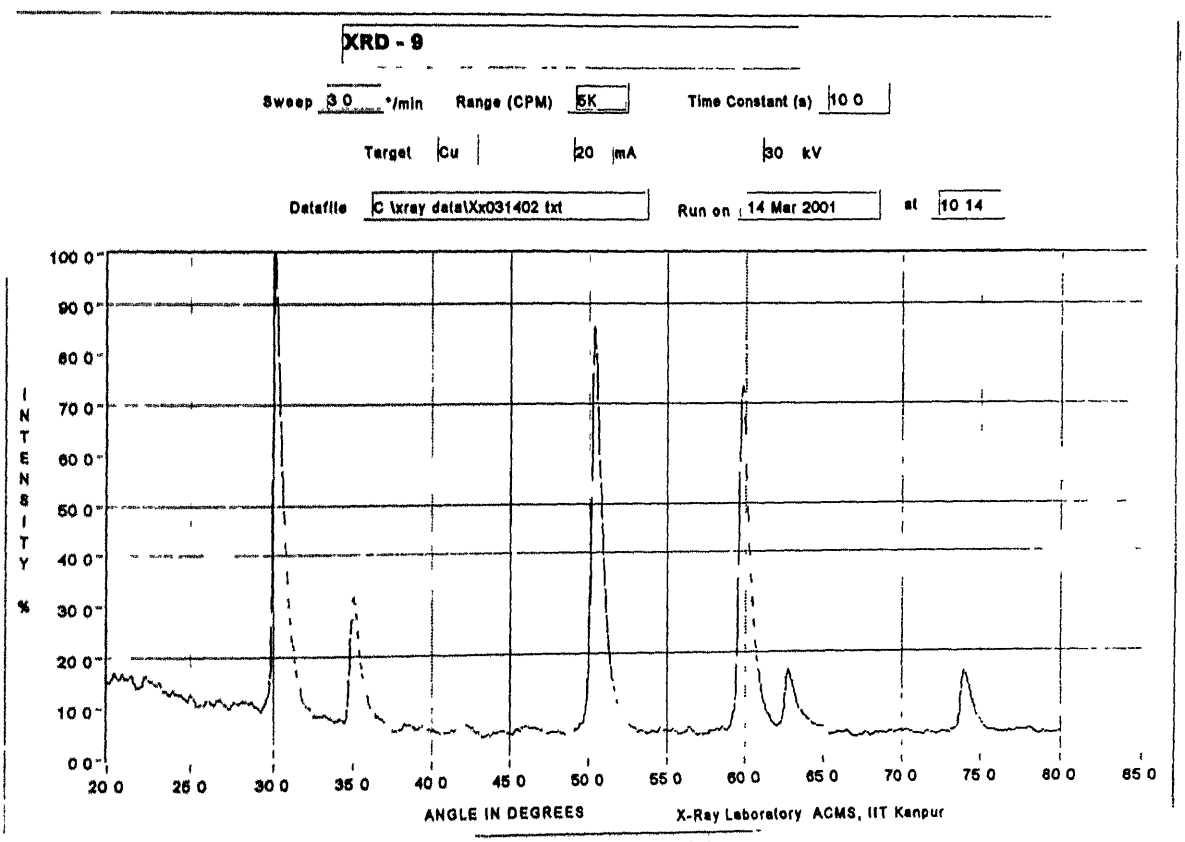

Fig. 3.6 XRD plot of 9 mole%

XRD - 11

Sweep 3 0 °/min Range (CPM) 5K Time Constant (s) 10 0

Target Cu 20 mA 30 kV

Datafile C \xray-data\Xx031403.txt Run on 14 Mar 2001 at 10 36

Intensity %	Angle°	d A
98 14	29 95	2 983516
35 25	34 75	2 581754
82 81	50 00	1 824153
69 40	59 44	1 554916
16 60	62 32	1 489834
15 42	73 33	1 290981

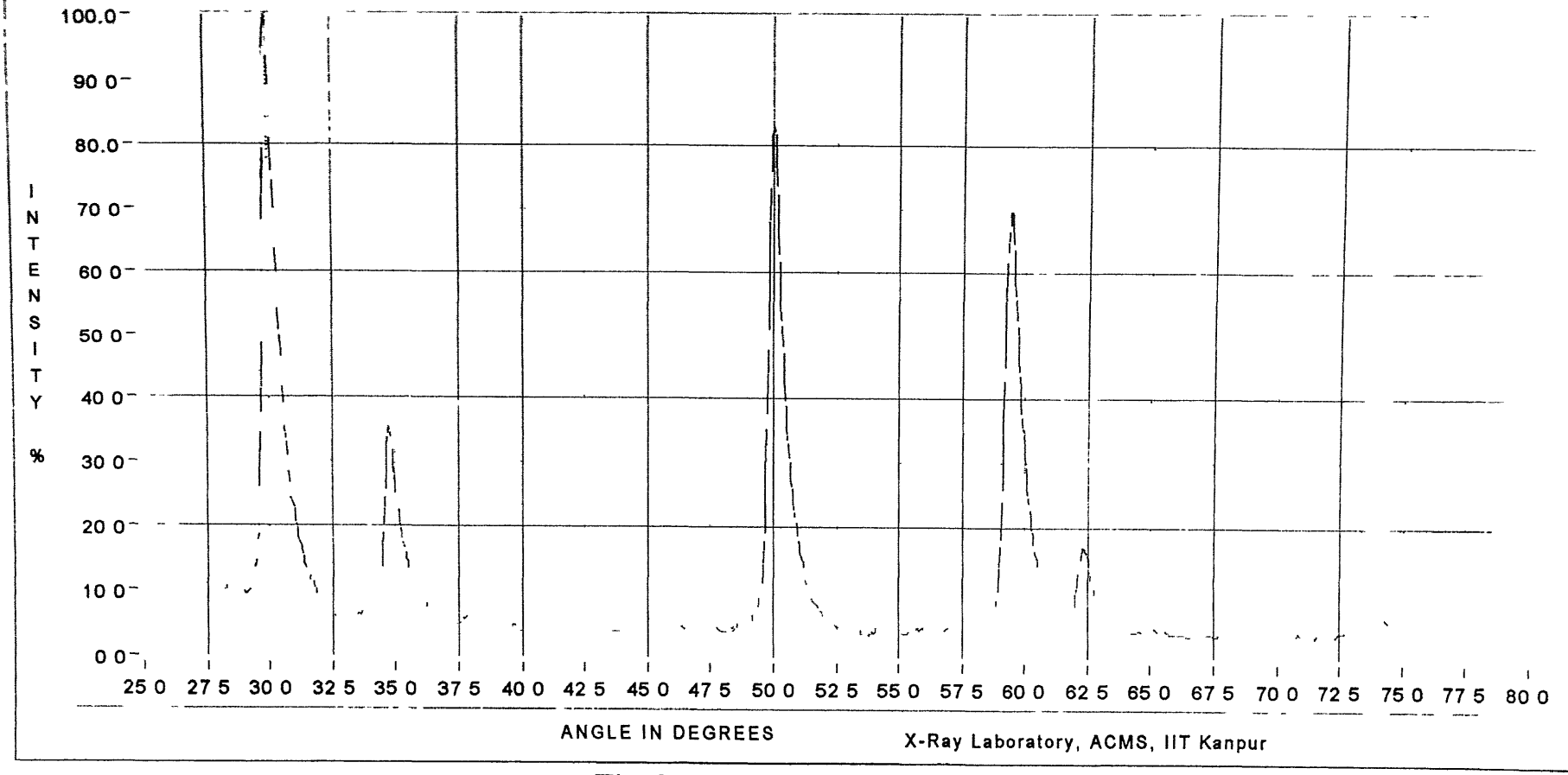

Fig. 3.7 XRD plot of 11 mol. %

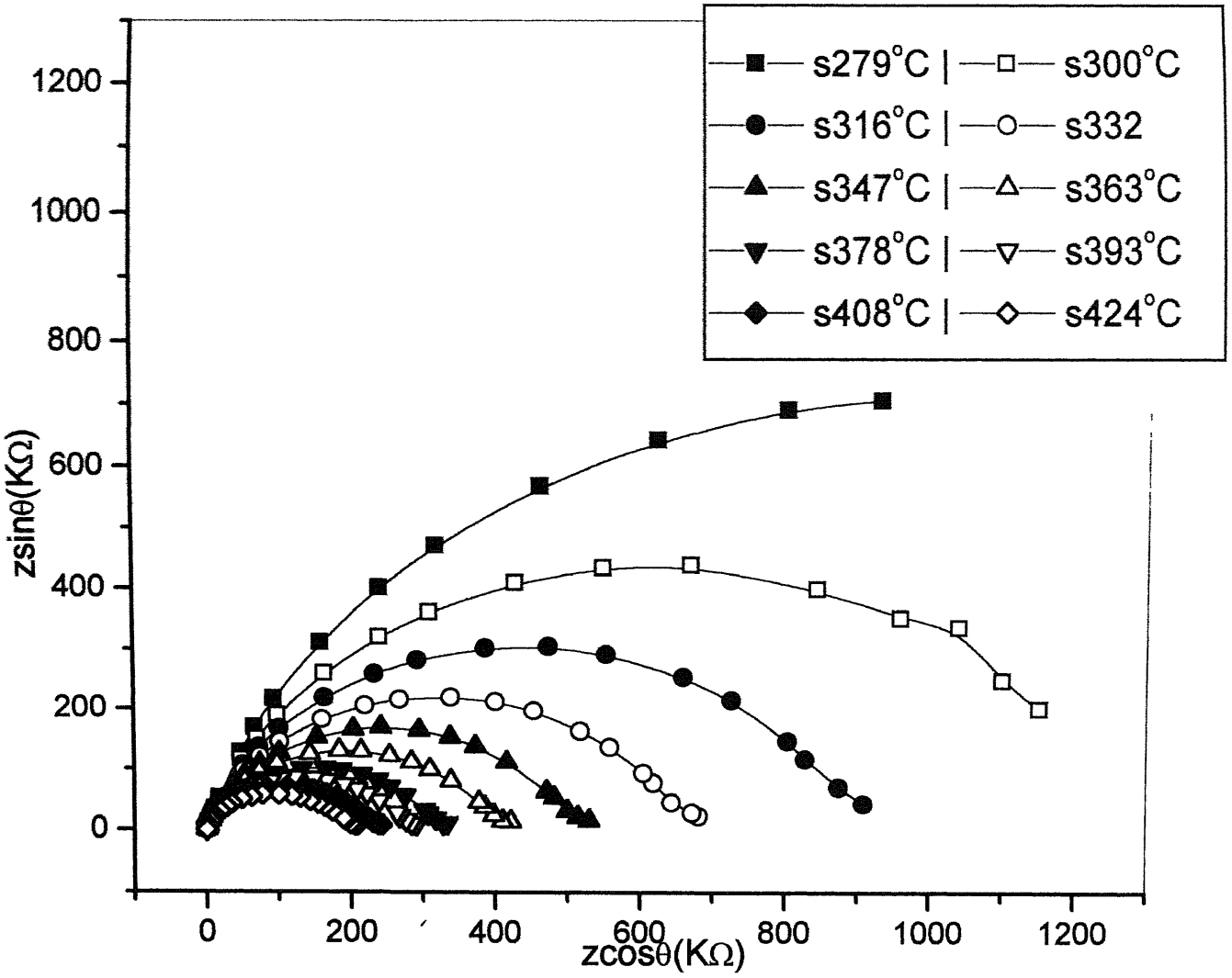

Fig.3.8 Cole-Cole plot for 1.75 mol% Gadolinia doped Samples from 279°to 424°C

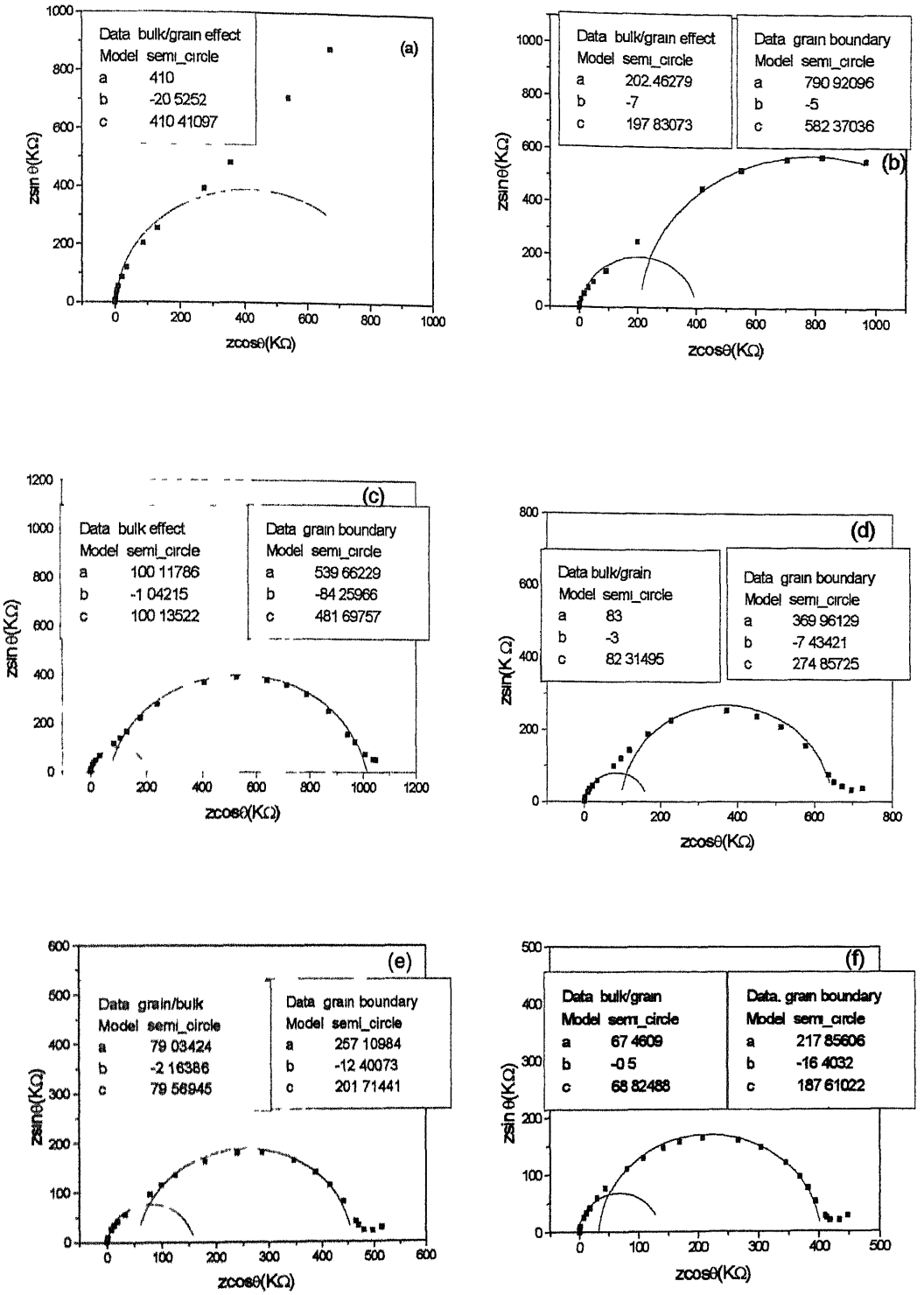

Fig. 3.9 Cole-Cole Plot for 2.5 mol% Gd_2O_3 doped ZrO_2 bulk samples at temperatures

(a) 309°C (b) 333°C (c) 348°C (d) 364°C (e) 379°C and (f) 396°C

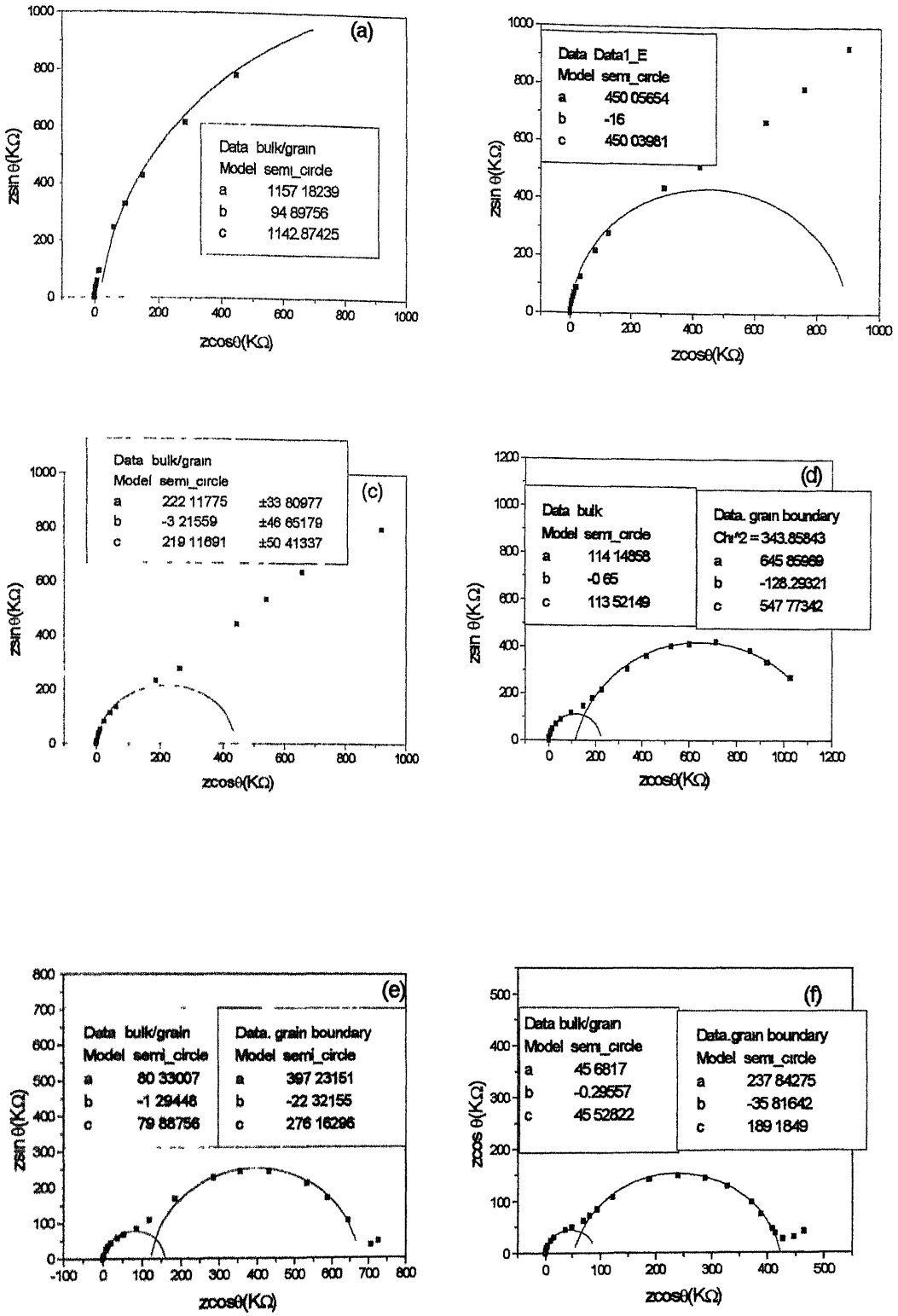
(a)
Data bulk/grain
Model semi_circle
a 1157 18239
b 94 89756
c 1142.87425
zsin θ(KΩ)
zcosθ(KΩ)
Data Data1_E
Model semi_circle
a 450 05654
b -16
c 450 03981
(c)
Data bulk/grain
Model semi_circle
a 222 11775 ±33 80977
b -3 21559 ±46 65179
c 219 11691 ±50 41337
(d)
Data bulk
Model semi_circle
a 114 14858
b -0 65
c 113 52149
Data. grain boundary
Chi^2 = 343.85843
a 645 85989
b -128.29321
c 547 77342
(e)
Data bulk/grain
Model semi_circle
a 80 33007
b -1 29448
c 79 88756
Data. grain boundary
Model semi_circle
a 397 23151
b -22 32155
c 276 16296
(f)
Data bulk/grain
Model semi_circle
a 45 6817
b -0.29557
c 45 52822
Data.grain boundary
Model semi_circle
a 237 84275
b -35 81642
c 189 1849
zcos θ(KΩ)

Fig. 3.10

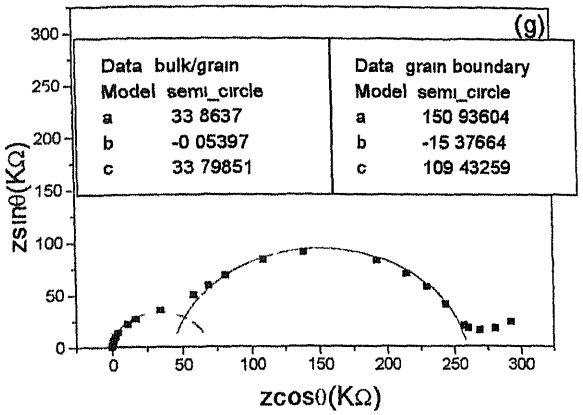

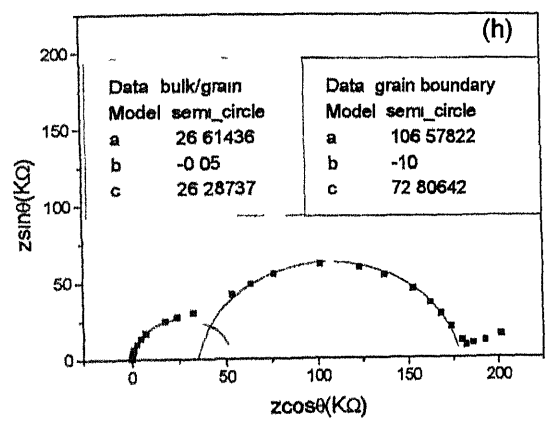

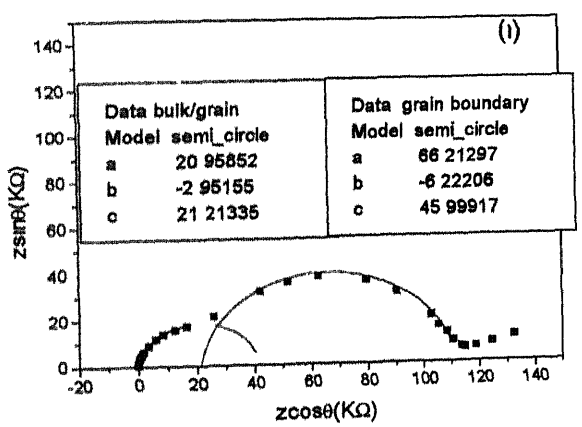

Fig 3.10. Cole-Cole plots for 4 mole% gadolinia doped zirconia bulk samples at temperatures (a) 255°C (b) 276°C (c) 308°C (d) 318°C (e) 333°C (f) 348°C (g) 365°C (h) 380°C and (i) 396°C

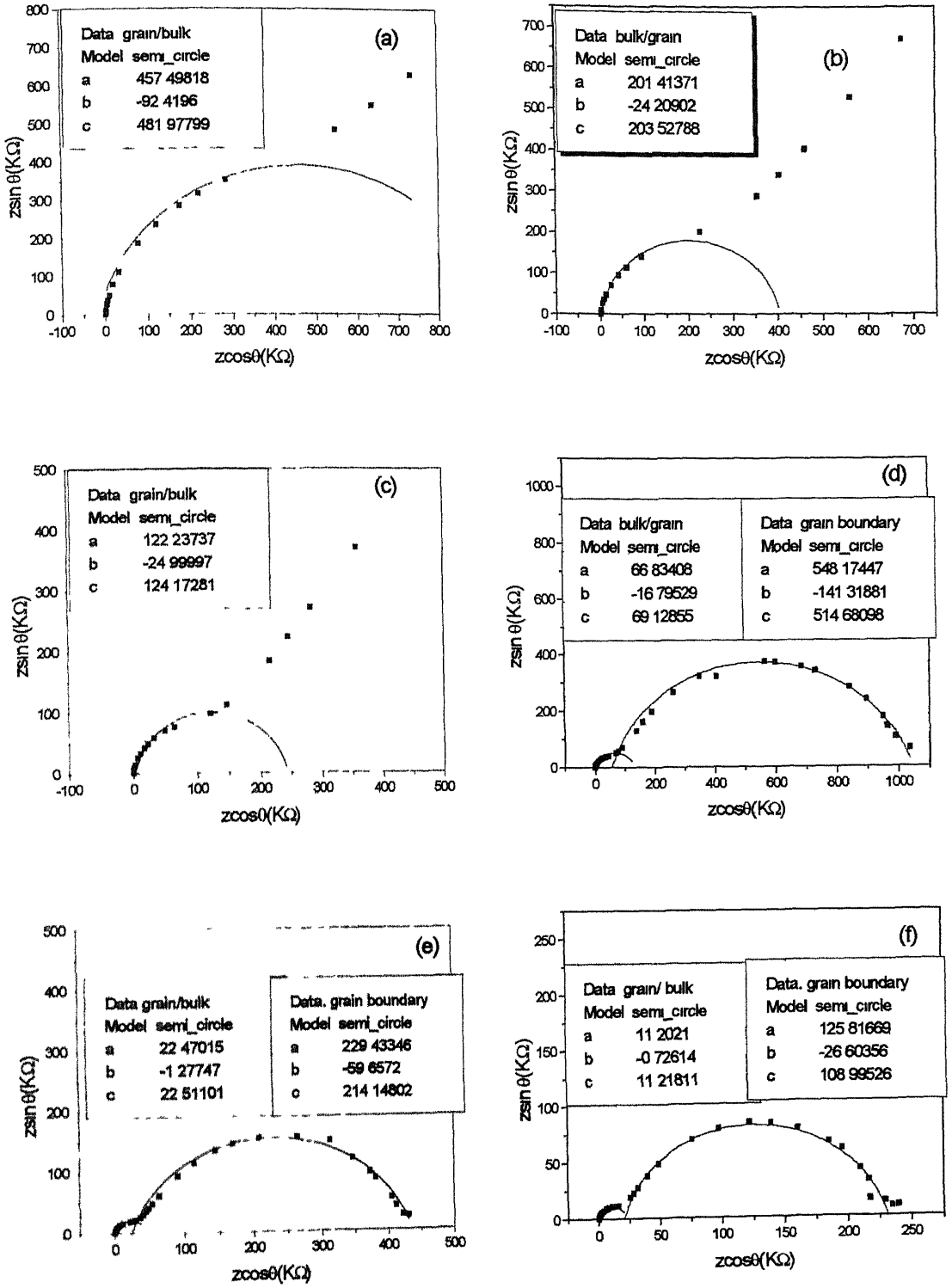

Fig 3.11. Cole-Cole plot for 5 mole % gadolinia doped zirconia at temperatures (a) 294°C (b) 285°C (c) 307°C (d) 330°C (e) 356°C (f) 374°C

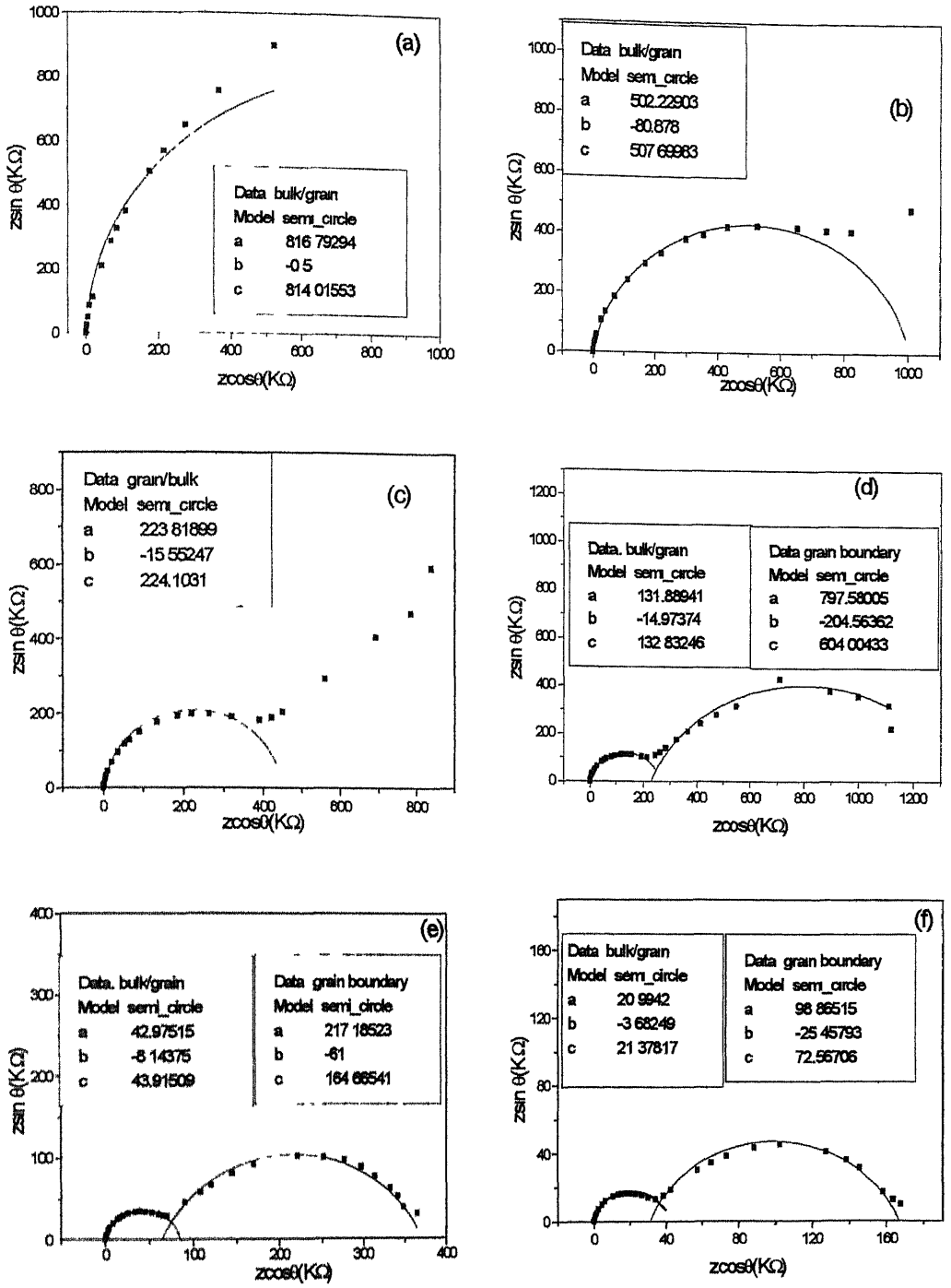
(a)
Data bulk/grain
Model semi_circle
a 816 79294
b -0 5
c 814 01553
zsin θ(KΩ)
zcosθ(KΩ)
(b)
Data bulk/grain
Model semi_circle
a 502.22903
b -80.878
c 507 69983
(c)
Data grain/bulk
Model semi_circle
a 223 81899
b -15 55247
c 224.1031
(d)
Data. bulk/grain
Model semi_circle
a 131.88941
b -14.97374
c 132 83246
Data grain boundary
Model semi_circle
a 797.58005
b -204.56362
c 604 00433
(e)
Data. bulk/grain
Model semi_circle
a 42.97515
b -5 14375
c 43.91509
Data grain boundary
Model semi_circle
a 217 18523
b -61
c 164 66541
(f)
Data bulk/grain
Model semi_circle
a 20 9942
b -3 68249
c 21 37817
Data grain boundary
Model semi_circle
a 98 86515
b -25 45793
c 72.56706

Fig. 3.12

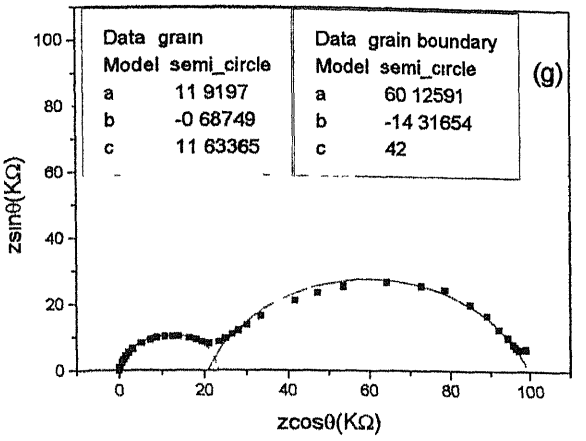

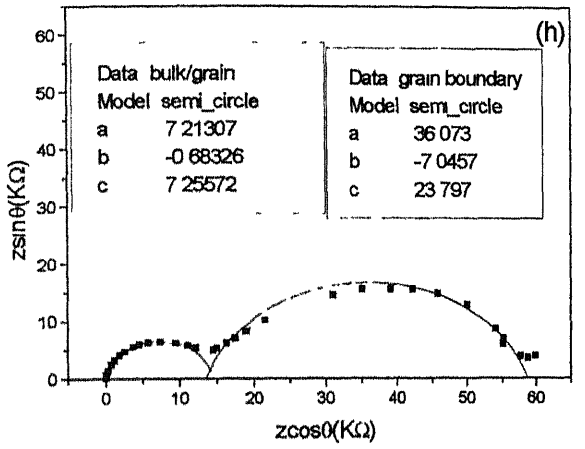

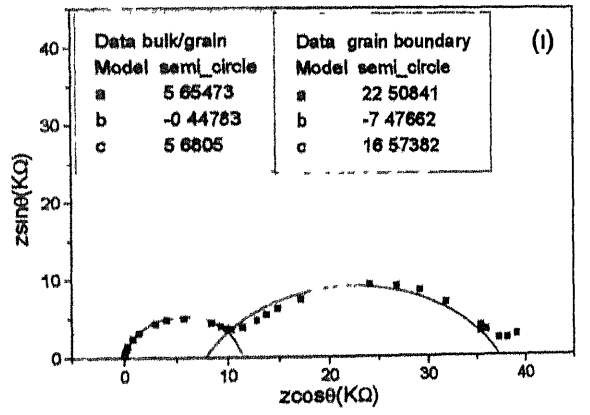

Fig 3.12. Cole-Cole plots for 8 mole % gadolinia doped zirconia bulk samples at temperatures (a) 236°C (b) 261°C (c) 279°C(d) 291°C (e) 324°C (f) 345°C (g) 362°C (h) 377°C and (i) 396°C

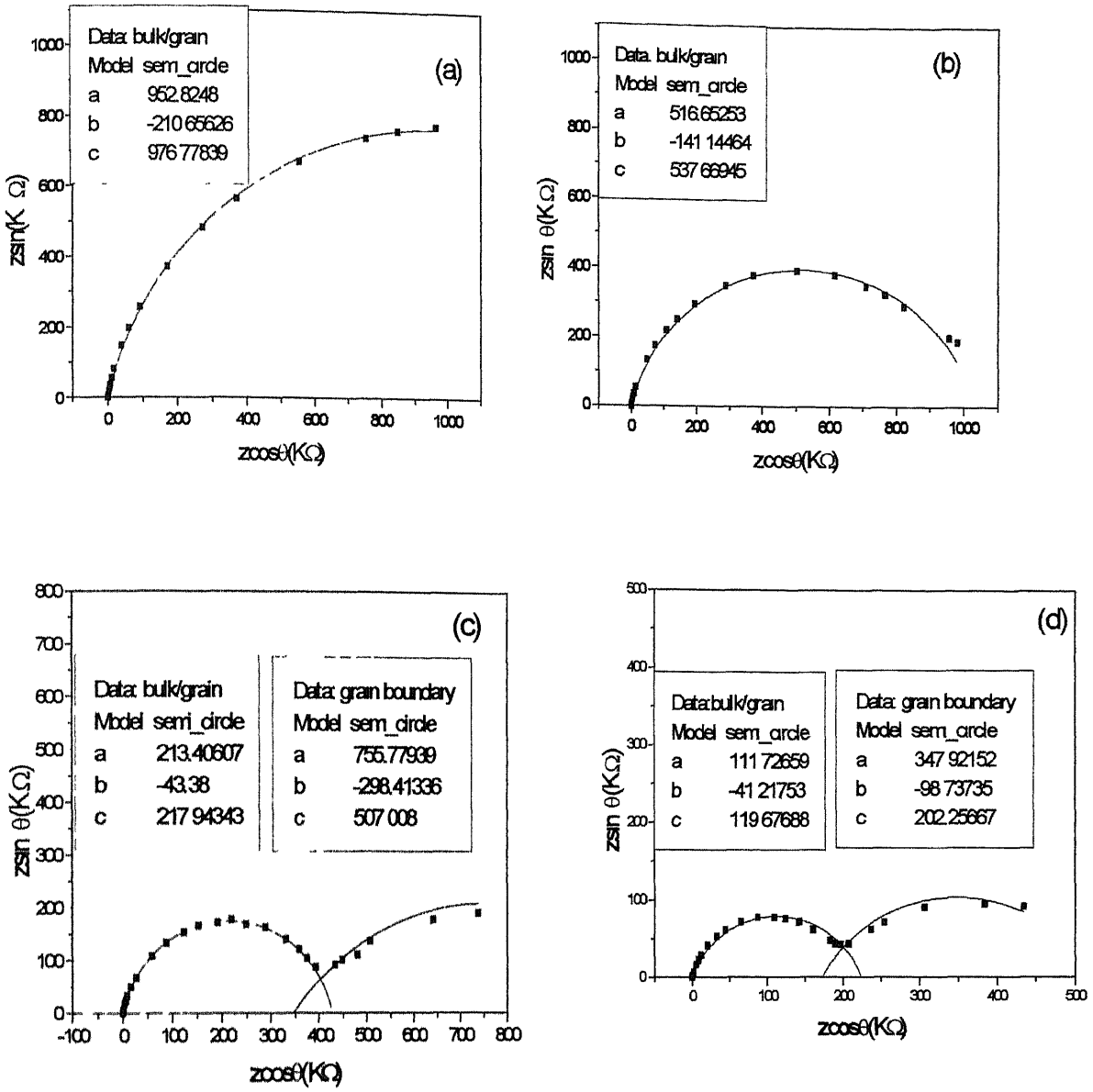
(a)
Data: bulk/grain
Model semi_circle
a 952.8248
b -210.65626
c 976.77839
zsin(K Ω)
zcosθ(KΩ)
(b)
Data: bulk/grain
Model semi_circle
a 516.65253
b -141.14464
c 537.66945
zsin θ(KΩ)
zcosθ(KΩ)
(c)
Data: bulk/grain
Model semi_circle
a 213.40607
b -43.38
c 217.94343
Data: grain boundary
Model semi_circle
a 755.77939
b -298.41336
c 507.008
zsin θ(KΩ)
zcosθ(KΩ)
(d)
Data: bulk/grain
Model semi_circle
a 111.72659
b -41.21753
c 119.67688
Data: grain boundary
Model semi_circle
a 347.92152
b -98.73735
c 202.25667
zsin θ(KΩ)
zcosθ(KΩ)

Fig. 3.13

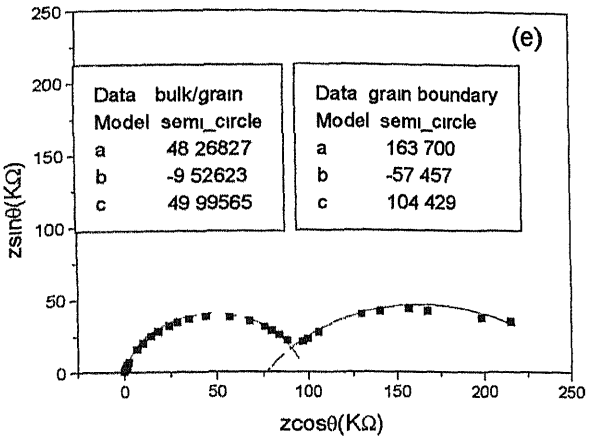

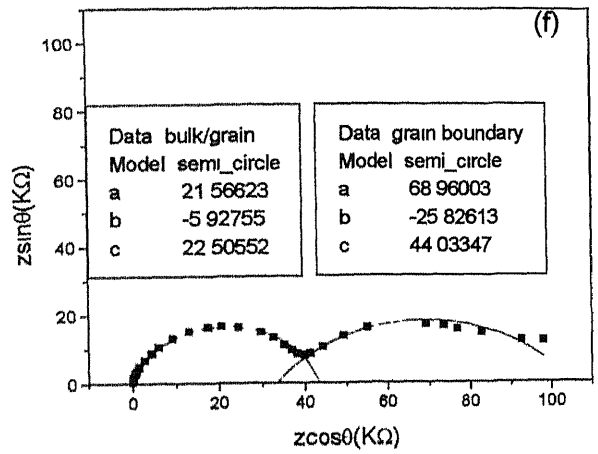

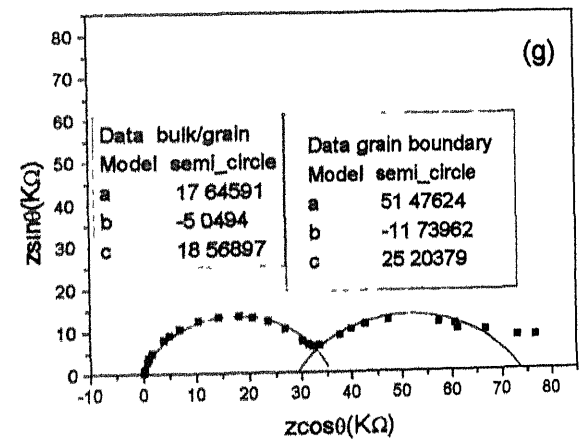

Fig 3.13. Cole-Cole plots for 9 mole % gadolinia doped zirconia bulk samples at temperatures (a) 201 (b) 230°C (c) 241°C (d) 262°C (e) 294°C (f) 311°C (g) 322°C

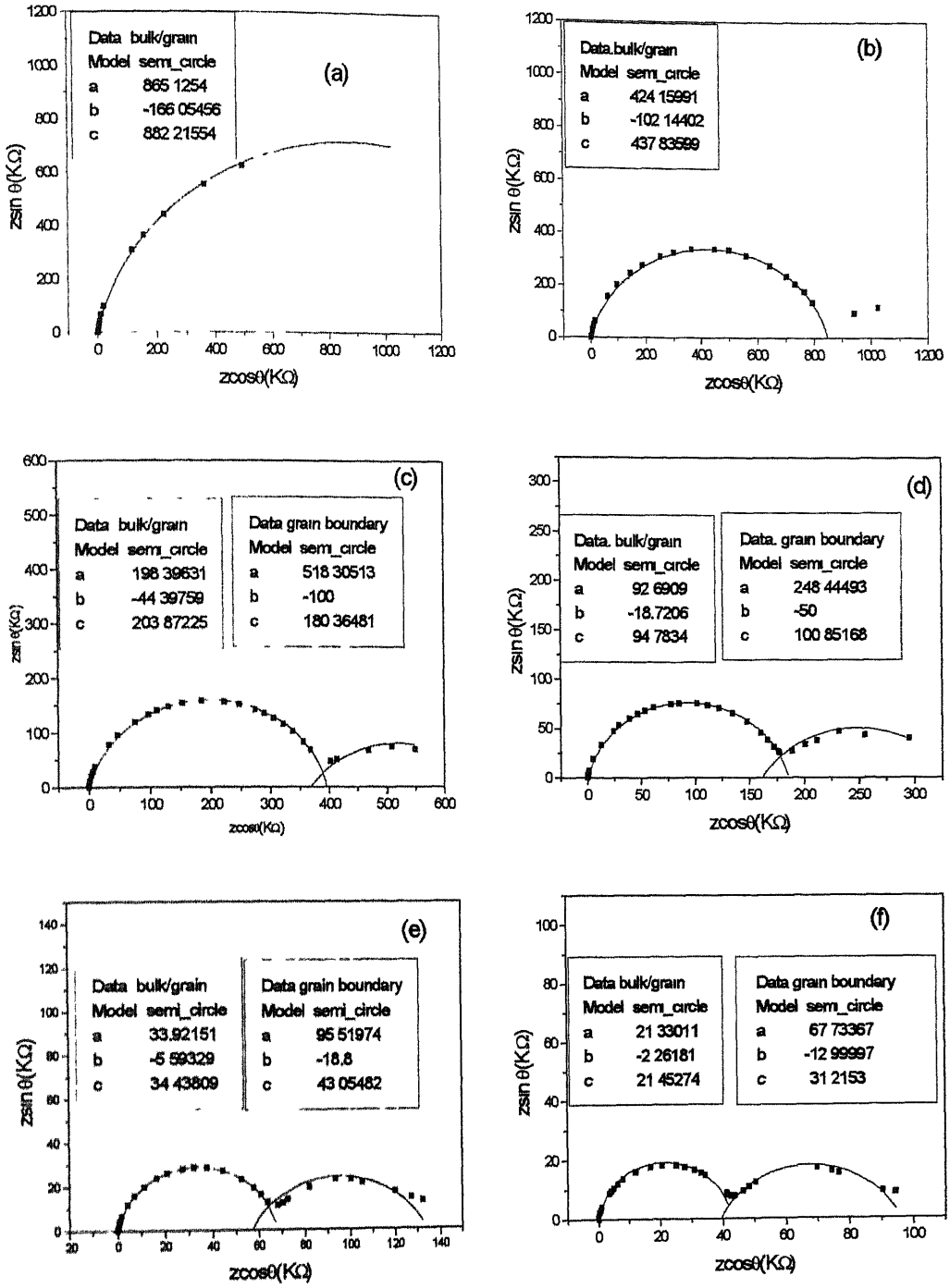
(a)
Data bulk/grain
Model semi_circle
a 865 1254
b -166 05456
c 882 21554
zsin θ(KΩ)
zcosθ(KΩ)
(b)
Data.bulk/grain
Model semi_circle
a 424 15991
b -102 14402
c 437 83599
zsin θ(KΩ)
zcosθ(KΩ)
(c)
Data bulk/grain
Model semi_circle
a 198 39631
b -44 39759
c 203 87225
Data grain boundary
Model semi_circle
a 518 30513
b -100
c 180 36481
zsin θ(KΩ)
zcosθ(KΩ)
(d)
Data. bulk/grain
Model semi_circle
a 92 6909
b -18.7206
c 94 7834
Data. grain boundary
Model semi_circle
a 248 44493
b -50
c 100 85168
zsin θ(KΩ)
zcosθ(KΩ)
(e)
Data bulk/grain
Model semi_circle
a 33.92151
b -5 59329
c 34 43809
Data grain boundary
Model semi_circle
a 95 51974
b -18.8
c 43 05482
zsin θ(KΩ)
zcosθ(KΩ)
(f)
Data bulk/grain
Model semi_circle
a 21 33011
b -2 26181
c 21 45274
Data grain boundary
Model semi_circle
a 67 73367
b -12 99997
c 31 2153
zsin θ(KΩ)
zcosθ(KΩ)

Fig 3 14

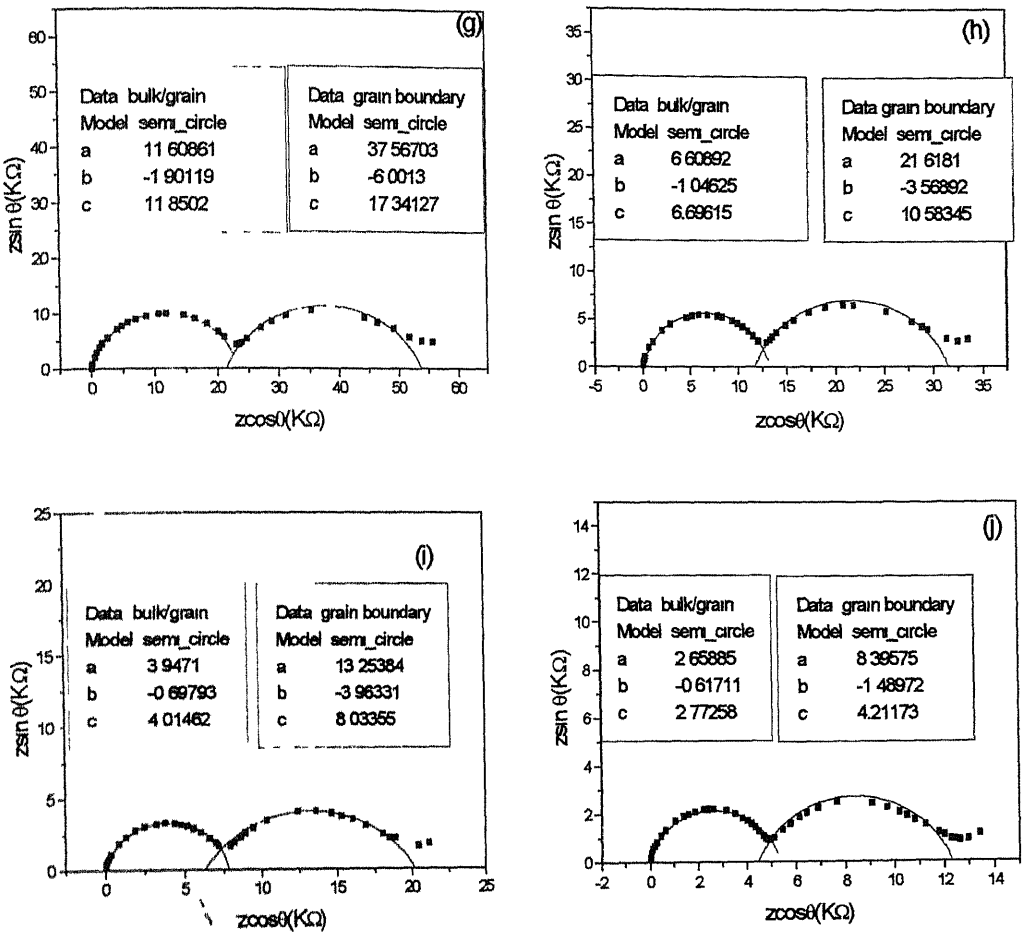

Fig 3.14. Cole-Cole plot of 11mole % gadolinia doped zirconia bulk samples at temperatures (a) 217°C (b) 240 °C (c) 261 °C (d) 282 °C (e) 312 °C (f) 327 °C (g) 348 °C (h) 368 °C (i) 388 °C and (j) 408 °C

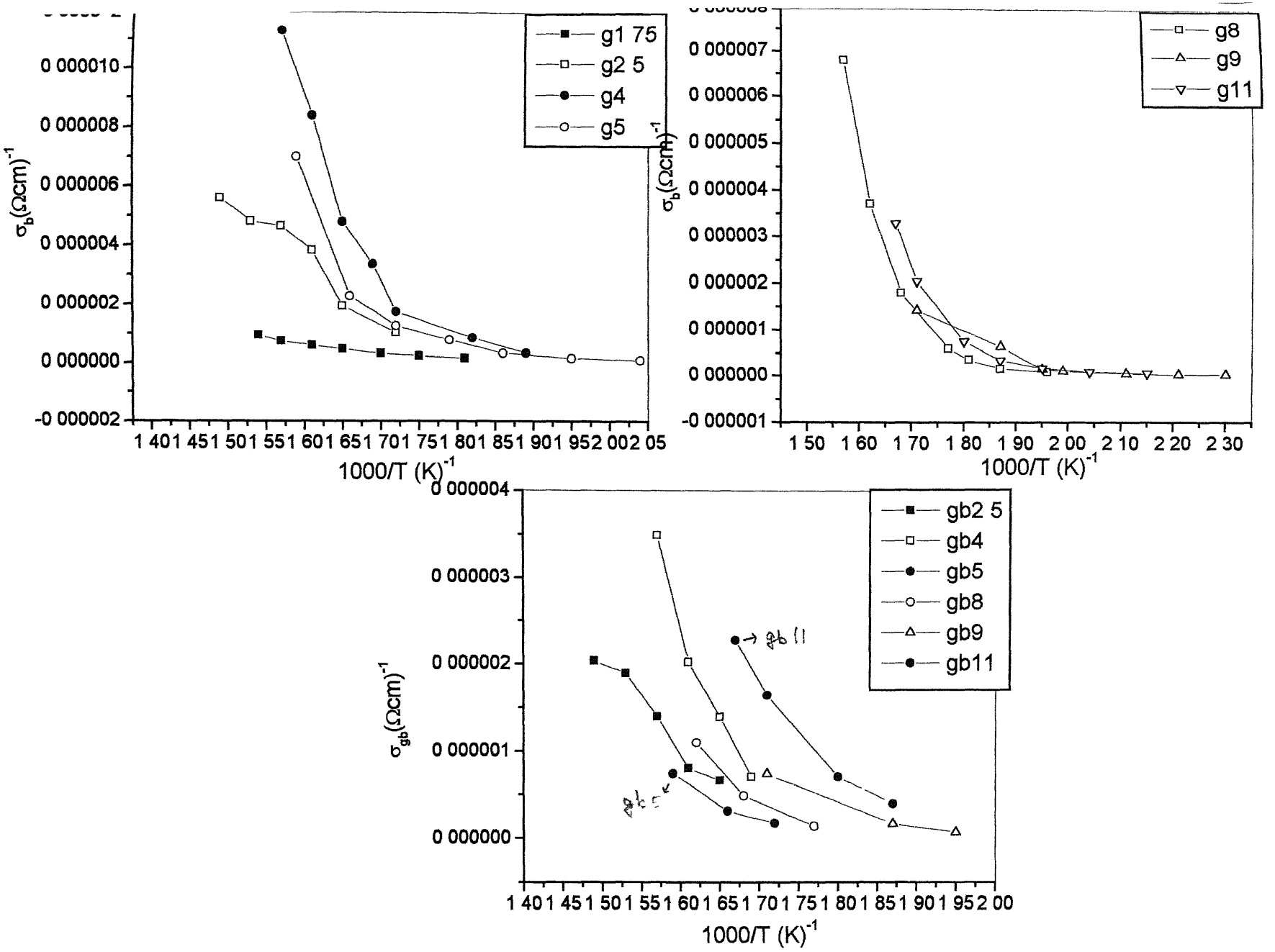

Fig.3.15 Variation of grain and grain boundary conductivity with temperature at different compositions in the gadolinia-zirconia system

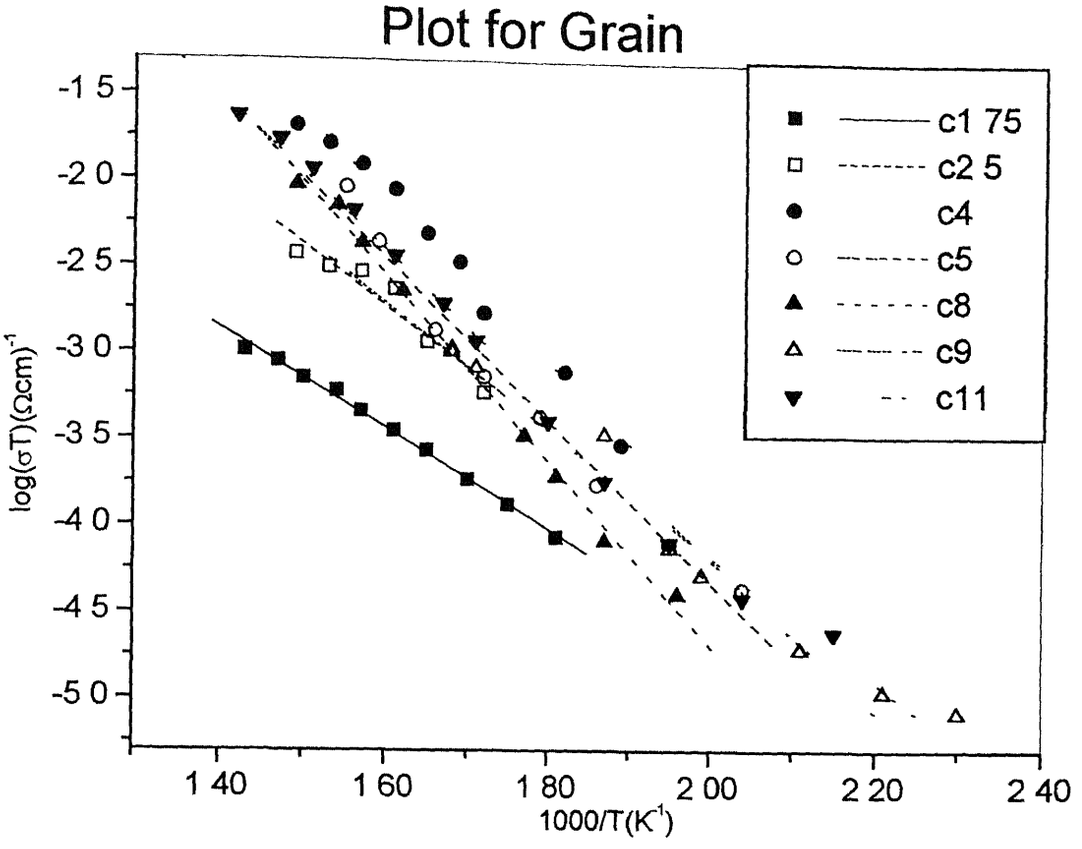

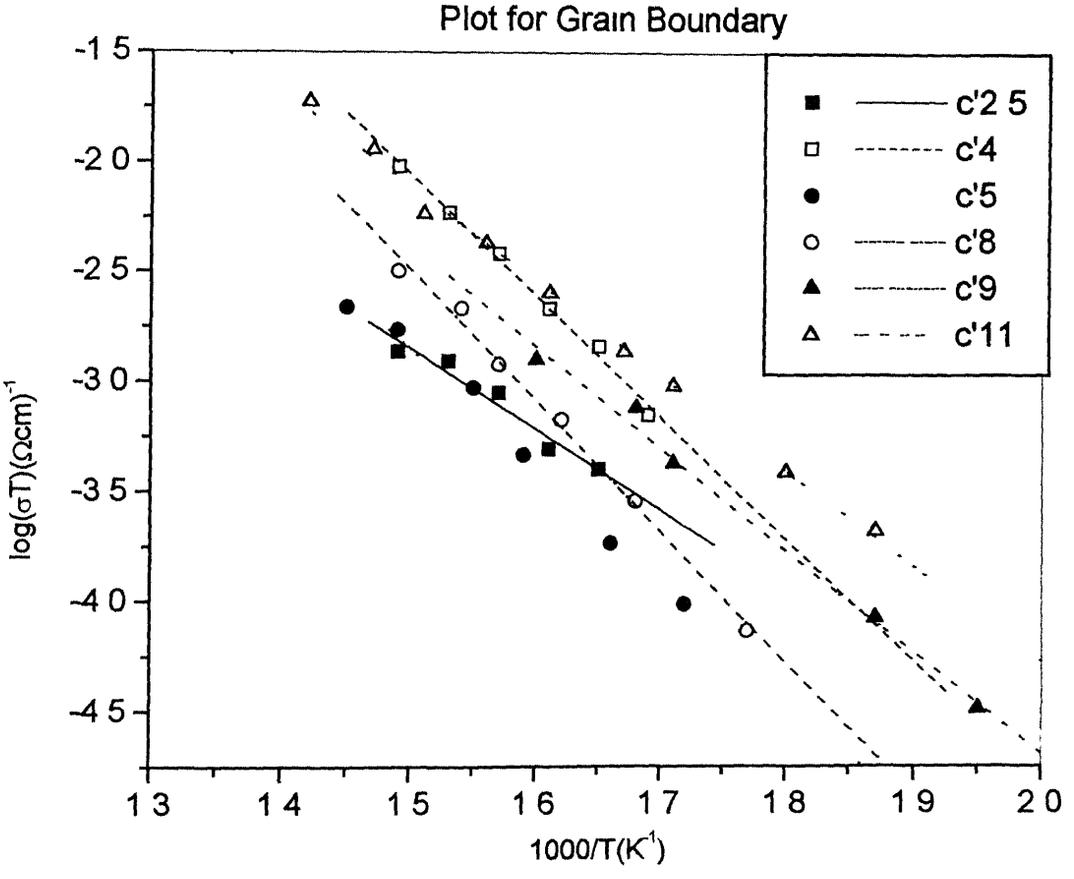

Fig.3.16 Arhennius plot showing linear fit to Log(σT) vs inverse of temperature for both grain and grain boundary effects for different mole% of Gd_2O_3

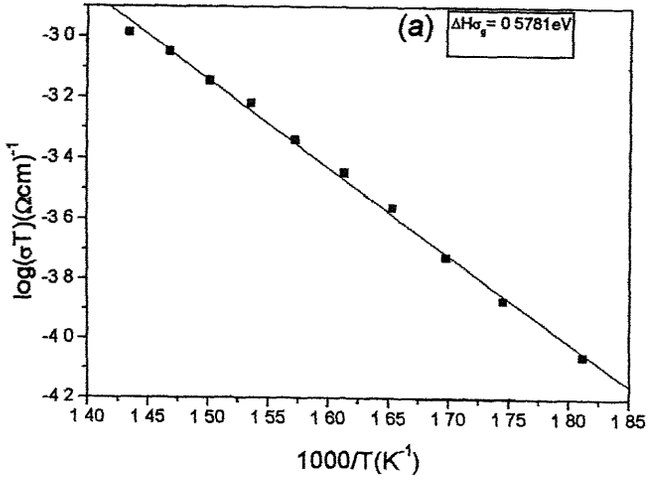
(a)
ΔHσg= 0 5781eV
log(σT)(Ωcm)-1
1000/T(K-1)

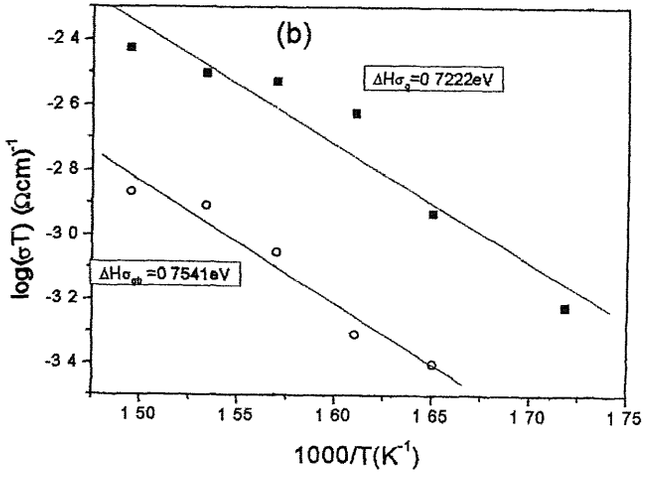
(b)
ΔHσg=0 7222eV
ΔHσgb =0 7541eV
log(σT) (Ωcm)-1
1000/T(K-1)

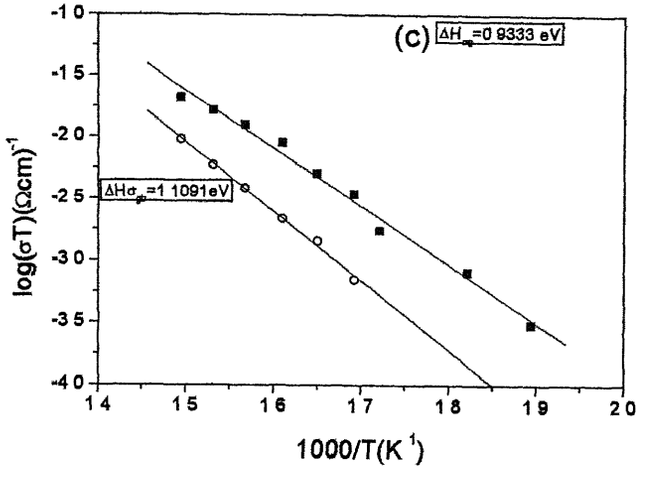
(c)
ΔHσgb=1 1091eV
log(σT)(Ωcm)-1
1000/T(K-1)

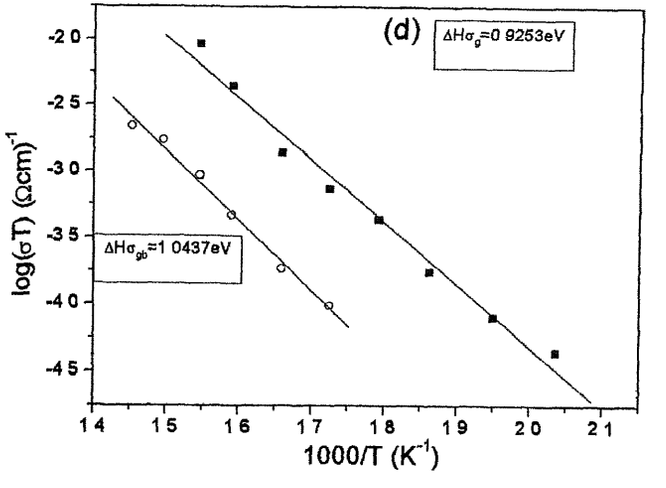
(d)
ΔHσg=0 9253eV
ΔHσgb=1 0437eV
log(σT) (Ωcm)-1
1000/T (K-1)

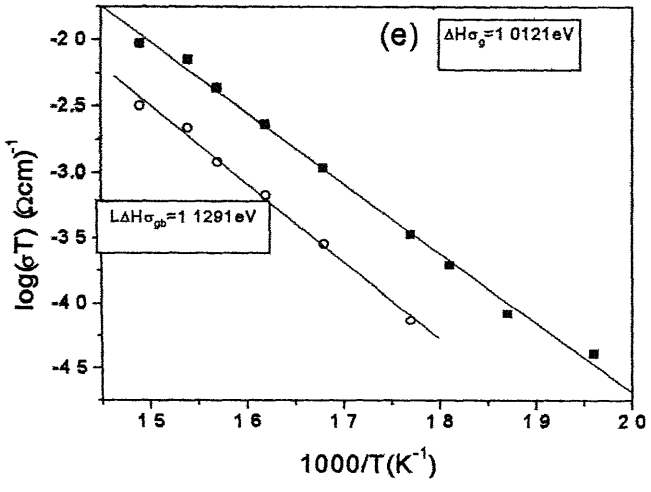

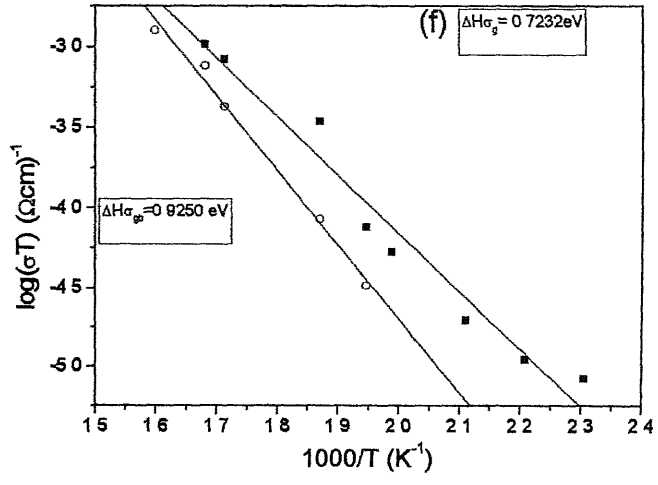

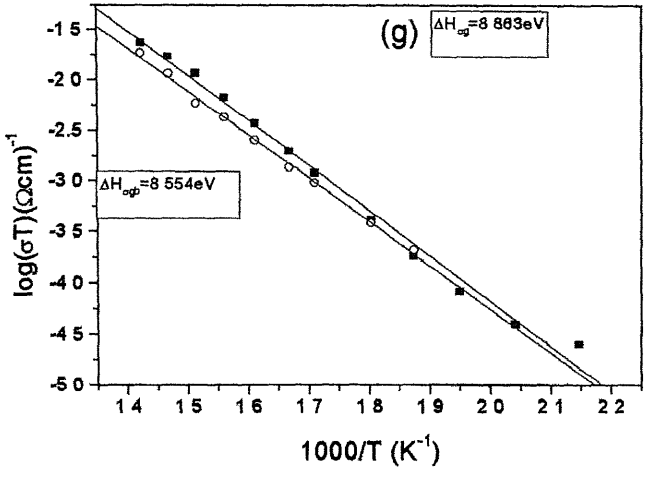

Fig 3.17. Arrhenius plots showing activation enthalpy for conduction for (a) 1.75 (b) 2.5 (c) 4.0 (d) 5.0 (e) 8.0 (f) 9.0 And (g) 11.0 mole % gadolinia doped zirconia bulk samples

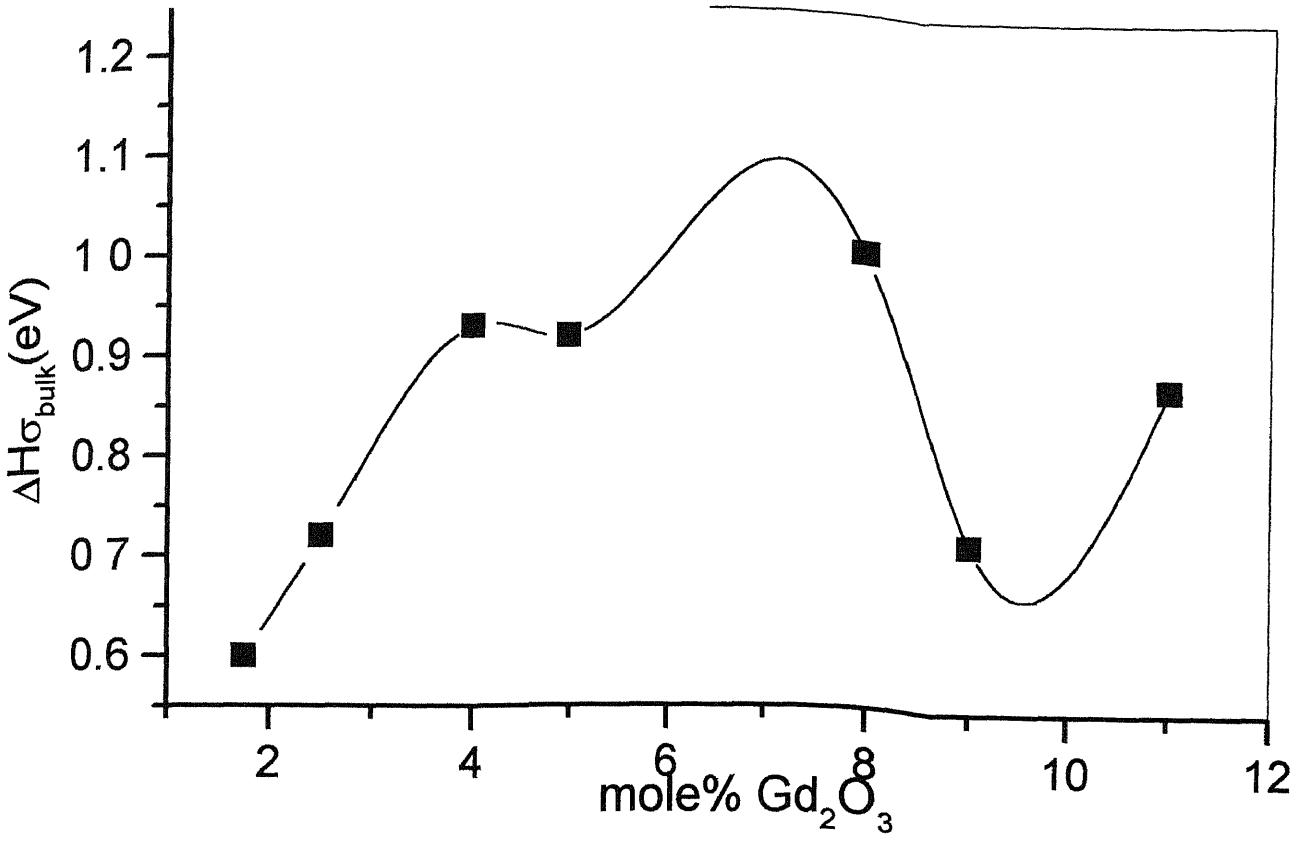

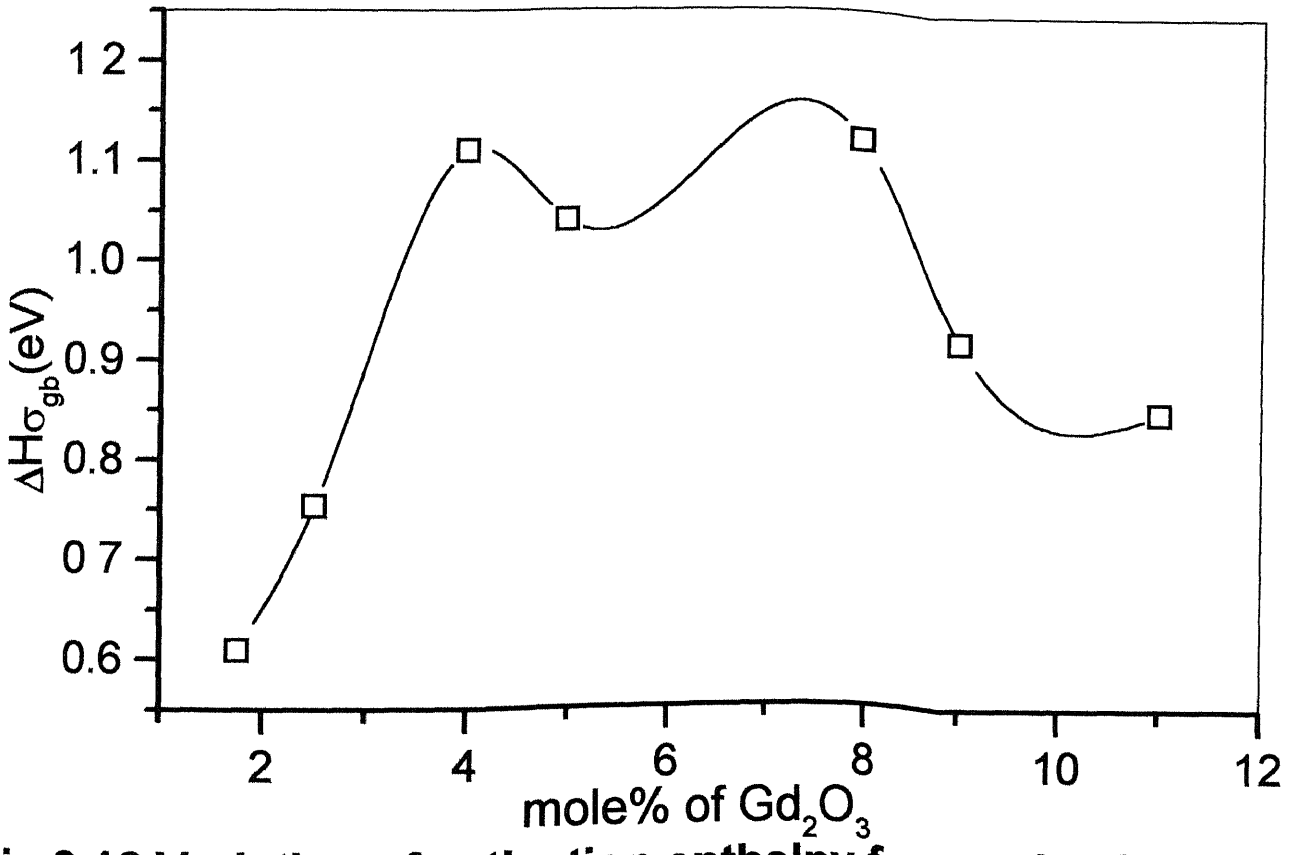

Fig.3.18 Variation of activation enthalpy for conduction with composition for both grain and grain boundary contribution

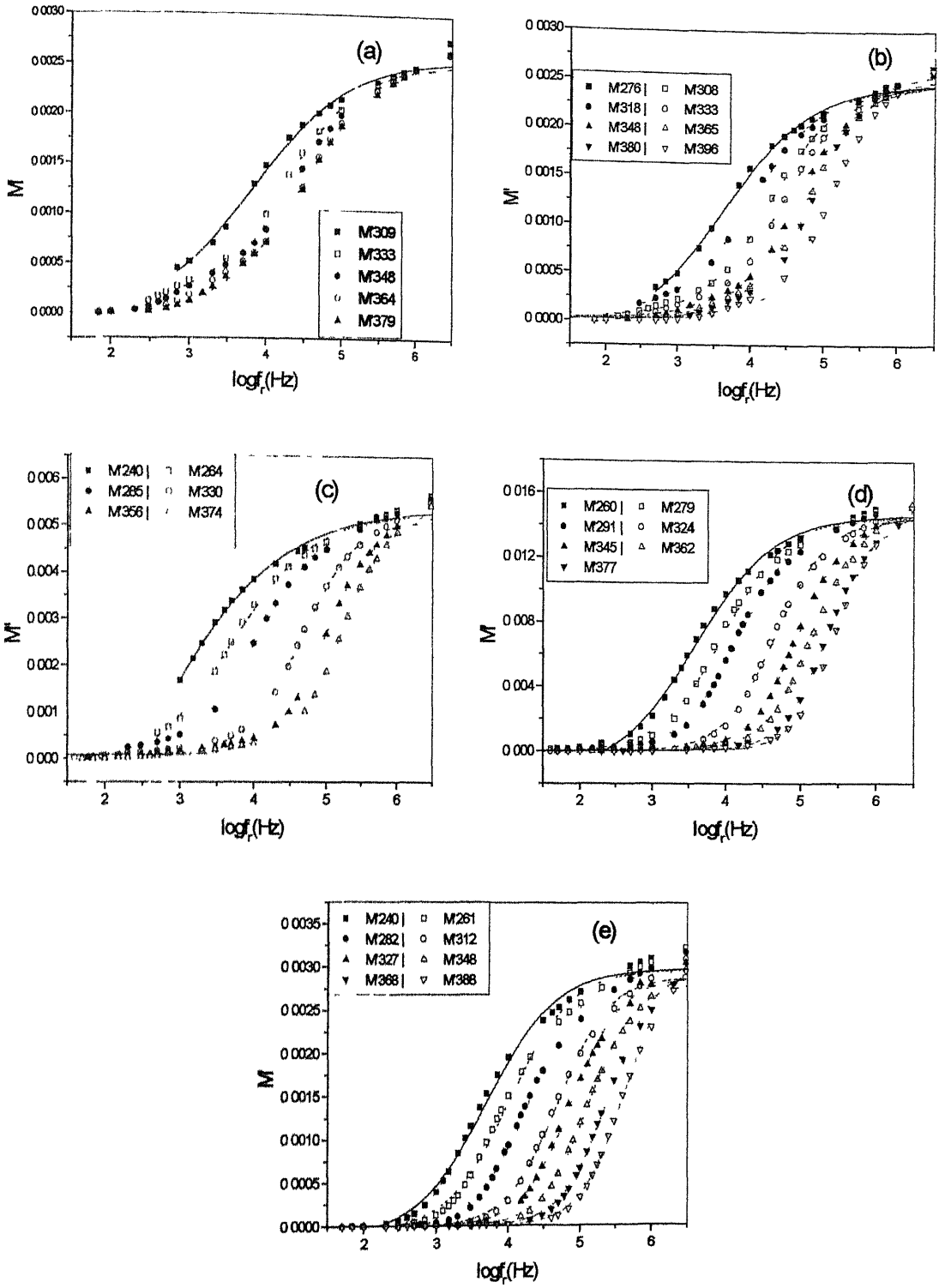

Fig. 3.19 Plots showing lorentzian fit of the imaginary part of modulus vs logarithm of frequency for (a) 2.5 (b) 4 (c) 5 (d) 8 (e) 9 and (f) 11 mole% gadolinia doped zirconia bulk samples

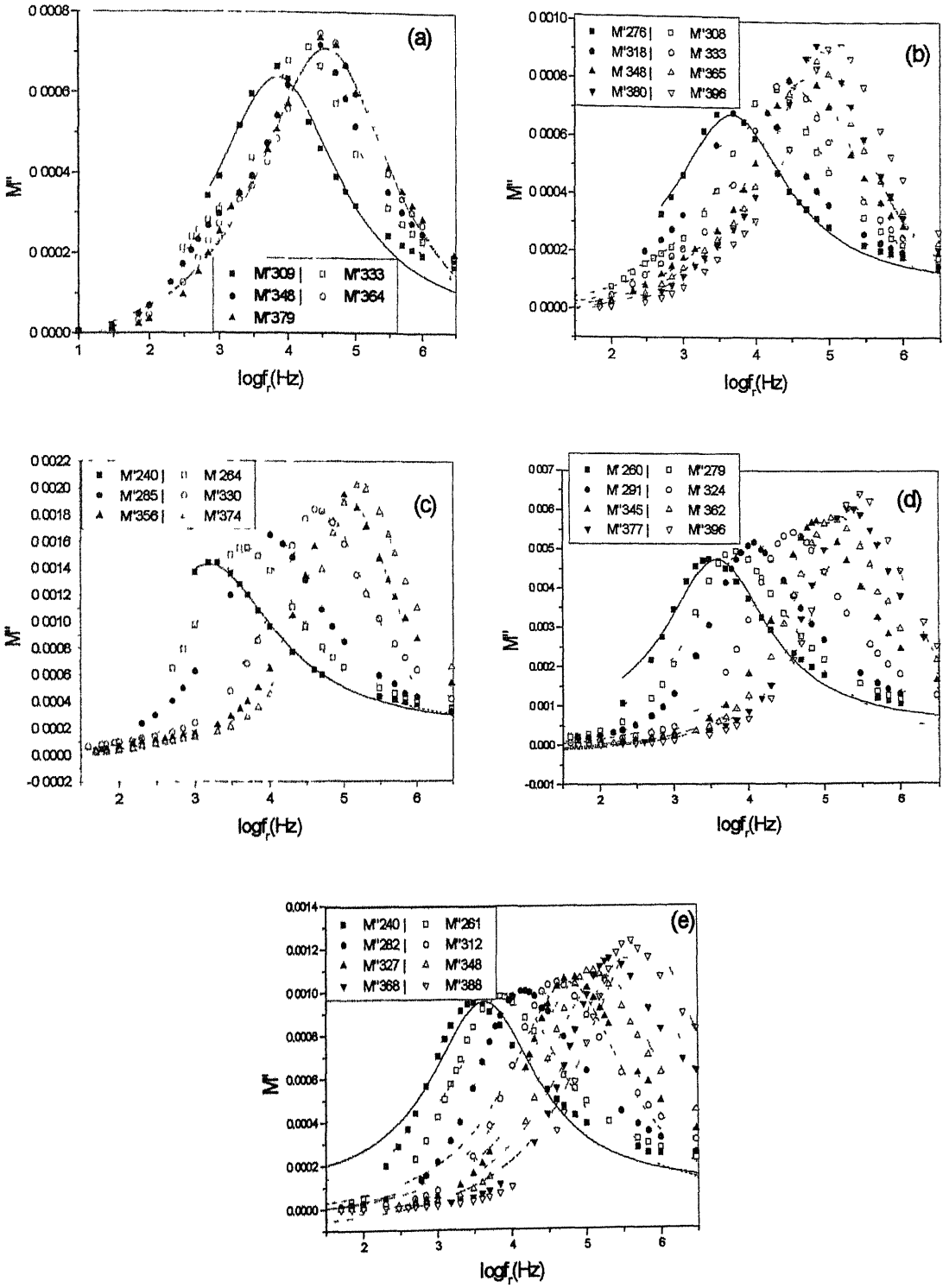

Fig. 3.20 Plots showing sigmoidal fit of the real part of modulus vs logarithm of frequency for (a) 2.5 (b) 4 (c) 5 (d) 8 ~~(e) 9~~ and ~~(f)~~ 11 mole% gadolinia doped zirconia bulk samples

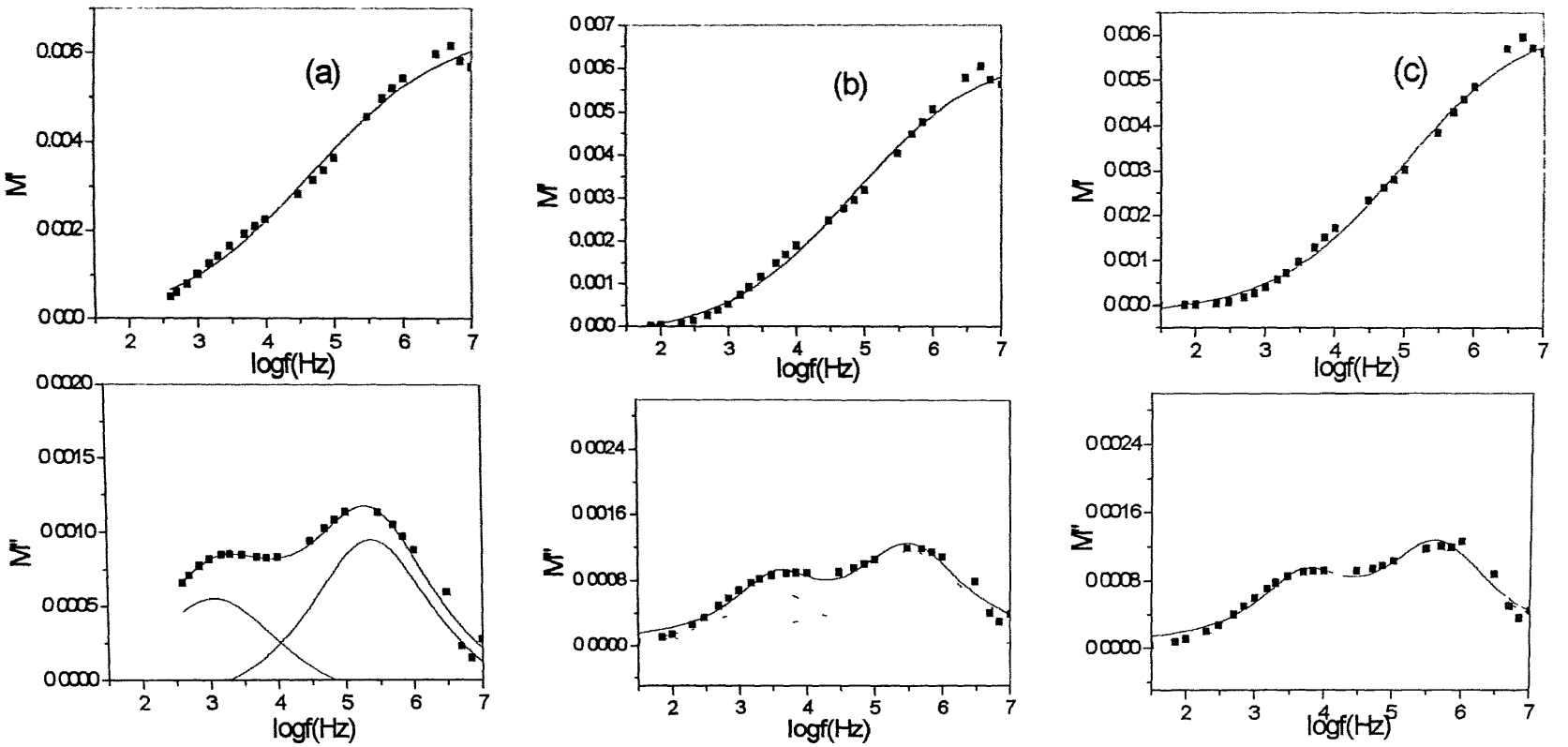
(a)
(b)
(c)
M'
M''
logf(Hz)

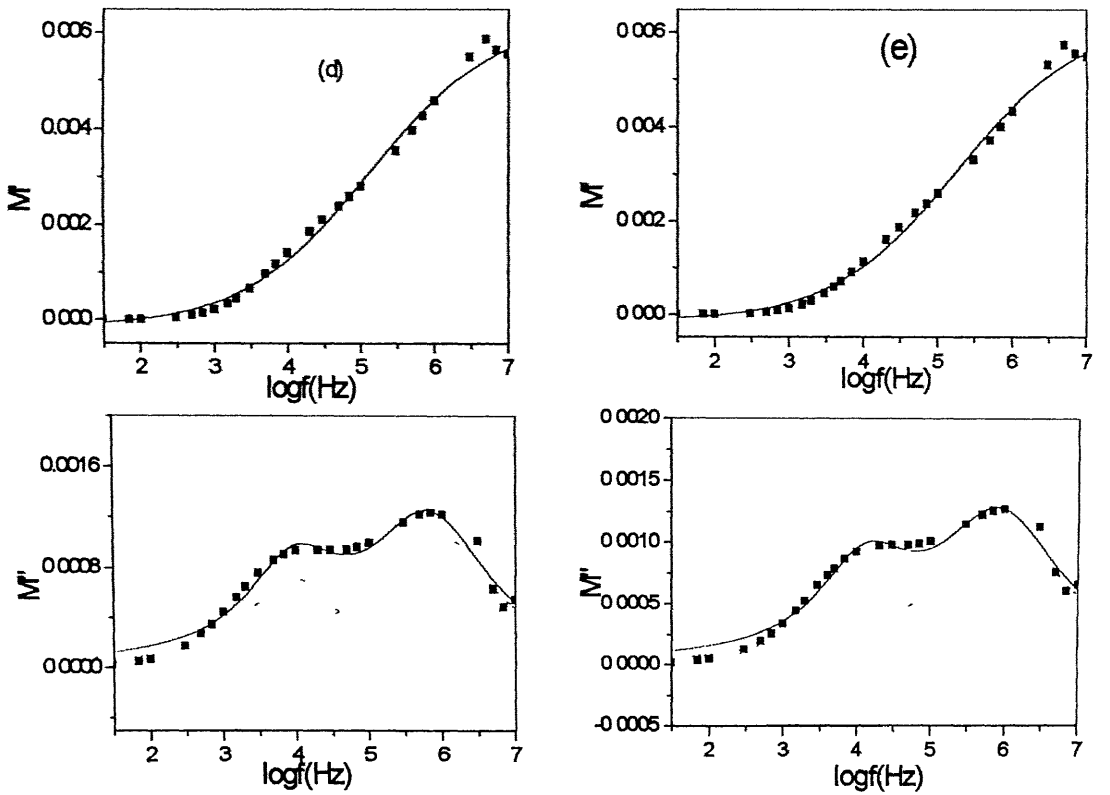

g. 3.21 Plots Showing Sigmoidal and Lorentzian Fits to the Real and Imaginary Parts of Modulus vs Logarithm of Frequency Respectively for 1.75 Mole% Gadolinia Doped Zirconia Bulk Samples at Temperatures a) 260°C (b) 300 °C (c) 332 °C (d) 363 °C and (e)393 °C

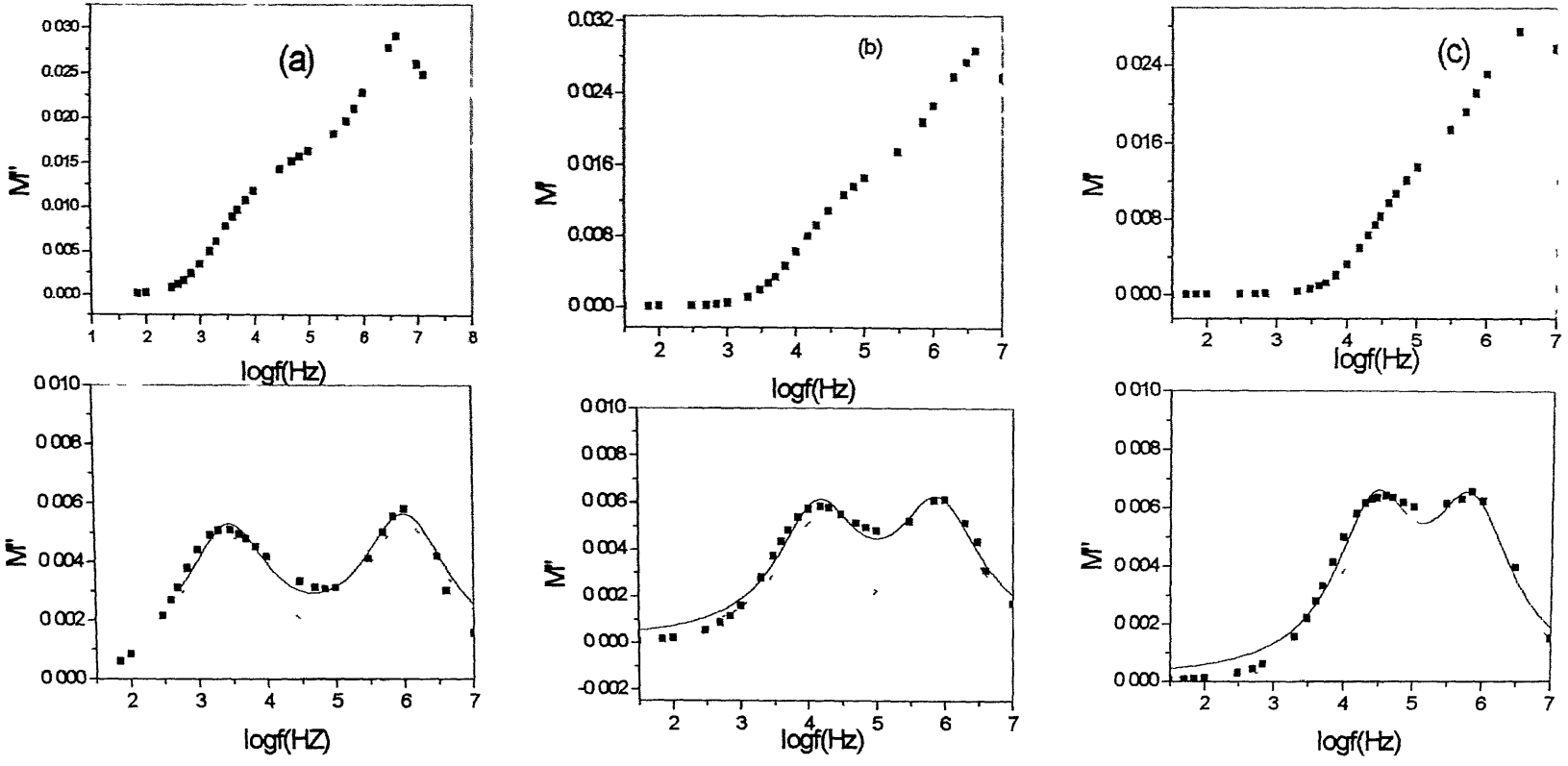
(a)
(b)
(c)
M'
logf(Hz)
logf(HZ)

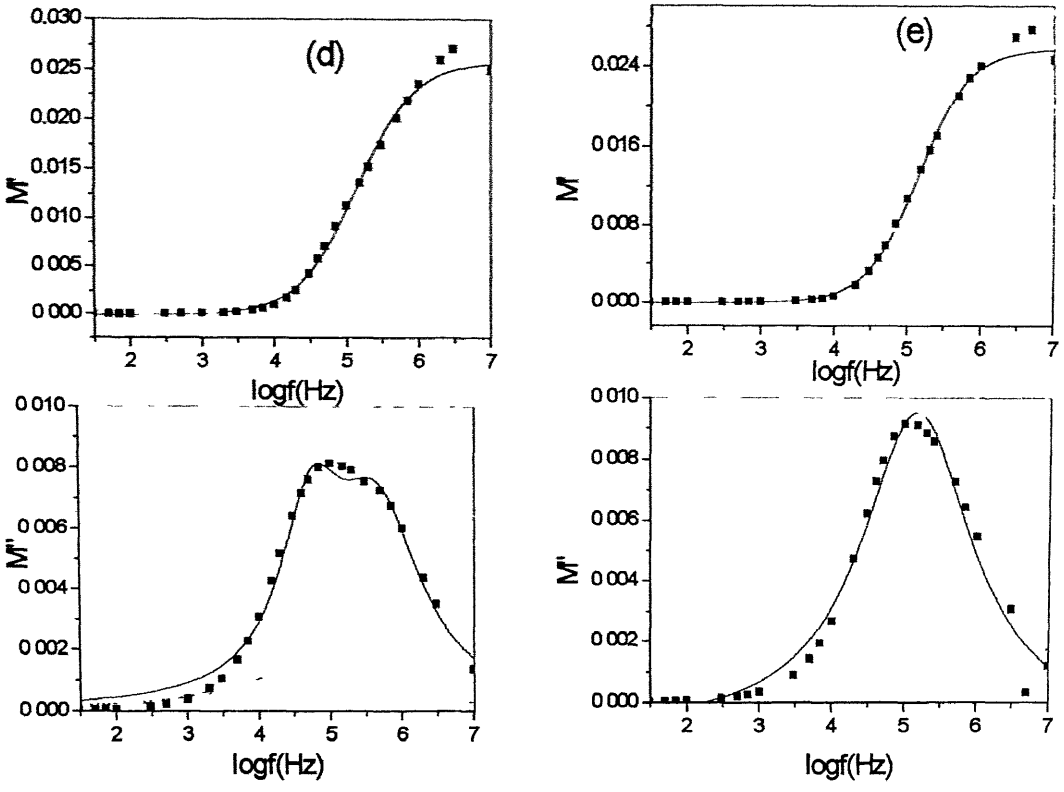

Fig. 3.22 Plots Showing the Real and Imaginary Parts of Modulus vs Logarithm of Frequency Respectively for 9 Mole% Gadolinia Doped Zirconia Bulk Samples at Temperatures a) 230°C (b) 262 °C (c) 294 °C (d) 311 °C and (e)322 °C

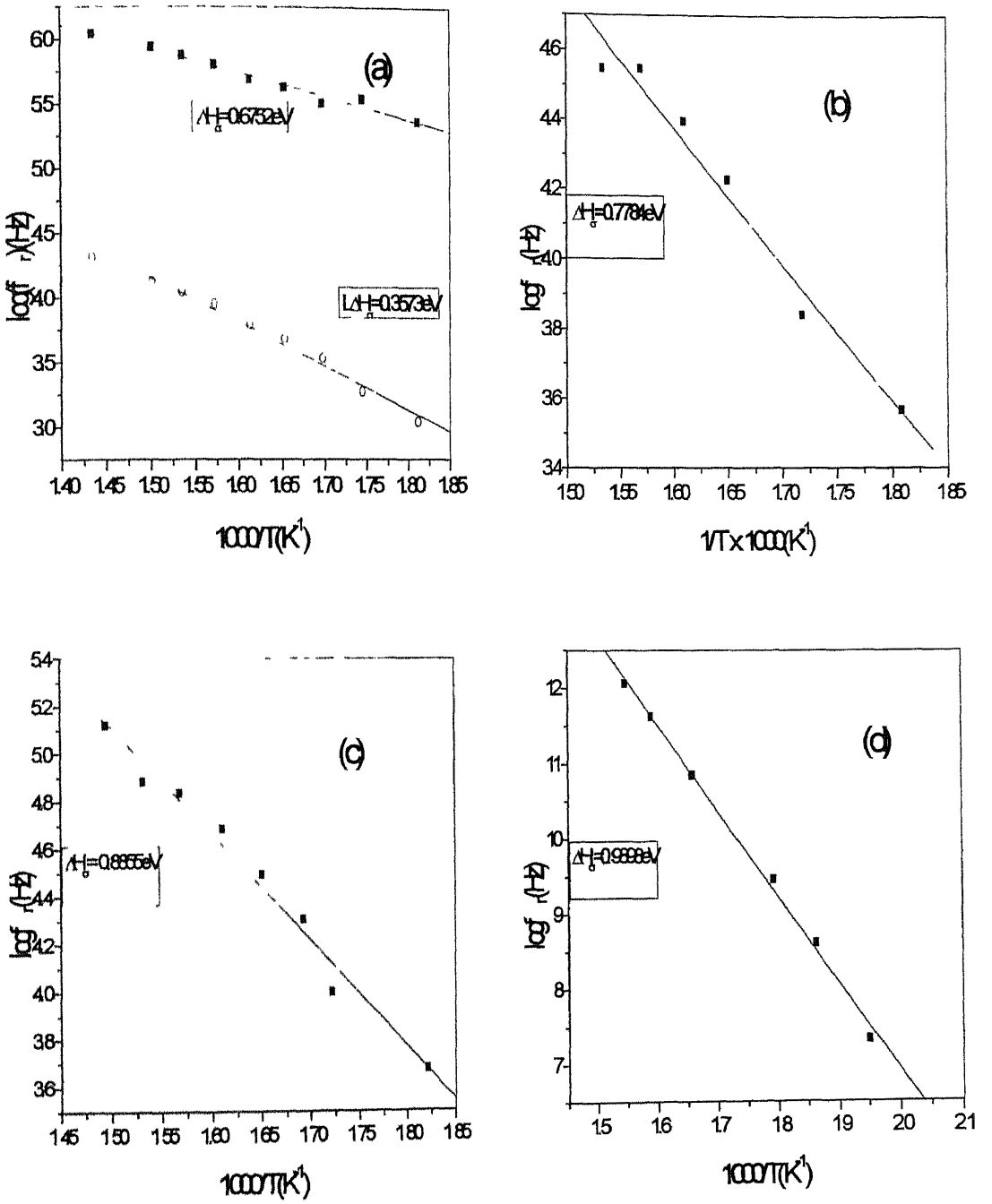
(a)
ΔH=0.6752eV
ΔH=0.3573eV
log f (Hz)
1000/T(K⁻¹)
(b)
ΔH=0.7784eV
log f (Hz)
1/T x 1000(K⁻¹)
(c)
ΔH=0.8855eV
log f (Hz)
1000/T(K⁻¹)
(d)
ΔH=0.9898eV
log f (Hz)
1000/T(K⁻¹)

Fig. 3.23

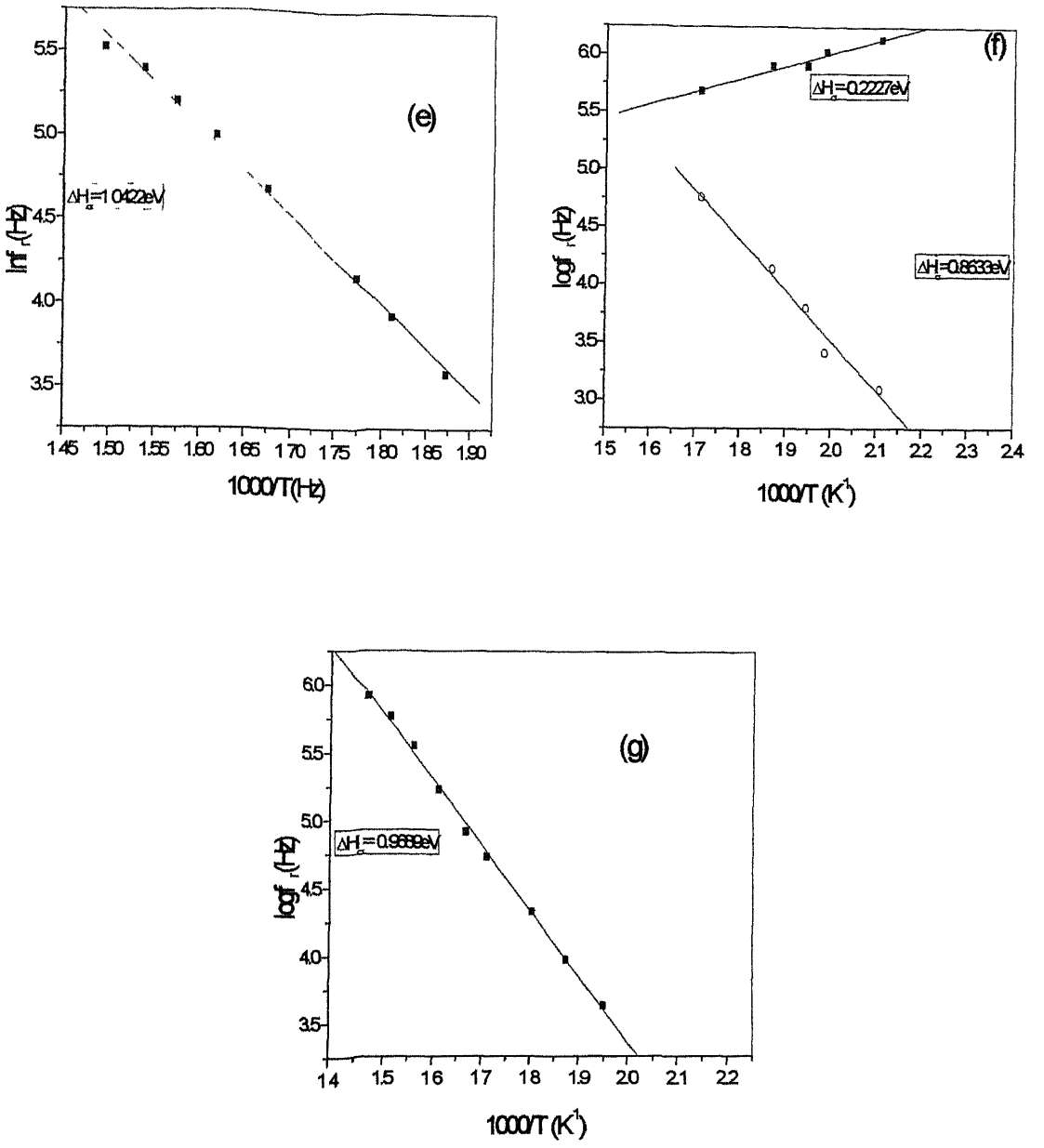

Fig. 3.23 Arhennius Plots showing activation enthalpy for conduction from modulus plots for (a) 1.7.5 (b)2.5 (c) 4 (d) 5 (e) 8 (f) 9 and (g) 11 mole% gadolinia doped zirconia bulk samples

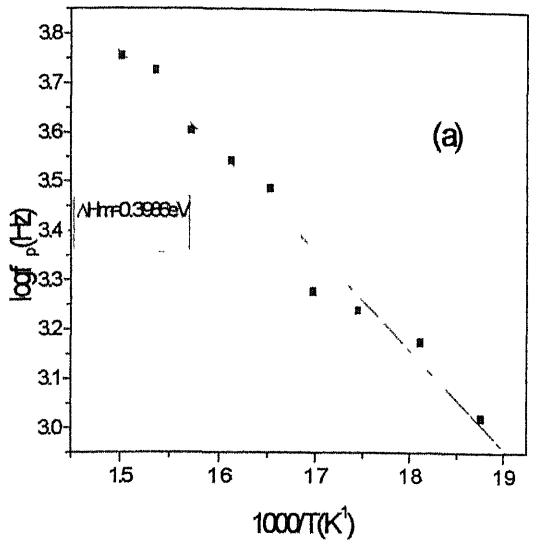
(a)
ΔHm=0.3988eV
logf p(Hz)
1000/T(K-1)

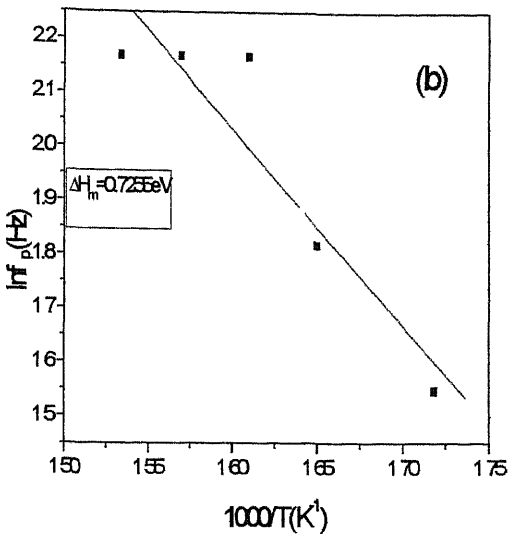
(b)
ΔHm=0.7255eV
lnf p(Hz)
1000/T(K-1)

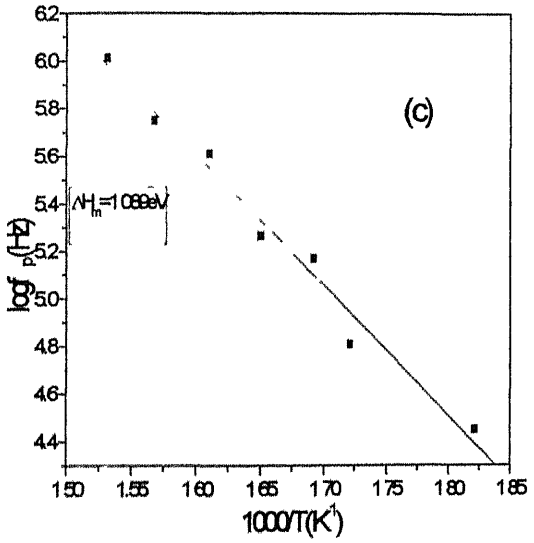
(c)
ΔHm=1.089eV
logf p(Hz)
1000/T(K-1)

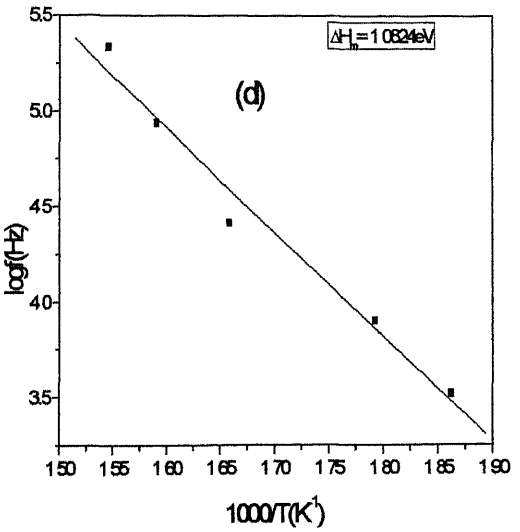
(d)
ΔHm=1.0824eV
logf(Hz)
1000/T(K-1)

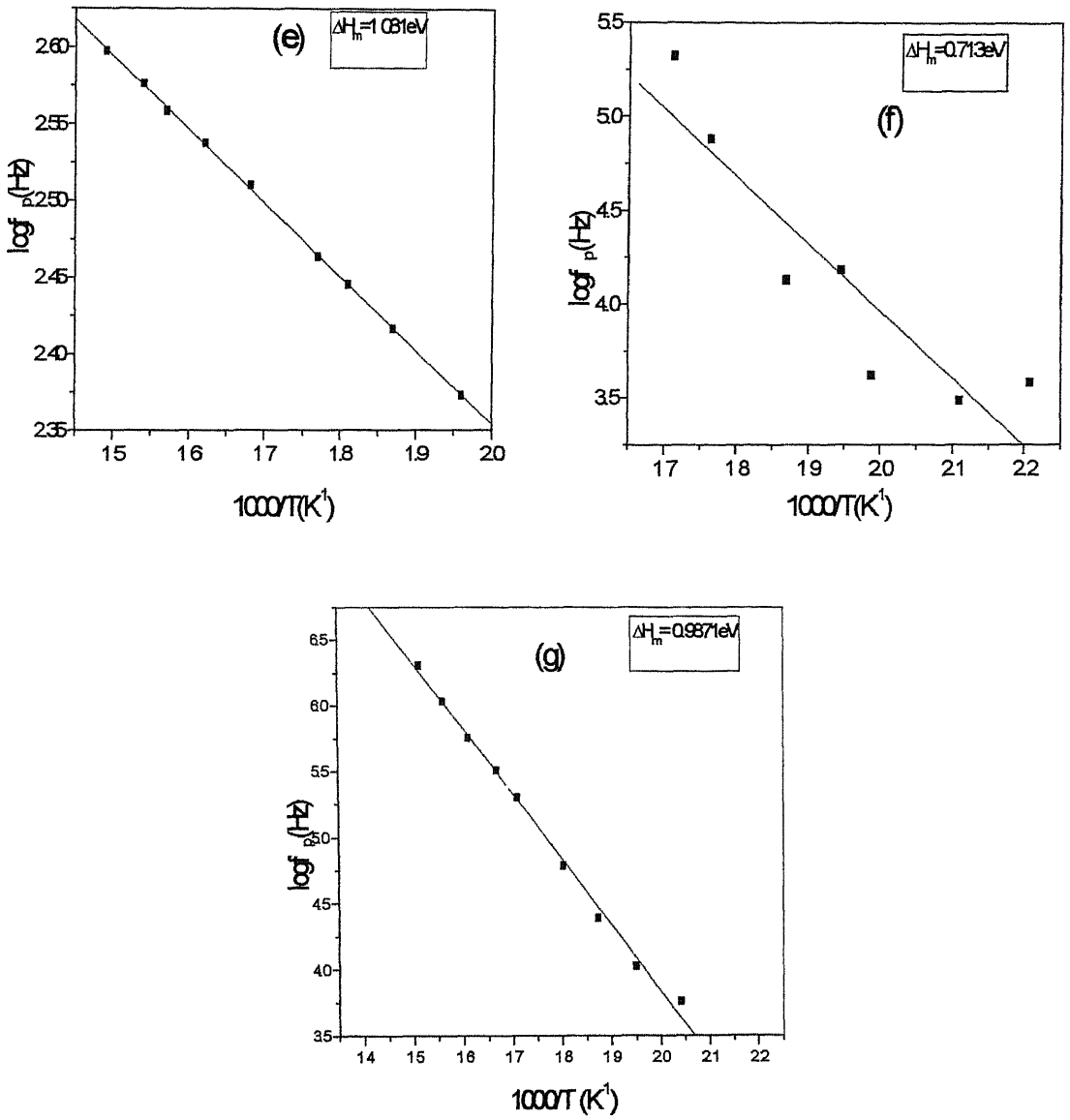

Fig. 3.24 Arhennius Plots showing activation enthalpy for migration for (a) 2.5 (b) 4 (c) 5 (d) 8 (e) 9 and (f) 11 mole% gadolinia doped zirconia bulk samples

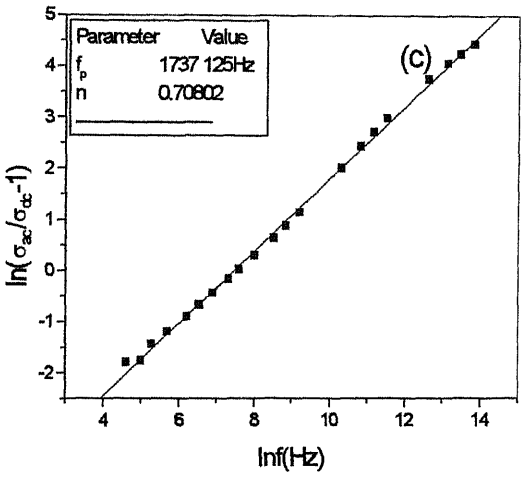
Parameter Value
f_p 1737.125Hz
n 0.70802
(c)
$\ln(\sigma_{ac}/\sigma_{dc}-1)$
lnf(Hz)

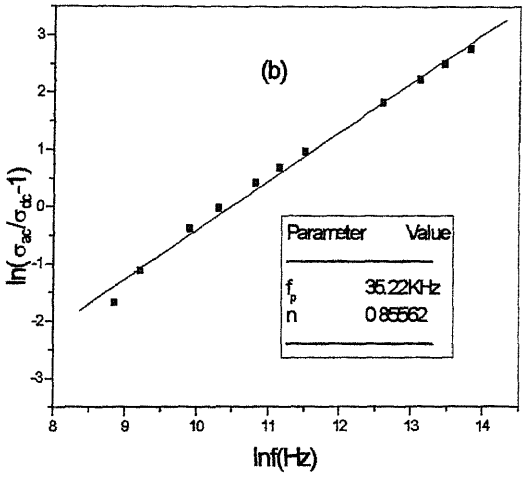
(b)
Parameter Value
f_p 35.22KHz
n 0.85562
$\ln(\sigma_{ac}/\sigma_{dc}-1)$
lnf(Hz)

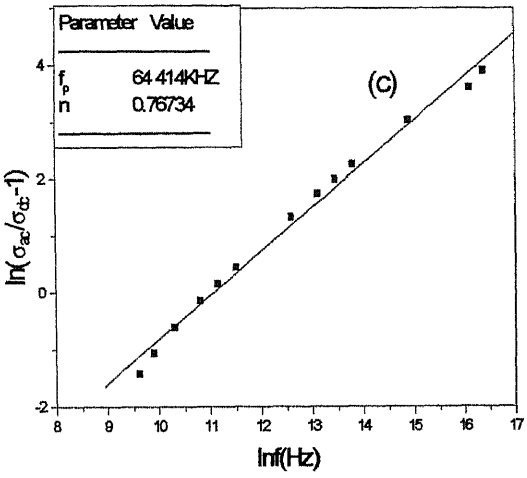
Parameter Value
f_p 64.414KHZ
n 0.76734
(c)
$\ln(\sigma_{ac}/\sigma_{dc}-1)$
lnf(Hz)

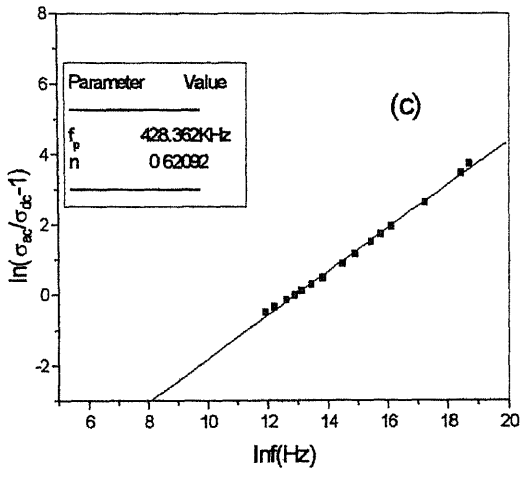
Parameter Value
f_p 428.362KHz
n 0.62092
(c)
$\ln(\sigma_{ac}/\sigma_{dc}-1)$
lnf(Hz)

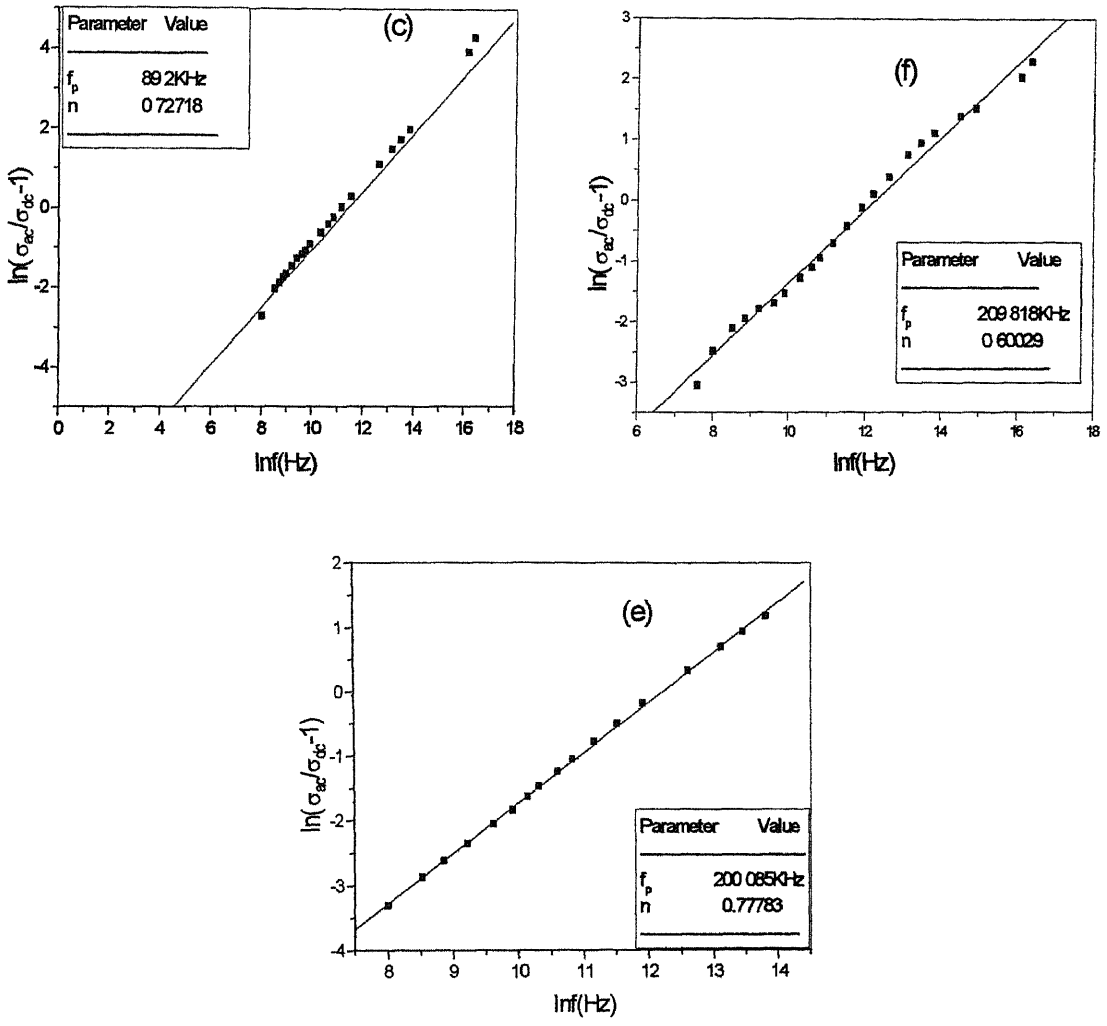

Fig. 3.2.5 Plots for curve fitting the Almond And West Equation to obtain the values of Jonscher's constant (n) and hopping frequency (f_p) for Gd_2O_3 content of (a) 1.75 mole% at 300°C(b) 2.5 mole% at 309°C (c) 4 mole% at 308°C (d) 5 mole% at 307°C (d) 8 mole% at 291°C(e) 9 mole% at 311 °C and (f) 11 mole% at 312 °C

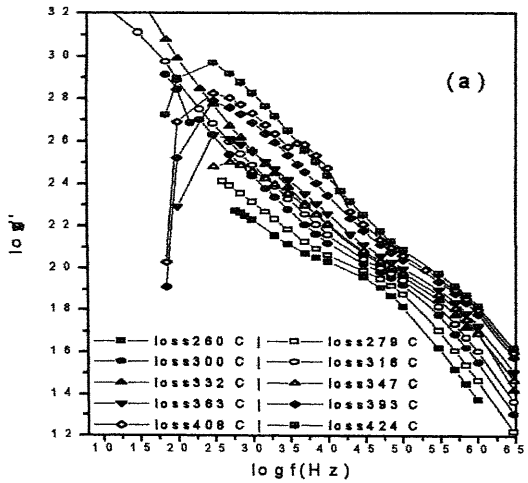
(a)
log g'
log f(Hz)
loss260 C | loss279 C
loss300 C | loss316 C
loss332 C | loss347 C
loss363 C | loss393 C
loss408 C | loss424 C

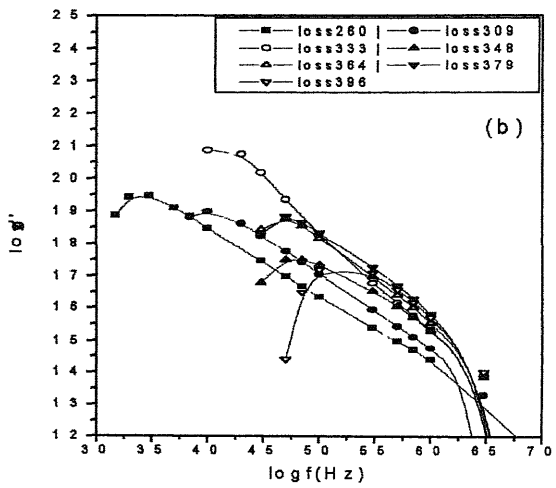
(b)
log g'
log f(Hz)
loss260 | loss309
loss333 | loss348
loss364 | loss379
loss396

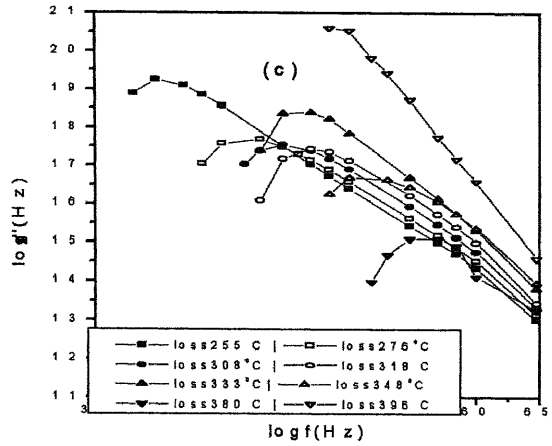
(c)
log g''(Hz)
log f(Hz)
loss255 C | loss276 °C
loss308 °C | loss318 C
loss333 °C | loss348 °C
loss380 C | loss396 C

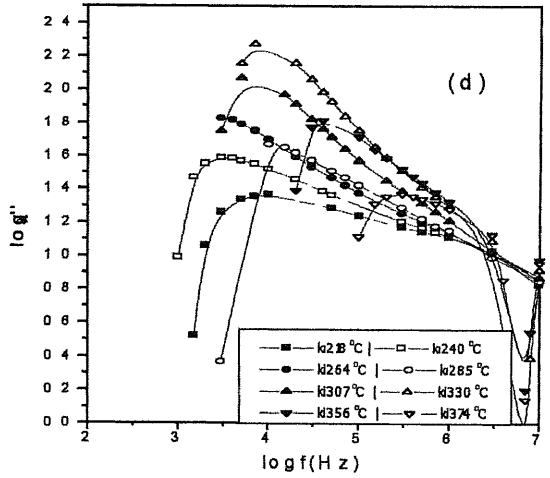
(d)
log g''
log f(Hz)
kl240 °C
kl264 °C | kl285 °C
kl307 °C | kl330 °C
kl356 °C | kl374 °C

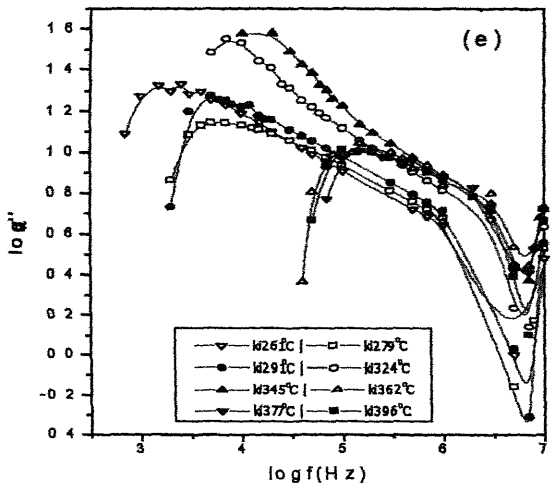

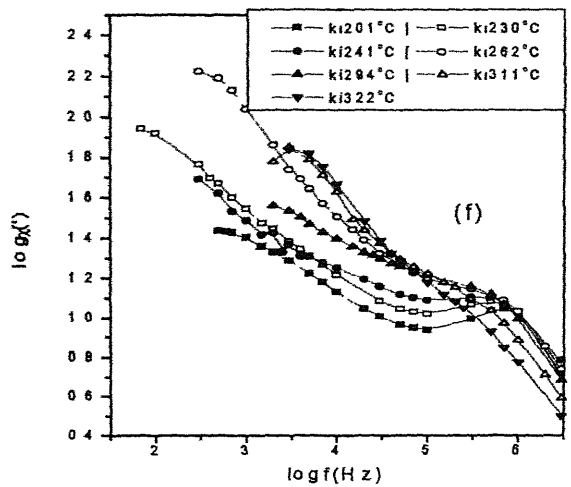

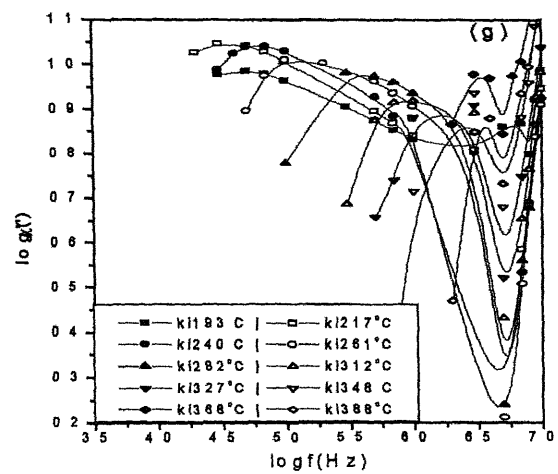

Fig. 3.26. Dielectric loss curves at different temperatures fo r(a) 1.75 (b) 2.5 (c) 4.0 (d) 5.0 (e) 8.0 (f) And (g) 11.0 mole % gadolinia doped zirconia bulk samples

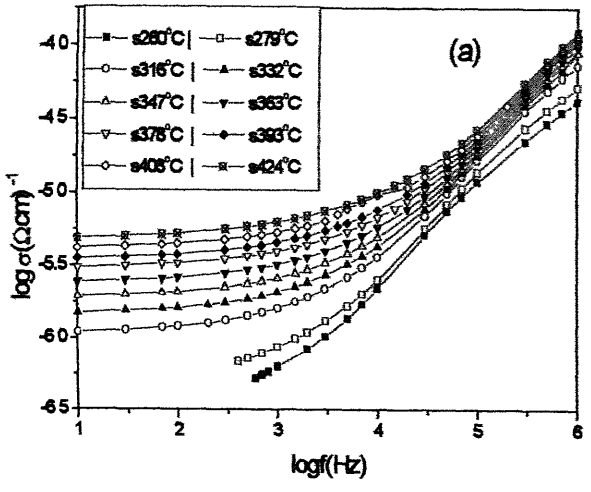
(a)
s260°C | s279°C
s316°C | s332°C
s347°C | s363°C
s378°C | s393°C
s405°C | s424°C
log σ(Ωcm)^-1
logf(Hz)

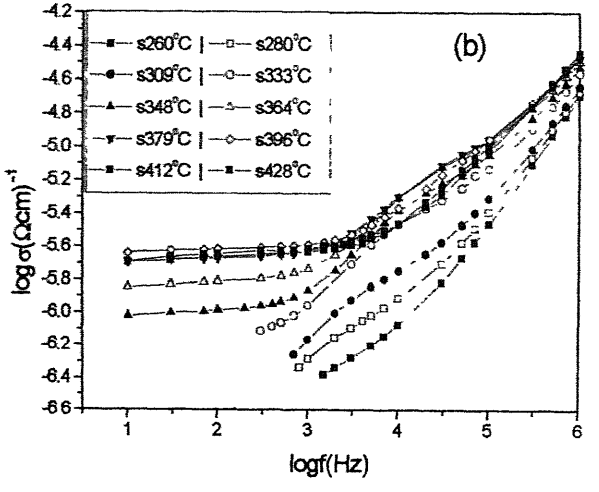
(b)
s260°C | s280°C
s309°C | s333°C
s348°C | s364°C
s379°C | s396°C
s412°C | s428°C
log σ(Ωcm)^-1
logf(Hz)

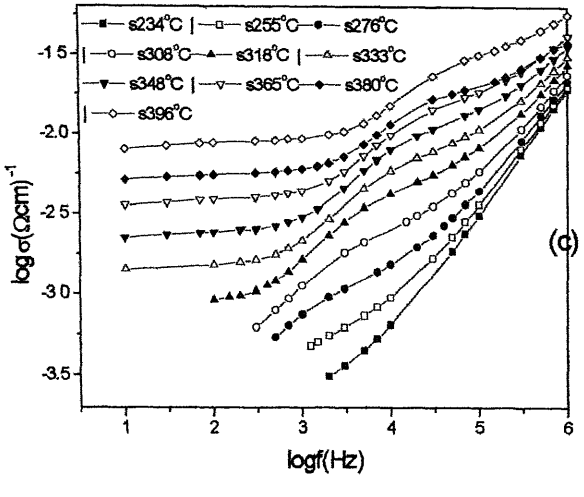
(c)
s234°C | s255°C | s276°C
s308°C | s316°C | s333°C
s348°C | s365°C | s380°C
s396°C
log σ(Ωcm)^-1
logf(Hz)

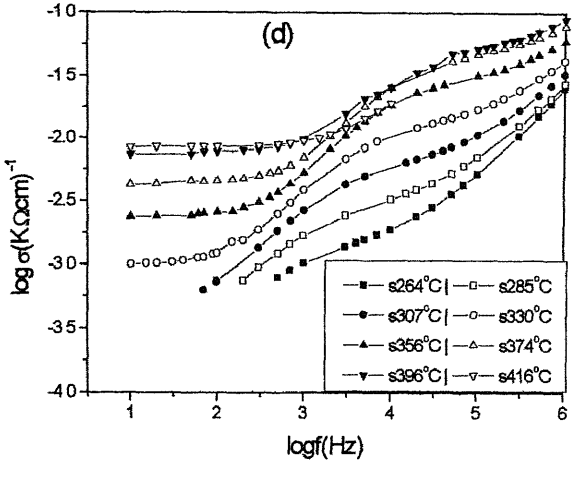
(d)
s264°C | s285°C
s307°C | s330°C
s356°C | s374°C
s396°C | s416°C
log σ(KΩcm)^-1
logf(Hz)

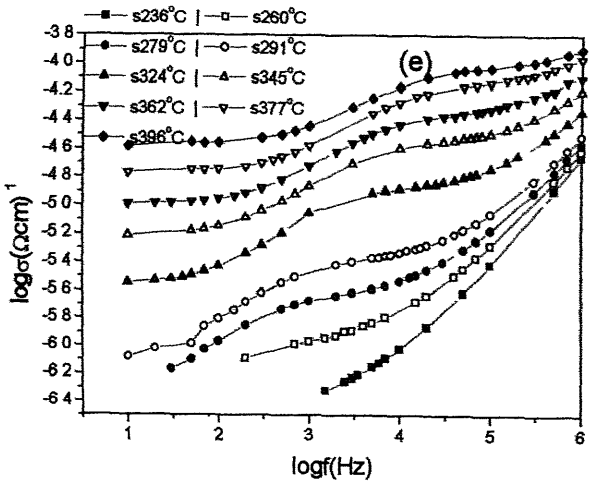

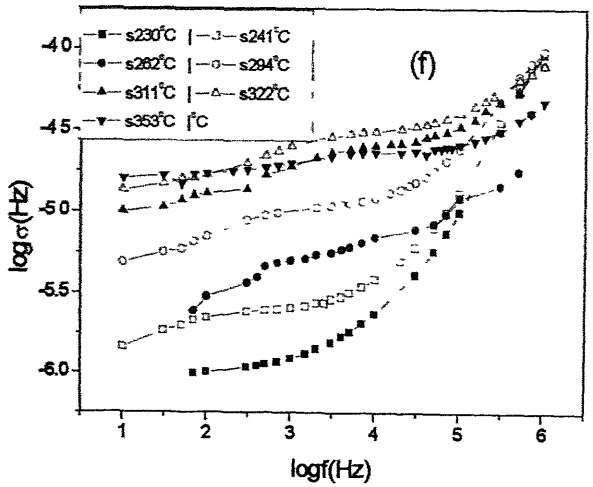

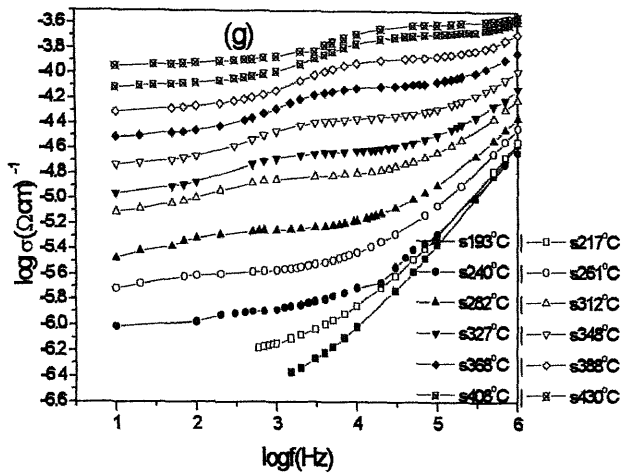

Fig. 3.27. Effect of Frequency on AC conductivity for (a) 1.75 (b) 2.5 (c) 4 (d) 5 (e) 8 and (f) 9 and (g) 11 mole% gadolinia doped zirconia bulk samples at different temperatures.

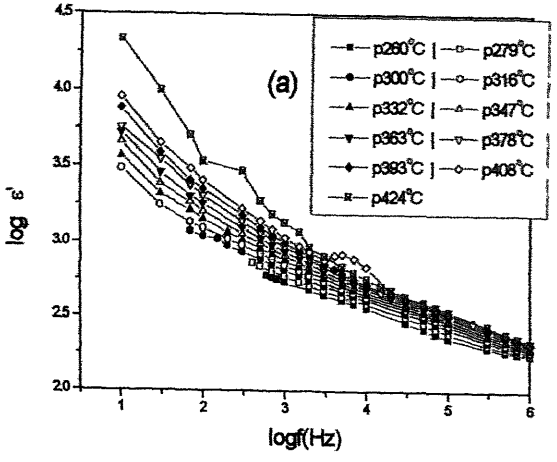
(a)
p260°C | p279°C
p300°C | p316°C
p332°C | p347°C
p363°C | p378°C
p393°C | p408°C
p424°C
log ε'
logf(Hz)

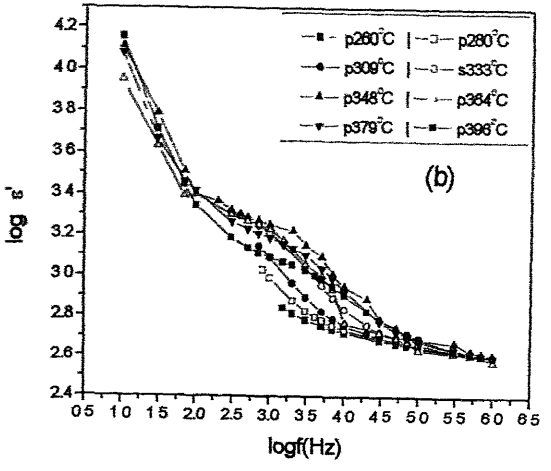
(b)
p260°C | p280°C
p309°C | s333°C
p348°C | p364°C
p379°C | p396°C
log ε'
logf(Hz)

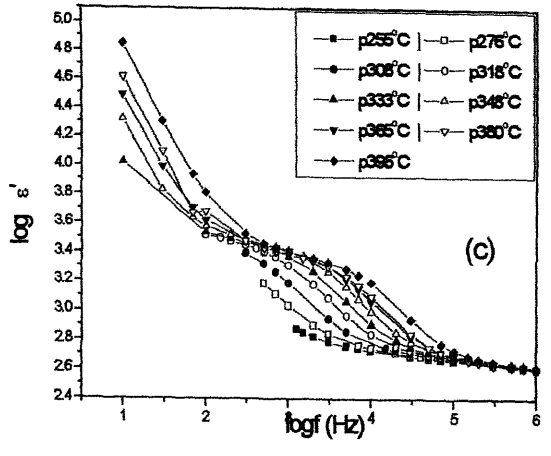
(c)
p255°C | p276°C
p306°C | p318°C
p333°C | p348°C
p365°C | p380°C
p396°C
log ε'
logf (Hz)

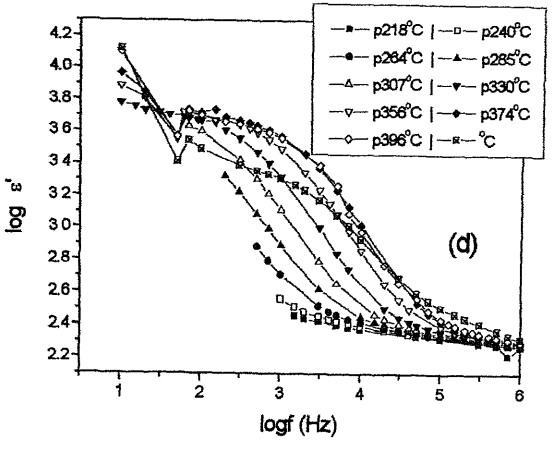
(d)
p218°C | p240°C
p264°C | p285°C
p307°C | p330°C
p356°C | p374°C
p396°C | °C
log ε'
logf (Hz)

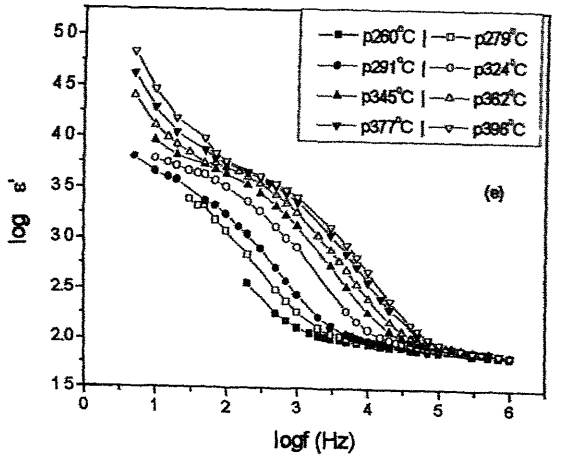

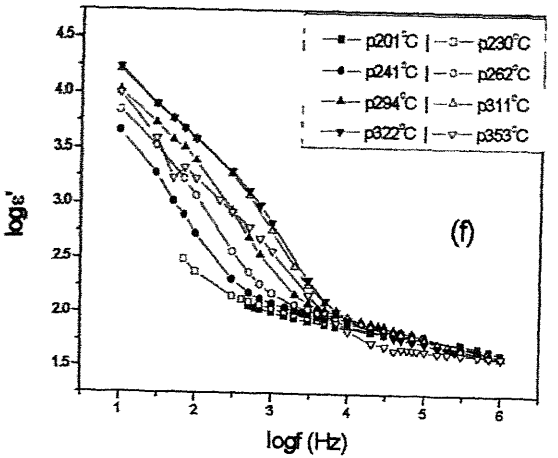

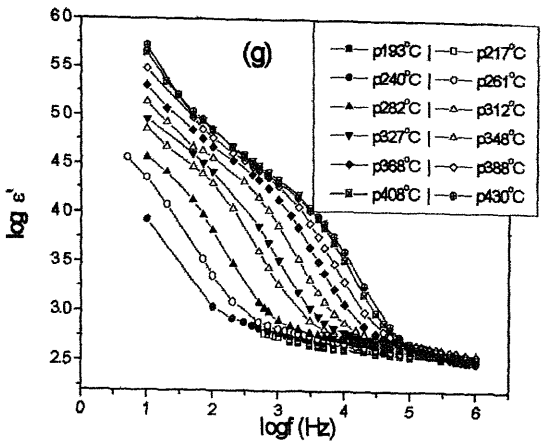

Fig. 3.28 Plots showing frequency dependence of real part of permittivity for (a) 1.75 (b) 2.5 (c) 4.0 (d) 5.0 (e) 8.0 (f) 9.0 And (g) 11.0 mole % gadolinia doped zirconia bulk samples at different temperatures

4 Summary and Conclusions

As mentioned in chapter 1, one of the motivations for studying the electrical conductivity of ZrO_2-Gd_2O_3 ceramics was the possibility of higher conductivity in this ceramics as compared to ZrO_2-Y_2O_3 ceramics because of the lower ionic size of Gd^{3+} However the results show that the conductivity and the activation enthalpy for ZrO_2-Gd_2O_3 system are not different from the values for ZrO_2-Y_2O_3 ceramics The main conclusions of this work are as follows.

1) The Cole-Cole plots for ZrO_2-Gd_2O_3 alloys at temperatures $\geq$ 380°C consist of two semicircles due to grain (high frequency) and grain boundary (low frequency) conduction and an arc due to electrode polarization.
2) The DC conductivity for both the grain and the grain boundary is seen to increase with temperature at all the compositions 4 mole% shows the highest conductivity at most of the temperatures. Around 585 K, except 4 mole% Gd_2O_3 grain conductivity of the rest of the compositions are nearly the same The grain boundary conductivity at this temperature is similar (around $0.6\times10^{-6}(\Omega cm)^{-1}$ for all the compositions except 2 5 mole% which shows a higher conductivity (1.5×10^{-6} $((\Omega cm)^{-1})$. If the data were to be extrapolated to higher temperature, the 8 mole% Gd_2O_3 sample would have shown the

maximum conductivity This is similar to the ZrO_2-Y_2O_3 ceramics

3) The activation enthalpies for conduction increase from 0 58 eV to 1 01 eV as the Gd_2O_3 content increases from 1 75 to 8 mole% Gd_2O_3 The activation enthalpies for all the compositions other than 1 75 and 2 5 mole% are nearly ~1 eV for grain and grain boundary conductivity which is again similar to observations in ZrO_2-Y_2O_3 system. The 9 and 11 mole% samples show the lower activation enthalpies compared to 8 mole% The reason could be that the 9 mole% is the lowest composition at which single cubic phase is seen Analysis of the data shows that the activation enthalpies for conduction and migration are nearly the same This shows that no significant formation of vacancy clusters in this system like ZrO_2-Y_2O_3

4) To the modulus plots M' vs log of frequency and M'' vs log of frequency, sigmoidal and lorentzian curve fit is done From the plot of log of relaxation frequency vs inverse of temperature, activation enthalpies for grain conduction are found. Values of determined by this method are nearly the same with those determined from the Cole-Cole plot except for 9 and 1 75 mole% At all compositions excepting 9 and 1 75 mole% a single relaxation mechanism is seen to be operating. At 1.75 mole% two thermally activated relaxation frequencies are seen. It may be attributed to conductivity relaxation due to ionic diffusion as well as dipole reorientation, which is still to be investigated The relaxation time is seen to decrease with composition and the relaxation peak is generally seen to increase with composition at any temperature

5) The carrier concentration N is of the order of 10^{21}/c c which is in good agreement with the data for ZrO_2-Y_2O_3 ceramics No correlation is seen between

N and composition of the ZrO_2-Gd_2O_3 system.

6) The values of Jonscher's constant (n) and hopping frequency (f_p) are found out by curve fitting to the universal dielectric response (UDR) relationship From the log of f_p vs inverse temperature, the activation enthalpies for migration are calculated The values of ΔH_m and $\Delta H_{\sigma g}$ are found to be nearly same. It indicates association of vacancy clusters is not significant in ZrO_2-Gd_2O_3 system The value of n is seen to decrease with temperature and f_p increases with temperature at a particular composition. The value of n varies between 0 6 and 0 85. On the other hand using the relationship between n and the depression angle in the Cole-Cole plot the values vary in the range of 0 8 to 1 Thus the AC curve fitting values are slightly lower than those from depression angle technique This is because the semicircle in the Cole-Cole plot is not exactly a semicircle

From the dielectric loss technique the values of conductivity could not be calculated as no frequency range showing linear trend for any composition was found. The dielectric loss peak is generally seen to decrease with increasing mole% of Gd_2O_3.

7) For all the compositions in the σ_{AC} vs logarithm of frequency plot, a plateau due to the frequency independent DC conductivity and a power law increase in the AC conductivity is seen. A dispersion step is seen due to the grain boundary relaxation in the curve The step is more prominent at higher mole% of Gd_2O_3 and becomes less significant at lower Gd_2O_3 concentration due to the overlapping nature of grain and the grain boundary semicircles.

8) Similar dispersion steps are seen in ε' vs logf plots Here the steps are

more prominent for grain boundary relaxation than σ_{AC} plots At lower frequencies ε' is seen to increase due to the blocking effect of space charge near the electrodes

References

1 S Chandra " Superionic Solids Theory and Principles" NorthHolland Publishing Company,(1981)

2 Green D J , R H J Hanik and M V Swain "Transformation Toughening of Ceramics" CRC Press , Inc Florida (1989)

3 T VanDijk, K J De Vries and A.J Burggraaf, "Electrical Conductivity of Flourite and Pyrochlore $Ln_x Zr_{1-x} O_{2-x/2}$ (Ln = Gd, Nd) Solid Solutions", Phys Stat Sol (a) **58**, 15 (1980)

4 Y Mizutani, M Kawai and Y Nakamura "High Electrical Conductivity and High Fracture Strength of Sc_2O_3 Doped Zirconia Ceramics with Submicrometer Grains", J Am Ceram Soc **82** [10] 2861-64 (1999)

5 E P Butlert and Bonanos, "The Characterization of ZrO_2 Engineering Ceramics by A C Impedance Spectroscopy", Mat Sci and Engg **1** (1985) 49-56.

6 S Bhattacharya, D C Agrawal, " Preparation of Tetragonal ZrO_2-Gd_2O_3", Journal of Materials Science **30** (1995) 1495-1499

7 T VanDijk and A.J Burggraaf, "Grain Boundary Effects on Ionic Conductivity in Ceramic $Gd_xZr_{1-x}O_{2-x/2}$ Solid Solutions", Phys Stat Sol (a) 63, 229 (1981)

8 J E Baurle, "Study of Solid Electrolyte Polarization by a Complex Admittance Method", J Phys Chem Solids, **30**,2657-70 (1969)

9 J R. Macdonald "Impedance Spectroscopy" John Wiley & Sam (1987)

10 B Scrosati, " Electrode Processes in Solid State Cells I The Metal Electrode" Solid State Batteries, Martinus Nijhoff Publishers (1985)

11 M.Kleitz & et al , "Impedence Spectroscopy & Electrical Resistance Measurement on Stabalized Zirconia" Advances in Ceramics , Vol 3 Science and Technology of Zirconia American Ceramic Society (1981)

12 J Luo, D P Almond, R. Stevens, "Ionic Mobilities and Association Energies from an Analysis of Electrical Impedance of $ZrO_2 - Y_2O_3$ Alloys" J Am Ceram Soc **83** [7] 1703-708 (2000)

13 J Luo, E F Hairetdinov, D P Almond, R. Stevens, "The Characteristic Frequencies for Ionic Conduction in 12 mol% Y_2O_3", Solid State Ionics **122** (1999) 205-210

14 Ramamoorthy, D Sundararaman, S Ramasamy, " Ionic Conductivity Studies of Ultrafine Grained Yttria Stabilized Zirconia Polymorphs", Solid State Ionics 91(1996) 39-44

15 A Pimenov et al "Ionic Conductivity and Relaxations in $ZrO_2 - Y_2O_3$ Solid Solutions", Solid State Ionics **109** (1998) 111-118

16 Thae-Khapp King, Takanori Nagasaki, Naoki Igawa, Kuk Il-Hiun, and Hideo Ohno, "Electrical Properties of Cubic, Stabalized ZrO_2-Gd_2O_3 Crystals," J Am Ceramics Soc , 75 {8} 2297-999 (1992)

17 T H Etsell and S N Flengas, "The Electrical properties of Solid Oxide Electrolytes," Chem Rev , 70, 339-76 (1970)

18 F Moztarzadeh, "Conductivity Measurements of Gd_2O_3-Stabalized ZrO_2 up to 2300 K", pp 901-905 in Advances in Ceramics, Vol 24 Science and Technology of Zirconia111 Edited by S Somiya, N Yamamoto, and 11 Yanagida American Ceramic Society, Westerville, OH, 1998

19 M Balog, M Schieber, "The Chemical Vapor Deposition and Characterization of ZrO_2 Films from Organometallic Compounds" Thin Solid Films, **129** (3-4), 1985, L71-73

20 C N Panagopoulos, "Charge Storage in Anodic ZrO_2 Films", Mater Lett 1997, **5** (1-2) 31-4

21 Akinune Yoshio, Ambe Satoshi, "Oxygen Sensor Element having a Thin Layer of Stabilized ZrO_2 Stabilized on a Substrate" Patent Nissan Motor Co Ltd GB, 2, 087, 569, 26 May 1982 Ceram Abstracts 62-054443P (1983)

22 J C Debsikdar, " Transparent Zirconia Gel-Monolith from Zirconium Alkoxide", J Non Cryst Solids **86** (1986) 231-240

23 Ph D Thesis of Santanu Bhattacharya under Dr D C Agrawal

24 V Provenzano et al "Electrical Relaxation in Na_2O –$3SiO_2$ Glass", J Am Ceram Soc **55** (100) 492-496 (1972)

APPENDIX

Use of Origin Software for Impedance Analysis

Origin 5 0 is used for plotting curves using raw data available from Impedance Analyzer i e z(Impedance), θ (phase shift) and f (frequency)

Double click Origin 5 0 icon Worksheet with two columns appears

I Cole-Cole Plot

Click on "Add New Columns" Enter f, z, θ in these three columns

(i) Convert θ to radians and enter in column D Click " Set Column Values" Enter the formula col(D) = (col(D)*pi/180)

(ii) Similarly put in column E values of zcosθ and in column F zsinθ

ColE = col(B) *cos (col(D)) and col(F) = col(B) *sin (col(D))

(iii) To plot click Plot icon Then click "Scatter" A new window titled " Select Columns For Plotting" appears Set col(E) as X and col(F) as Y click "O K "

(iv) Plot of zsinθ vs zcos θ appears on a new graph window

(v) Click on the abscissa or the ordinate to modify the range of x and y values Gridlines can be added and other formatting can be done

(vi) Click on "X axis title" A new screen named "Text Control" appears on the screen zcosθ can be put as name of the axis

(vii) Repeat for Y axis

(viii) Two semicircles are fitted to the data, one at a higher frequency for grain contribution and the other at the lower frequency part for the grain boundary contribution

(ix) To start with the semicircular fitting, click on "Analysis", and then click on "Non-Linear Curve Fit" In the new window that appears, click on "Origin Basic Functions" in the category section and then click on "semi_circle" Then click on "Start Fitting"

(x) Enter values for parameters a, b and c Approximate values of abscissa, ordinate of the center and the radius are entered respectively according to the equation $(x-a)^2 + (y-b)^2 = c^2$ Click on iterations At a minimum value of χ^2, click on "Done"

(xi) Semicircular fit is done on one part of the data and the results appear on the graph window Similarly another semicircle can be fitted The b values should be always negative as the semicircles are depressed ones The resistances are calculated as $R = c \times 2\ \Omega$

(xii) Column names in the datasheet can be changed by double clicking it

II Arrhenius Plots

At all the temperatures R is calculated for both grain and the grain boundary semicircles Then conductivity is obtained using equation (1 35)

1 In a new project, values of σ and T are entered Then log (σT) and T are entered in new columns Then scattered curve of log (σT) vs I/T is plotted

2 Click on the Linear Fit to fit a straight line to the data

3 A straight line is fitted to the data The result shows a straight line equation $y = A + Bx$, where A gives the value of the pre-exponential factor and B gives the value of activation enthalpy for conduction (ΔH_σ)

IV Migration Enthalpy Plot

Using the Almond-West equation (1 34), ΔH_m is calculated

1 $\ln(R^*\cos\theta/z-1)$ is calculated and entered $\ln(\sigma_{ac}/\sigma_{dc}-1)$ or $\ln(R^*\cos\theta/z-1)$ is plotted against lnf Scattered plot is obtained

2 Linear fit is done to the data The slope of the straight line gives the value of n or Jonscher's constant The intercept gives the value of $n\ln f_p$, the hopping frequency f_p is calculated from it

V Modulus Spectroscopy Plots

Real and imaginary parts of modulus are plotted against logf ($M' = z\sin\theta C_o$ and $M'' = z\cos\theta C_o$ where $C_o = \varepsilon_o \times A/L$, ε_o being the permittivity of the free space)

1 Values of M' and M'' are calculated and entered in the columns of worksheet Sigmoidal fit from non-linearfit is done to M' vs lnf and Lorentzian fit is done to the M'' vs lnf curve

2 The frequency at which peak values are seen is the relaxation frequency f_r a plot of $\log f_r$ vs 1/T is plotted Slope of the straight line gives the value of activation enthalpy for conduction for grain using the modulus spectra

VI AC Conductivity and Permittivity Plots

σ_{AC} ($\cos\theta/z$ *L/A) is plotted against logf for all temperatures

Real part of permittivity ε' ($\sin\theta/z\cos\theta/z\omega C_o$) is plotted against logf for all the temperatures

If there are different plots at different temperatures in one project as in the

'cases of conductivity and permittivity vs logf, then these plots can be combined to a single plot Click on Edit menu and then click on "Merge All Graph Windows" Then a single graph window containing plots at different temperatures is plotted


139593


139593
Date Slip

This book is to be returned on the date last stamped.


A139593